Artificial Brownian motors: controlling transport on the nanoscale

Peter Hänggi, Fabio Marchesoni

Angaben zur Veröffentlichung / Publication details:

Hänggi, Peter, and Fabio Marchesoni. 2009. "Artificial Brownian motors: controlling transport on the nanoscale." *Reviews of Modern Physics* 81 (1): 387–442. https://doi.org/10.1103/revmodphys.81.387.

Artificial Brownian motors: Controlling transport on the nanoscale

Peter Hänggi*

Institut für Physik, Universität Augsburg, Universitätsstrasse 1, D-86135 Augsburg, Germany
and Department of Physics and Centre for Computational Science and Engineering, National University of Singapore, Singapore 117542, Singapore

Fabio Marchesoni†

Dipartimento di Fisica, Università di Camerino, I-62032 Camerino, Italy
and School of Physics, Korea Institute for Advanced Study, Seoul 130-722, Korea

(Published 30 March 2009)

In systems possessing spatial or dynamical symmetry breaking, Brownian motion combined with unbiased external input signals, deterministic and random alike, can assist directed motion of particles at submicron scales. In such cases, one speaks of "Brownian motors." In this review the constructive role of Brownian motion is exemplified for various physical and technological setups, which are inspired by the cellular molecular machinery: the working principles and characteristics of stylized devices are discussed to show how fluctuations, either thermal or extrinsic, can be used to control diffusive particle transport. Recent experimental demonstrations of this concept are surveyed with particular attention to transport in artificial, i.e., nonbiological, nanopores, lithographic tracks, and optical traps, where single-particle currents were first measured. Much emphasis is given to two- and three-dimensional devices containing many interacting particles of one or more species; for this class of artificial motors, noise rectification results also from the interplay of particle Brownian motion and geometric constraints. Recently, selective control and optimization of the transport of interacting colloidal particles and magnetic vortices have been successfully achieved, thus leading to the new generation of microfluidic and superconducting devices presented here. The field has recently been enriched with impressive experimental achievements in building artificial Brownian motor devices that even operate within the quantum domain by harvesting quantum Brownian motion. Sundry akin topics include activities aimed at noise-assisted shuttling other degrees of freedom such as charge, spin, or even heat and the assembly of chemical synthetic molecular motors. This review ends with a perspective for future pathways and potential new applications.

DOI: 10.1103/RevModPhys.81.387 PACS number(s): 05.60.−k, 47.61.−k, 81.07.−b, 85.25.−j

CONTENTS

*peter.hanggi@physik.uni-augsburg.de
†fabio.marchesoni@pg.infn.it

I. INTRODUCTION

Over the past two decades advances in microscopy and microscale control have allowed scientists and engineers to delve into the workings of biological matter. One century after Kelvin's death, today's researchers aim to explain how the engines of life actually work by stretching thermodynamics beyond its 19th-century limits (Haw, 2007).

Carnot realized that all engines transform energy from one form into another with a maximum possible efficiency that does not depend on the technology developed or on the fuel utilized, but rather on fundamental quantities such as heat and temperature. Kelvin and Clausius came up with two "rules of the engine," later known as the first two laws of thermodynamics. The first law states that energy cannot be destroyed or created but only transformed; the second law sets fundamental limitations on the practical achievements of energy transformation. Just as the first law was centered on the notion of energy (from the Greek for "work capability"), the second law revolved around the new concept of entropy (a term coined by Clausius, also from Greek, for "change capability").[1] When expressed in such terms, the second law states that entropy cannot decrease during any spontaneous or natural process. Notably, within the whole virtual factory of all natural processes, the first law takes on the role of an account clerk, keeping track of all energy changes, while the second law takes on the role of the director, determining the direction and action of all processes.

The fathers of thermodynamics developed their laws having in mind macroscopic systems that they could describe in terms of state (i.e., average) quantities such as pressure and temperature, a reasonable assumption when dealing with the monster steam engines of Victorian industry. A typical protein, however, is a few nanometers in size and consists of just a few tens of thousands of atoms. As a consequence, the movements of a protein engine are swamped by fluctuations resulting from the Brownian motion of its surroundings, which causes the energy of any of its parts to fluctuate continually in units of kT, with k denoting the Boltzmann constant and T the temperature. The effects of such energy fluctuations were demonstrated by Yanagida and coworkers (Nishiyama *et al.*, 2001, 2002), who observed kinesin molecules climbing the cytoskeletal track in a juddering motion made up of random hesitations, jumps, and even backward steps. Similar results have been reported for a host of protein engines. The key question in modern thermodynamics is therefore how far energy fluctuations drive microengines and nanoengines beyond the limits of the macroscopic laws.

A revealing experiment was performed by Bustamante *et al.* (2005), who first stretched a single RNA molecule by optically tugging at a tiny plastic bead, attached to one end, and then released the bead, to study the effect of random energy fluctuations on the molecule recovery process. By repeating many identical stretching cycles, they found that the molecule "relaxation path" was different every time. In fact, the bead was drawing useful energy from the thermal motion of the suspension fluid and transforming it into motion. However, by averaging over increasingly longer bead trajectories, that is, approaching a macroscopic situation, Bustamante *et al.* (2005) were able to reconcile their findings with the second law. These results led to the conclusion that the straightforward extension of the second law to microscopic systems is unwarranted; individual small systems do evolve under inherently nonequilibrium conditions.

However, a decade ago Jarzynski (1997) showed that the demarcation line between equilibrium and nonequilibrium processes is not always as clear-cut as we used to think. Imagining a microscopic single-molecule process, Jarzynski evaluated not the simple average of the change of the (random) work of the underlying perturbed nanosystem, as it was pulled away from equilibrium according to an arbitrary protocol of forcing, but rather the average of the *exponential* of that tailored nonequilibrium work. This quantity turned out to be the same as for an adiabatically slow version of the same process, and, most remarkably, equals the exponential of the system's equilibrium free energy change. This result, also experimentally demonstrated by Bustamante *et al.* (2005), came as a great surprise because it meant that

[1]Rudolf Julius Emanuel Clausius throughout his life allegedly preferred the German word *Verwandlungswert* rather than entropy, although his colleagues suggested that he choose a name for his new thermodynamic quantity S (his chosen symbol for labeling entropy, possibly in honor of Sadi Carnot) that sounded as close as possible to the word energy.

information about macroscopic equilibrium was somehow buried inside individual, randomly fluctuating microscopic systems far from equilibrium (see also Gallavotti and Cohen, 1995; Crooks, 1999; Jarzynski, 2007; Talkner *et al.*, 2007, 2008).

There is an additional limitation of 19th-century thermodynamics that is potentially even more significant in the design and operation of engines at submicron scale. Kelvin's thermodynamics was based on the simplifying notion of an isolated system. The laws of macroscopic thermodynamics therefore apply only to systems that are either separated from their environment or coupled to it under controlled operating conditions, that is, measured in terms of the state variables of the system itself. However, unlike cylinders inside steam engines, protein engines do not (cannot) work in isolation.

Following very much in the footsteps of 19th-century scientists and engineers, modern experimenters have individually probed the proteins that play a crucial role in the cell, feeding them with energy by injecting some chemical fuel "by hand" (e.g., ATP molecules) or exerting mechanical action of some sort (Astumian, 1997; Bustamante *et al.*, 2005). In their natural setting, however, life engines are just parts of a closely interconnected functional web that keeps a cell alive. The great challenge of systems biology is therefore to put our understanding of isolated life engines back into the real world of the cell.

A. Artificial nanodevices

Nanotechnology has been intricately linked with biological systems since its inception. Fascinated by the complexity and smallness of the cell, Feynman (1960) challenged the scientific community to "make a thing very small which does what we want." In his visionary response, Drexler (1992) proposed to focus on protein synthesis as a pathway for creating nanoscale devices. Both Feynman's and Drexler's propositions were met with much skepticism, as accurate manipulations at the nanoscale were deemed impossible. However, in view of the recent advances in systems biology (Gross, 1999), cellular mechanisms are now being cited as the key proof of the nanotechnological viability of devices with atomic precision. In spite of their established complementarity, a fundamental difference between systems biology and nanotechnology is their ultimate goal. Systems biology aims to uncover the fundamental operations of the cell in an effort to predict the exact response to specific stimuli and genetic variations, whereas nanotechnology is chiefly concerned with useful design.

Manufacture of nanodevices through positional assembly and self-assembly of biological components available at the cellular level is the goal of the so-called biomimetic approach—as opposed to the inorganic approach aimed at fabricating nanomechanical devices in hard, inorganic materials (e.g., using modern lithographic techniques, atomic force, and scanning tunneling microscopy, etc.). Nature has already proven that it is possible to engineer complex machines on the nanoscale; there is an existing framework of working components manufactured by nature that can be used as a guide to develop our own *biology-inspired* nanodevices. It is also true that the molecular machinery still outperforms by many orders of magnitude anything that can be artificially manufactured. Nevertheless, inorganic nanodevices are attracting growing interest as a viable option due to their potential simplicity and robustness; in addition, inorganic nanodevices may provide additional experimental access to the molecular machinery itself.

In this review we intend to pursue further the inorganic approach to nanodevices, based on three main assumptions: (i) In view of the most recent developments in nonequilibrium thermodynamics, the science of nanodevices, regardless of the fabrication technique, is inseparable from the thermodynamics of microscopic engines (Hänggi *et al.*, 2005). (ii) Fabrication techniques on the nanoscale will perform better and better following the trend of the last two decades. (iii) A better understanding of the molecular machinery can help us to devise and implement new transport and control mechanisms for biology-inspired nanodevices. In other words, we bet on a two-way cross fertilization between the biomimetic and inorganic approaches.

B. Brownian motors

Nature has provided microorganisms with characteristic sizes of about 10^{-5} m with a variety of self-propulsion mechanisms, all of which pertain to motion induced by cyclic shape changes. During one such cycle the configuration changes follow an asymmetric sequence, where one half cycle does not simply retrace the other half, in order to circumvent the absence of hydrodynamic inertia at the microscale, i.e., for low Reynolds numbers (Purcell, 1977). A typical example is motile bacteria that "swim" in a suspension fluid by rotating or waving their flagella (Astumian and Hänggi, 2002; Astumian, 2007). As anticipated above, a further complication arises when the moving parts of a (sub)micron-sized engine have molecular dimensions of 10^{-8} m or so. In that case, diffusion caused by Brownian motion competes with self-propelled motion. For example, a molecular motor mechanism becomes efficient if, at room temperature and in a medium with viscosity close to that of water, a bacterium needs more time to diffuse a body length than it does to swim the same distance.

A solution common to most cell machinery is to have molecular motors operating on a track that constrains the motion to essentially one dimension along a periodic sequence of wells and barriers. The energy barriers significantly suppress diffusion, while thermal noise plays a constructive role by providing a mechanism, thermal activation (Hänggi *et al.*, 1990), by which motors can escape over the barriers. The energy necessary for directed motion is supplied by *asymmetrically* raising and lowering the barriers and wells, either via an external time-dependent modulation (e.g., due to the coupling with other motors) or by energy input from a nonequi-

librium source such as a chemical reaction, like ATP hydrolysis. Thus, in agreement with the reasoning underlying the analysis[2] of the Smoluchowski-Feynman stylized ratchet engine (Smoluchowski, 1912; Feynman *et al.*, 1963), under appropriate nonequilibrium conditions structural anisotropy can sustain directed motion. Such a device does not violate the second law of thermodynamics because the very presence of nonequilibrium renders inoperative those limiting (thermal equilibrium) restrictions.

In the case of a bacterium, as for any ordinary heat engine, the relevant state variables, namely, its position and the phase of the flagellum stroke, always cycle through one and the same periodic time sequence; the two variables are tightly coupled and almost synchronized. In clear contrast to this familiar scenario, the state variables of artificial motors are often loosely coupled due to the prominent action of fluctuations, a salient feature captured by Hänggi, who coined the term Brownian motors in this context (Bartussek and Hänggi, 1995).[3]

Important hallmarks of any genuine Brownian motor are as follows (Astumian and Hänggi, 2002; Hänggi *et al.*, 2005): (i) The presence of some amount of (not necessarily thermal) noise. The intricate interplay among nonlinearity, noise-activated escape dynamics, and nonequilibrium driving implies that, generally, not even the direction of transport is predictable *a priori*. (ii) Some sort of symmetry breaking supplemented by temporal periodicity (typically via an unbiased, nonequilibrium forcing), if a cyclically operating device is involved. Therefore not every small ratchet device falls in the category of Brownian motors. This holds true especially if the governing transport principle is deterministic, as in mechanical ratchet devices of macroscopic or mesoscopic size.

The following prescriptions should be observed when designing an efficient Brownian motor: (a) Spatial and temporal periodicity critically affect rectification. (b) All acting forces and gradients must vanish after averaging over space, time, and statistical ensembles. (c) Random forces (of thermal, nonthermal, or even deterministic origin) assume a prominent role. (d) Detailed balance symmetry, ruling thermal equilibrium dynamics, must be broken by operating the device away from thermal equilibrium. (e) A symmetry-breaking mechanism must apply. There exist several possibilities to induce symmetry breaking. First, the spatial inversion symmetry of the periodic system itself may be broken intrinsically, that is, already, in the absence of nonequilibrium perturbations. This is the most common situation and typically involves a type of periodic, asymmetric ratchet potential. A second option consists of the use of an unbiased driving force (either deterministic or stochastic) possessing nonvanishing, higher-order odd time correlations. Yet a third possibility arises via collective effects in coupled, perfectly symmetric nonequilibrium systems, namely, in the form of spontaneous symmetry breaking. Note that in the latter two cases we speak of Brownian motor dynamics even though a ratchet potential is not necessarily involved.

The idea of using unbiased thermal fluctuations and/or unbiased nonequilibrium perturbations to drive directed motion of particles and the like has seen several rediscoveries since the visionary works by von Smoluchowski (1912) and Feynman *et al.* (1963). From a historical perspective, the theme of directed transport and Brownian motors was put into the limelight of statistical and biological physics research with the appearance of several ground-breaking works, both theoretical and experimental, which appeared during the period 1992–1994. Most notably, Ajdari and Prost (1992), Astumian and Bier (1994), Bartussek *et al.* (1994), Chauwin *et al.* (1994), Doering *et al.* (1994), Magnasco (1993), Millonas and Dykman (1994), Prost *et al.* (1994), and Rousselet *et al.* (1994) helped ignite tumultuous interest in this topical area which kept growing until the present day. Readers may deepen their historical insight by consulting earlier introductory reports such as those published by Hänggi and Bartussek (1996), Astumian (1997), Jülicher *et al.* (1997), Astumian and Hänggi (2002), Reimann (2002), Reimann and Hänggi (2002), and Hänggi *et al.* (2005).

This review focuses on recent advances in the science of nonbiological, *artificial* Brownian motors. In contrast to those reviews and articles mentioned above, which cover the rich variety of possible Brownian motor scenarios and working principles, our focus is on nonbiological, artificial, mostly solid-state-based Brownian motors. In this spirit we have attempted to present a comprehensive overview of today's status of this field, including the newest theory developments, most compelling experimental demonstrations, and first successful technological applications. Some closely related topics, such as the engineering of synthetic molecular motors and nanomachines based on chemical species, are only briefly discussed because detailed, up-to-date reviews have been published by groups active in those areas (Kottas *et al.*, 2005; Balzani *et al.*, 2006; Kay *et al.*, 2007).

II. SINGLE-PARTICLE TRANSPORT

Signal rectification schemes in the absence of noise have been known for a long time, especially in the electrical engineering literature. However, rectification in nanodevices cannot ignore fluctuations and Brownian motion, in particular. New experiments on both biological and artificial devices showed how noise rectification can actually be utilized to effectively control particle transport on the small scale. By now, noise rectification

[2]Note also the examination of Feynman's analysis by Parrondo and Español (1996).

[3]The notion of a molecular motor is reserved for motors specifying biological, intracelluar transport. Likewise, the notion of a Brownian or thermal ratchet is reserved for the operating principle of protein translocation processes. The latter term was introduced by Simon *et al.* (1992) to describe isothermal trapping of Brownian particles to drive protein translocation; see also Wang and Oster (2002).

has become one of the most promising techniques for powering microdevices and nanodevices.

In order to set the stage, in the next section we first consider the case of systems where rectification cannot occur. In the subsequent sections we single out all ingredients that do make rectification possible.

Consider a Brownian particle with mass m, coordinate $x(t)$, and friction coefficient γ in one dimension, subjected to an external static force F and thermal noise $\xi(t)$. The corresponding stochastic dynamics is described by the inertial Langevin equation

$$m\ddot{x} = -V'(x) - m\gamma\dot{x} + F + \xi(t), \tag{1}$$

where $V(x)$ is a periodic potential with period L, namely, $V(x+L)=V(x)$, the prime indicates differentiation with respect to x, and the overdot differentiation with respect to time t. Thermal fluctuations are modeled by a stationary Gaussian noise of vanishing mean, $\langle\xi(t)\rangle=0$, satisfying the fluctuation-dissipation relation

$$\langle\xi(t)\xi(0)\rangle = 2D_p\delta(t), \tag{2}$$

where the momentum-diffusion strength reads $D_p = m\gamma kT$, with k denoting the Boltzmann constant and T the temperature of an equilibrium heat bath.

In extremely small systems, particle dynamics and fluctuations occurring in biological and liquid environments are often well described by the *overdamped* limit of Eq. (1)—for a discussion see Purcell (1977)—in terms of a massless Langevin equation, which is driven by position diffusion $D_x = kT/m\gamma \equiv D$, i.e.,

$$\dot{x} = -V'(x) + F + \xi(t), \tag{3}$$

with

$$\langle\xi(t)\xi(0)\rangle = 2D\,\delta(t). \tag{4}$$

In this overdamped regime, the inertia term $m\ddot{x}$ can be dropped altogether with respect to the friction term $-m\gamma\dot{x}$ (the Smoluchowski approximation). In the following, $m\gamma$ has been scaled to unity for convenience, i.e., $D \equiv kT$.

In the absence of an external bias, i.e., $F=0$, the equilibrium stochastic mechanism in Eq. (1) cannot sustain a nonzero stationary current, i.e., $\langle\dot{x}(t)\rangle=0$, no matter what $V(x)$. This can be readily proven by solving the corresponding Fokker-Planck equation with periodic boundary conditions (Risken, 1984; Mel'nikov, 1991).

A. Symmetric substrates

We consider first the case when a periodic substrate with potential $V(x)$ is symmetric under reflection, that is, $V(x-x_0)=V(-x+x_0)$ for certain x_0 with $0 \leqslant x_0 < L$. The most studied example is the symmetric washboard potential (Risken, 1984)

$$V(x) = -V_0 \sin(2\pi x/L), \tag{5}$$

displayed in the presence of a static tilt force F in Fig. 1(a). The particle mobility $\mu(F) \equiv \langle\dot{x}\rangle/F$ is symmetric for $F \to -F$, namely, $\mu(F)=\mu(-F)$. For this reason we restrict ourselves to $F \geqslant 0$.

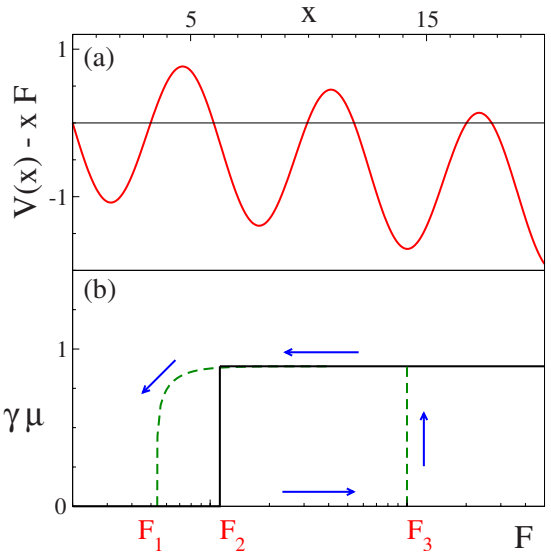

FIG. 1. (Color online) Transport in a tilted washboard potential. (a) Tilted periodic potential of Eq. (5), $V(x)-xF$, with $F=0.1$. (b) Locked-to-running transitions. The thresholds F_1 and F_3 of the hysteretic loop (dashed curves) and the zero temperature step at F_2 (solid curve) are marked explicitly. Parameter values: $m=V_0=1$, i.e., $F_3=1$, and $\gamma=0.03$.

1. dc drive

The Brownian motion, Eq. (1), in the washboard potential, Eq. (5), has been detailed in the Risken (1984) textbook. To make contact with Risken's notation one must rewrite Eq. (1) in terms of the rescaled quantities $x \to (2\pi/L)x$, $F \to (2\pi/L)F/m$, and $T \to (2\pi/L)^2 T/m$, so that

$$\ddot{x} = -\gamma\dot{x} + \omega_0^2 \cos x + F + \xi(t). \tag{6}$$

The angular frequency $\omega_0=(2\pi/L)\sqrt{V_0/m}$ characterizes the oscillating motion of the particle at the bottom of the potential wells. To reconcile Eq. (6) with Eq. (1) for the potential in Eq. (5), it suffices to scale $m=1$ and $L=2\pi$, as assumed throughout unless stated otherwise.

The dynamics of Eq. (6) is characterized by random switches occurring either between two locked states, dwelling in a well minimum (large friction γ), or between a locked state with zero average velocity and a (downhill) running state with a finite, average asymptotic velocity $\langle\dot{x}\rangle = F/\gamma$ (small friction γ). In terms of mobility, locked and running states correspond to $\gamma\mu=0$ and 1, respectively.

In the overdamped regime, Eq. (3), the particle is trapped most of the time at a local minimum of the tilted substrate as long as $F \leqslant F_3 = \omega_0^2$; for $F > F_3$ there exist no such minima and the particle runs in the F direction with average speed approaching F/γ. This behavior is described quantitatively by the mobility formula (Risken, 1984)

$$\mu(F) = L/\langle t(L,F)\rangle F, \tag{7}$$

where $\langle t(L,F)\rangle$, the mean first-passage time of the particle across a substrate unit cell in the F direction, can be computed explicitly for any choice of $V(x)$ (Hänggi *et al.*, 1990).

In the underdamped regime $\gamma \ll \omega_0$ the locked-to-running transition depends crucially on the presence of noise, no matter how weak. In the *noiseless* case, $\xi(t) \equiv 0$, the average speed of a Brownian particle with coordinate $x(t)$ depends on the initial conditions according to the hysteretic cycle illustrated in Fig. 1(b): The transition from the locked to the running state occurs on raising F above F_3 (depinning threshold), while the opposite transition takes place on lowering F below $F_1 = (4/\pi)\gamma\omega_0$ (repinning threshold). Of course, for sufficiently large values of γ, say, in the damped regime with $\gamma > \gamma_0 = (\pi/4)\omega_0$, the distinction between F_1 and F_3 becomes meaningless; the locked-to-running transition occurs at $F = F_3$, no matter what the initial conditions.

At zero temperature, $T = 0+$, we have a totally different scenario, as the *stationary* dynamics of $x(t)$ is controlled by one threshold $F_2 = 3.3576\ldots\gamma\omega_0$ only (Risken, 1984): For $F < F_2$ the Brownian particle remains trapped in one potential well; for $F > F_2$ it falls down the tilted washboard potential with speed close to F/γ. At the threshold F_2 the quantity $\gamma\mu$ jumps from 0 to (very close to) 1, stepwise [Fig. 1(b)]. Note that, unlike F_3, F_2 indicates a dynamical transition occurring in the presence of a relatively small tilt. Nevertheless, at low damping, switches between locked and running states correspond to long forward particle jumps, which can span many substrate unit cells L; the distributions of the relevant jump lengths exhibit persistent nonexponential tails (Pollak *et al.*, 1993; Ferrando *et al.*, 1995; Costantini and Marchesoni, 1999; Borromeo and Marchesoni, 2000; Shushin, 2002).

For finite but low temperatures, $kT \ll V_0$, the transition from the locked to the running state is continuous but still confined within a narrow neighborhood of F_2; the relevant locked-to-running transition threshold $F_{\rm th}$ is numerically identifiable with high accuracy as a convex function of γ; F_2 and F_3 are, respectively, the $\gamma \to 0$ and $\gamma \to \infty$ asymptotes of the numerical curve $F_{\rm th}(\gamma)$ (Risken, 1984).

2. ac drive

Suppose now that the external force $F(t)$ acting on the unit-mass Brownian particle is periodic in time. The simplest case possible is represented by a noiseless particle, $\xi(t) \equiv 0$, moving on a sinusoidal potential, Eq. (5), under the action of a harmonic force

$$F(t) = A_1 \cos(\Omega_1 t + \phi_1). \tag{8}$$

The wide class of devices thus modeled may be assimilated to a damped-driven pendulum operated at zero noise level, a chaotic system investigated in depth in the 1980s (Baker and Gollub, 1990). The dynamics of a massive particle in a sinusoidal potential was reproduced in terms of a climbing-sine map (Geisel and Nierwetberg, 1982; Grossmann and Fujisaka, 1982): Running orbits, leading to a spontaneous symmetry breaking, can be either periodic or diffusive, depending on the value of the map control parameter (viz., the amplitude of the sine term). The phase-space portrait of the actual damped-driven pendulum was computed by Huberman *et al.* (1980), who revealed the existence of delocalized strange attractors with an intricate structure on all scales, later recognized to be fractal objects (Baker and Gollub, 1990). This means that, despite the global reflection symmetry of the dynamics in Eqs. (1) and (8), for sufficiently small γ the particle drifts either to the right or to the left, depending on the initial conditions, but with equal probability in phase space.

Coupling the particle to a heat bath, no matter how low the temperature, changes this scenario completely. The action of the noise source $\xi(t)$ amounts to scrambling the initial conditions, which therefore must be averaged over. As a consequence, trajectories to the right and to the left compensate one another and the symmetry is restored: No Brownian drift is expected in the zero-temperature limit.

The system symmetry can be broken by adding a dc component A_0 to the external force,

$$F(t) = A_0 + A_1 \cos(\Omega_1 t + \phi_1). \tag{9}$$

The most evident effect of such a periodic drive is the appearance of hysteresis loops (Borromeo *et al.*, 1990) in the parametric curves of the mobility $\mu(t)$ vs $F(t)$. For $\Omega_1 \ll \omega_0$ and $A_0 \ll F_{\rm th}$, the mobility hysteresis loop is centered on the static mobility curve $\mu(A_0)$ and traversed counterclockwise; with decreasing Ω_1, its major axis approaches the tangent to the curve $\mu(A_0)$. Hysteresis loops have been observed even for Ω_1 much smaller than the relevant Kramers rate, the smallest relaxation rate in the unperturbed stationary process of Eq. (6) with $F = 0$. The area encircled by the hysteretic loops is maximum for $A_0 \simeq F_{\rm th}$, that is, close to the transition jump. Even more interestingly, it exhibits a resonant dependence on both the forcing frequency and the temperature, thus pointing to a dynamical stochastic resonance (Gammaitoni *et al.*, 1998) mechanism between locked and running states (Borromeo and Marchesoni, 2000).

Finally, Machura, Kostur, *et al.* (2007) showed that, under special conditions, involving small Brownian motion at temperature T and appropriate relaxation constants $\gamma \lesssim \Omega_1 \lesssim \omega_0$, the damped process in Eq. (6) occasionally exhibits the phenomenon of absolute negative mobility: The ac cycle-averaged drift velocity $\langle \dot{x} \rangle$ may be oriented against the dc bias A_0, as the result of a delicate interplay of chaotic and stochastic dynamics. This observation was corroborated theoretically by Speer *et al.* (2007) and Kostur *et al.* (2008) and experimentally by Nagel *et al.* (2008). Yet another artificial Brownian motor system where this phenomenon can likely be validated experimentally is a system of cold atoms dwelling in periodic optical lattices.

3. Diffusion peak

Diffusive transport of particles or, more generally, small objects, is a ubiquitous feature of physical and chemical reaction systems (Burada *et al.*, 2009). Directed Brownian motor transport is typically controlled by both the fluctuation statistics of the jittering objects and the phase space available to their dynamics. For example, as the particle in Eq. (6) drifts with average speed $\langle \dot{x} \rangle$ in the direction of the external force F, the random switches between locked and running states cause a spatial dispersion of the particle around its average position. The corresponding normal diffusion constant

$$D(F) = \lim_{t\to\infty}[\langle x(t)^2\rangle - \langle x(t)\rangle^2]/2t \tag{10}$$

was computed numerically as a function of F at constant temperature by Costantini and Marchesoni (1999). A peak in the curves of D vs F is detectable in the vicinity of the transition threshold $F_{\rm th}$, irrespective of the value of γ. In particular, at low damping, where $F_{\rm th} \simeq F_2$, and low temperature, $kT \ll \omega_0^2$, the peak of D at $F=F_2$ is very pronounced; as the damping is increased, the diffusion peak eventually shrinks down to a bump corresponding to the threshold $F_{\rm th} \simeq F_3$. In any case, in an appropriate neighborhood of $F_{\rm th}$, the diffusion constant can grow larger than Einstein's diffusion constant for the free Brownian motion in one dimension, $D_0 = kT/\gamma$. On increasing T the diffusion peak eventually disappears, no matter what the value of γ.

A refined analytical formula for the diffusion peak was obtained by Reimann and collaborators, who regarded the locked-to-running transition in the overdamped regime as a renewal process, that is (Reimann *et al.*, 2001, 2002),

$$D(F) = \frac{L^2}{2}\frac{\langle t^2(L,F)\rangle - \langle t(L,F)\rangle^2}{\langle t(L,F)\rangle^3}, \tag{11}$$

where the nth moments of the first-passage time $\langle t^n(L,F)\rangle$ can be computed explicitly. For $F\to 0$, Eq. (11) reproduces the zero-bias identity $D/D_0 = \gamma\mu$ (Festa and d'Agliano, 1978).

4. Single-file diffusion

When a gas of particles is confined to a linear path, an individual particle cannot diffuse past its neighbors. This constrained one-dimensional (1D) geometry is often called a "single-file" or Jepsen gas (Jepsen, 1965; Harris, 1974). Consider a file of N indistinguishable, unit-mass Brownian particles moving on the tilted sinusoidal substrate of length L_S. If the particle interaction is hard core (zero radius), the file constituents can be labeled according to a given ordered sequence, and the long-time diffusion of an individual particle is strongly suppressed. In early studies (Jepsen, 1965; Lebowitz and Percus, 1967; Levitt, 1973; Harris, 1974; Marchesoni and Taloni, 2006), the mean square displacement of a single particle in the thermodynamic limit ($L_S, N \to \infty$ with constant density $\rho = N/L_S$) was calculated analytically. Those results were generalized to the diffusion of a single file of driven Brownian particles on a periodic substrate by Taloni and Marchesoni (2006), who derived the subdiffusive law

$$\lim_{t\to\infty}[\langle x(t)^2\rangle - \langle x(t)\rangle^2] = \frac{2}{\rho}\sqrt{\frac{D(F)t}{\pi}}, \tag{12}$$

with $D(F)$ given in Eq. (11). This result applies to any choice of the substrate potential $V(x)$ (Burada *et al.*, 2009) and to the transport of composite objects (Heinsalu *et al.*, 2008), as well. Excess diffusion peaks have been obtained experimentally in the context of particle transport in quasi-1D systems (Sec. III).

B. Rectification of asymmetric processes

Stochastic transport across a device can be induced by applying a macroscopic gradient, like a force or a temperature difference. However, under many practical circumstances this is not a viable option: (i) currents induced by macroscopic gradients are rarely selective; (ii) a target particle that carries no charge or dipole can hardly be manipulated by means of an external field of force; (iii) external controls, including powering, critically overburden the design of a small device. Ideally, the optimal solution would be a self-propelled device that operates by rectifying environmental signals. In the quest for rectification mechanisms of easy implementation, we start from the symmetric dynamics of Eq. (1) and add the minimal ingredients needed to induce and control particle transport.

If $V(x)$ is symmetric under reflection, the only way to induce a drift of the Brownian particle consists in driving it by means of a nonsymmetric force $F(t)$, either deterministic or random (Luczka *et al.*, 1995; Hänggi *et al.*, 1996; Chialvo *et al.*, 1997; Astumian and Hänggi, 2002; Reimann and Hänggi, 2002). Here symmetric means that all force moments are invariant under sign reversal, $F \to -F$. Note that the condition of a vanishing dc component, $\lim_{t\to\infty}(1/t)\int_0^t F(s)ds = 0$, would not be sufficient. For instance, a biharmonic signal with commensurate frequencies and arbitrary phase constants, although zero-mean valued, is in general nonsymmetric.

On the contrary, particles in an asymmetric potential can drift on average in one direction even when all perturbing forces or gradients are symmetric. However, as pointed out in Sec. II.D, to achieve directed transport in such a class of devices the external perturbation is required to be time correlated, as in the presence of a non-Markovian noise source (correlation ratchets) or a time-periodic drive (rocked and pulsated ratchets).

The interplay of time and space asymmetry in the operation of a Brownian motor has been established mathematically by Reimann (2001) and Yevtushenko *et al.* (2001). We slightly generalize the overdamped dynamics in Eq. (3) to incorporate the case of time-dependent substrates, that is,

$$\dot{x} = -V'[x,F_2(t)] + F_1(t) + \xi(t). \tag{13}$$

The potential $V[x,F_2(t)]$ is termed supersymmetric (Marchesoni *et al.*, 1988; Jung and Hänggi, 1991) if, for an appropriate choice of the x and t origins,

$$-V[x,F_2(t)] = V[x + L/2,F_2(-t)]. \tag{14}$$

Analogously, the additive drive $F_1(t)$ is supersymmetric if for an appropriate t origin

$$-F_1(t) = F_1(-t). \tag{15}$$

Should $F_i(t)$, with $i=1,2$, be stationary noises, clearly no restriction can be set on the t origin; the equalities in Eqs. (14) and (15) must then hold in a statistical sense, meaning that the two terms of each equality must be statistically indistinguishable.

Consider now the time-reversed process $z(t) = x(-t) + L/2$. By definition, $\langle \dot{z} \rangle = -\langle \dot{x} \rangle$, whereas, on simultaneously imposing the supersymmetry conditions (14) and (15), the Langevin equation (13) yields $\langle \dot{z} \rangle = \langle \dot{x} \rangle$; hence $\langle \dot{x} \rangle = 0$. As a consequence, a nonzero rectification current requires that either the substrate or the additive drive (or both) is *nonsupersymmetric*.

We remark that the above theorem has been proven only for zero-mass particles, that is, when the Smoluchowski regime $m\ddot{x}=0$ applies. In the presence of inertia, instead, rectification may occur, under special conditions, also in fully supersymmetric devices, as shown recently by Machura *et al.* (2007) for a rocked cosine potential.

C. Nonlinear mechanisms

In this section we review transport on symmetric substrates driven by asymmetric forces. The rectification mechanisms outlined below can be traced back to the nonlinear nature of the substrate; for this reason, unlike Brownian motors, they work also, if not more effectively, in the absence of noise.

We remind the reader that these mechanisms have been introduced and demonstrated experimentally in the most diverse fields of physics and engineering. Direct applications to various categories of artificial nanodevices will be discussed in the subsequent sections.

1. Harmonic mixing

A charged particle spatially confined by a nonlinear force is capable of mixing two alternating input electric fields of angular frequencies Ω_1 and Ω_2, its response containing all possible higher harmonics of Ω_1 and Ω_2. For commensurate input frequencies, i.e., $\Omega_1/\Omega_2 = n/m$ with n and m coprime integer numbers, the output contains a dc component too (Schneider and Seeger, 1966); harmonic mixing thus induces a rectification effect of the $(n+m)$th order in the dynamical parameters of the system (Marchesoni, 1986; Goychuk and Hänggi, 1998).

Consider the overdamped stochastic dynamics of Eq. (3) in the potential of Eq. (5), driven by the biharmonic force

$$F(t) = A_1 \cos(\Omega_1 t + \phi_1) + A_2 \cos(\Omega_2 t + \phi_2). \tag{16}$$

Let the two harmonic components of $F(t)$ be commensurate with one another, meaning that Ω_1 and Ω_2 are integer-valued multiples of a fundamental frequency Ω_0, i.e., $\Omega_1 = n\Omega_0$ and $\Omega_2 = m\Omega_0$. For small amplitudes and low frequencies of the drive in Eq. (16), a simple expansion of the mobility function Eq. (7) in powers of $F(t)$ yields, after time averaging, the following approximate expression for the nonvanishing dc component of the particle velocity:

$$\langle \dot{x} \rangle = 2\bar{\mu}\frac{m+n}{m!n!}\left(\frac{A_1}{2}\right)^m \left(\frac{A_2}{2}\right)^n \cos(\Delta_{m,n}), \tag{17}$$

where $\bar{\mu}$ is the positive $(n+m-1)$th derivative of $\mu(F)$ at $F=0$, $\Delta_{m,n} = n\phi_2 - m\phi_1$, and $m+n$ is an odd number. Harmonic mixing currents $j = \langle \dot{x} \rangle / L$ clearly result from a spontaneous symmetry-breaking mechanism: indeed, averaging j over ϕ_1 or ϕ_2 would eliminate the effect completely. This is true under any regime of temperature and forcing, as proven by means of standard perturbation techniques (Wonneberger and Breymayer, 1981; Marchesoni, 1986). In particular, rectification of two small commensurate driving signals, $A_1, A_2 \ll \omega_0^2$, is a noise-assisted process and therefore is strongly suppressed for $kT \ll \omega_0^2$, when $\bar{\mu}$ decays exponentially to zero (Risken, 1984). Moreover, we anticipate that accounting for finite inertia effects requires introducing in Eq. (17) an additional damping and frequency-dependent phase lag, as discussed in Sec. IV.A.

In all calculations of $\langle \dot{x} \rangle$, including Eq. (17), the reflection symmetry of $V(x)$ plays no significant role; rectification via harmonic mixing is caused solely by the nonlinearity of the substrate. However, it must be noted that a symmetric nonlinear device cannot mix rectangular wave forms, like

$$F(t) = A_1 \operatorname{sgn}[\cos(\Omega_1 t + \phi_1)] + A_2 \operatorname{sgn}[\cos(\Omega_2 t + \phi_2)], \tag{18}$$

with $A_1, A_2 \geqslant 0$ and sgn[$\cdots$] denoting the sign of [$\cdots$] (Savel'ev, Marchesoni, Hänggi, *et al.*, 2004a, 2004b). As shown in Sec. II.D.4, *asymmetric* devices do not exhibit this peculiarity. Moreover, we underscore that for incommensurate frequencies, where Ω_1/Ω_2 is not a rational number, harmonic mixing takes place only in the presence of spatial asymmetry, as reported in Sec. II.D.4.

For practical applications, any commensuration condition, like $\Omega_1/\Omega_2 = n/m$ for harmonic mixing (but see also Secs. II.C.2 and II.D.4), is affected by an uncertainty that is inversely proportional to the observation time, i.e., the code running time for numerical simulations or the data recording time for real experiments. As such time is necessarily finite, only a limited number of commensuration spikes can be actually detected.

We conclude by recalling that the notion of harmonic mixing has been introduced long ago, e.g., to interpret the output of certain charge wave density experiments (Schneider and Seeger, 1966) and to design laser ring gyroscopes (Chow *et al.*, 1985) and annular Josephson

junctions (Ustinov *et al.*, 2004); applications in the context of nanoparticle transport are more recent (see Secs. II.C.3 and IV).

2. Gating

A periodically driven Brownian motion can also be rectified by modulating the amplitude of the substrate potential $V(x)$. We specialize the overdamped dynamics in Eq. (13) as follows:

$$\dot{x} = -V'(x)[1 + F_2(t)] + F_1(t) + \xi(t). \tag{19}$$

To avoid interference with possible harmonic mixing effects we follow the prescription of Sec. II.C.1, namely, we take $F_i(t) = A_i \,\mathrm{sgn}[\cos(\Omega_i t + \phi_i)]$, $i = 1,2$, with $A_1 > 0$ and $0 < A_2 < 1$. Mixing of the additive $F_1(t)$ and the multiplicative signal $F_2(t)$ provides a control mechanism of potential interest in device design.

In the adiabatic limit, the Brownian particle moves cyclically back and forth subjected to opposite dc forces with amplitude A_1; the substrate potential $V(x,t) = V(x)[1 + F_2(t)]$ switches, in turn, periodically between the two symmetric configurations $V_\pm(x) = V(x)(1 \pm A_2)$. The relevant mobilities $\mu_\pm(A_1)$ can be easily related to the static mobility function $\mu(A)$ for the tilted potential $V(x)$ studied in Fig. 1, namely (Savel'ev, Marchesoni, Hänggi, *et al.*, 2004a, 2004b),

$$\mu_\pm(A_1) = (1 \pm A_2)\mu[A_1/(1 \pm A_2)] \tag{20}$$

with $T \to T/(1 \pm A_2)$.

In particular, for any pair of commensurate frequencies Ω_1 and Ω_2 such that $\Omega_2/\Omega_1 = (2m-1)/(2n-1)$ (with m,n positive integers), the net particle velocity mediated over an integer number of cycles of both $F_1(t)$ and $F_2(t)$ can be cast in the form

$$\langle \dot{x} \rangle = -\frac{(-1)^{m+n} A_1}{(2m-1)(2n-1)} \Delta\mu(A_1, A_2) p(\Delta_{n,m}), \tag{21}$$

where $\Delta\mu(A_1,A_2) = [\mu_-(A_1) - \mu_+(A_1)]/2$ and $p(\Delta_{n,m}) \equiv |\pi - \Delta_{n,m}|/\pi - 0.5$ is a modulation factor with $\Delta_{n,m} = (2n-1)\phi_2 - (2m-1)\phi_1$, mod (2π). Note that for any other choice of the ratio Ω_2/Ω_1, no induced drift is predicted (see Fig. 2).

As a consequence, a relatively small modulation of the sinusoidal potential amplitude at low temperatures results in a net transport current as illustrated in Fig. 2. Consider the simplest possible case, $\Omega_1 = \Omega_2$ and $\phi_1 = \phi_2$: As the ac drive points to the right, the amplitude of $V(x,t)$ is set at its maximum value $\omega_0^2(1 + A_2)$; at low temperatures the Brownian particle can hardly overcome the substrate barriers within a half ac-drive period π/Ω_1. In the subsequent half period $F_1(t)$ switches to the left, while the potential amplitude drops to its minimum value $\omega_0^2(1 - A_2)$: The particle has a better chance to escape a potential well to the left than to the right, thus inducing a negative current with maximum intensity for Ω_1 of the order of the Kramers rate [resonant activation (Borromeo and Marchesoni, 2004)]. Of course, the amplitude and sign of the net current may be controlled via the modulation parameters A_2 and ϕ_2 too (see the inset of Fig. 2).

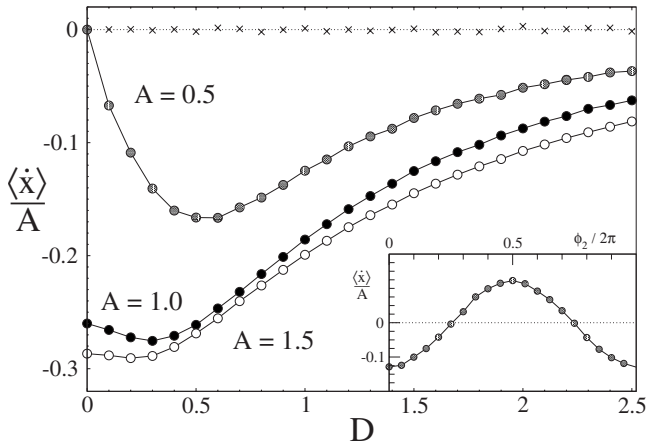

FIG. 2. Gating mechanism. Equation (19) has been simulated numerically for $\Omega_1 = \Omega_2 = 0.01$, $\phi_1 = \phi_2 = 0$, $A_1 = A_2 = A$, and $V(x) = \omega_0^2(1 - \cos x)$ with $\omega_0 = 1$; the net velocity $\langle \dot{x} \rangle$ has been plotted vs $D = kT$ for different amplitudes A. For a comparison we show also $\langle \dot{x} \rangle$ vs D for $\Omega_1 = 0.01$, $\Omega_2/\Omega_1 = \sqrt{2}$, and $A = 0.5$ (crosses). Inset: $\langle \dot{x} \rangle$ vs ϕ_2 for $\phi_1 = 0$, $A = 0.5$, and $D = 1$. Note the resonant behavior of $\langle \dot{x} \rangle$ for subthreshold drives, $A < 1$, where a low noise level may enhance rectification; increasing D for $A > 1$ degrades the rectification effect. From Borromeo and Marchesoni, 2005b.

3. Noise induced transport

Induced transport in the symmetric dynamics can be achieved also by employing two *correlated* noisy signals.

a. Noise mixing

Borromeo and Marchesoni (2004) showed that the gating process in Eq. (19) can also be driven by two stationary, zero-mean-valued Gaussian noises $F_i(t) = \eta_i(t)$ with $i = 1,2$. The two random drives may be cross correlated and autocorrelated with

$$\langle \eta_i(t)\, \eta_j(0) \rangle = \sqrt{Q_i Q_j}(\lambda_{ij}/\tau_{ij}) \exp(-|t|/\tau_{ij}), \quad i,j = 1,2. \tag{22}$$

Without loss of generality, one sets $\lambda_{11} = \lambda_{22} = 1$ and $\lambda_{12} = \lambda_{21} = \lambda$, and to avoid technical complications $\tau_{ij} \equiv \tau$. Of course $\tau \to 0$ corresponds to taking the white noise limit of $\eta_i(t)$, Eq. (4). The parameter λ characterizes the cross correlation of the two signals; in particular, $\lambda = 0$, independent signals; $\lambda = 1$, identical signals, $\eta_2(t) \equiv \eta_1(t)$; $\lambda = -1$, signals with reversed sign, $\eta_2(t) \equiv -\eta_1(t)$. Two such signals may have been generated by a unique noise source and then partially decorrelated through different transmission or coupling mechanisms.

In the white noise limit, $\tau \to 0$, the Fokker-Planck equation associated with the process of Eqs. (19) and (22) contains a stationary solution in closed form. Nonvanishing values of $\langle \dot{x} \rangle$ for $\lambda \neq 0$ are the signature of a stochastic symmetry breaking due to nonlinear noise

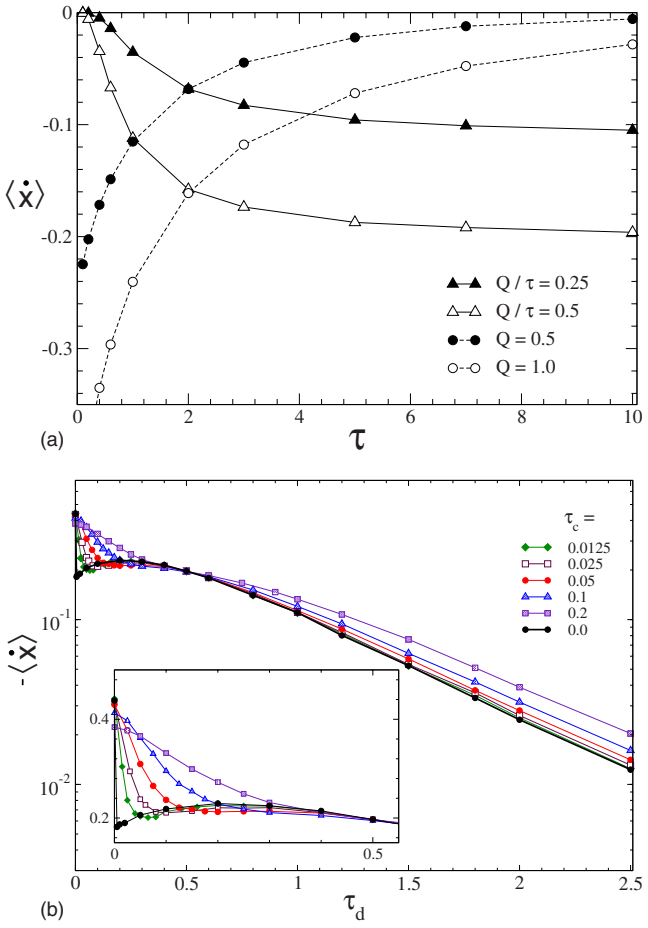

FIG. 3. (Color online) Numerical simulation of Eq. (19), with $F_i(t)=\eta_i(t)$, $i=1,2$, and $V(x)=-\sin x$. The noises $\eta_i(t)$, Eq. (22), have the same strength, $Q_1=Q_2=Q$. (a) Nonlinear noise mixing: Characteristic curve $\langle\dot{x}\rangle$-τ for different intensities Q of the noises and $\lambda=1$, $D=0.1$. (b) Noise recycling: Characteristic curve $\langle\dot{x}\rangle$-τ_d, where τ_d is the relative time delay of η_i (see text). Data are for different τ and $Q=1$, $D=0$; see Borromeo *et al.*, 2006. From Borromeo and Marchesoni, 2005b.

mixing; the sign of λ, similarly to the relative phase $\Delta_{m,n}$ in the gating setup of Sec. II.C.2, determines the direction of the particle drift. The interpretation of this result is straightforward. Consider, for instance, the case of the symmetric potential in Eq. (5), rocked and pulsated by the same signal, i.e., $\eta_1(t)=\eta_2(t)$: For $\lambda=1$, when pushed to the left ($\eta_i<0$), the Brownian particle encounters lower substrate barriers than when pushed to the right ($\eta_i>0$), hence the negative average drift current detected by means of numerical simulation (Borromeo and Marchesoni, 2005b; Borromeo *et al.*, 2006).

The magnitude of the induced current is controlled by the correlation time τ (Borromeo and Marchesoni, 2005b). While one can easily estimate $\langle\dot{x}\rangle$ for $\lambda\neq 0$ and $\tau=0$ [white noise (Risken, 1984)] or $\tau\to\infty$ [strongly correlated noise (Hänggi *et al.*, 1989)], the intermediate τ values are accessible solely through numerical simulation. In Fig. 3(a) we show $\langle\dot{x}\rangle$ vs τ for different noise intensities: the two sets of curves at Q and Q/τ fixed illustrate the noise mixing effect for $\tau\to 0$ and $\tau\to\infty$, respectively.

b. Noise recycling

If the noises $\eta_i(t)$ are generated by the same source and then coupled to the diffusing particle through different paths, it may well happen that they are simply delayed in time. Under stationary conditions, we can assume that $\eta_2(t)=\eta_1(t-\tau_d)$, with $\eta_i(t)$ given by Eq. (22) and, for simplicity, $\lambda=0$. In the notation of Borromeo *et al.* (2006) and Borromeo and Marchesoni (2007b), $\eta_1(t)$ represents the primary noise source and $\eta_2(t)$ a recycled noise to be used as a control signal.

By the same argument as for noise mixing, we expect that the Brownian dynamics becomes rectified to the left with negative velocity $\langle\dot{x}(\tau_d)\rangle$. Note that $\langle\dot{x}(-\tau_d)\rangle=\langle\dot{x}(\tau_d)\rangle$ and $\langle\dot{x}(\tau_d)\rangle\to-\langle\dot{x}(\tau_d)\rangle$, upon changing the relative signs of η_i. The dependence of the characteristic curve $\langle\dot{x}(\tau_d)\rangle$ on the time constants τ_d and τ displayed in Fig. 3(b) is important in view of practical applications. Indeed, in many circumstances, it would be extremely difficult to recycle a control signal $\eta_2(t)$ so that $\tau_d\ll\tau$, stated otherwise, measurement of $\langle\dot{x}(0)\rangle$ requires a certain degree of experimental sophistication. On the contrary, if we agree to work on the resonant tail of its response curve $|\langle\dot{x}(\tau_d)\rangle|$, a noise-controlled rectification device can be operated with less effort; its net output current may be not the highest for $\tau_d>\tau$ but is still appreciable, and, more importantly, stable against the accidental floating of the time constant τ_d.

In this sense both schemes discussed are a simple attempt at implementing the operation of a Maxwell's demon: The ideal device we set up is intended to gauge the primary random signal η_1 at the sampling time t and, depending on the sign of each reading, to lower or raise the gate barriers accordingly at a later time $t+\tau_d$, i.e., to open or close the trap door. The rectifying power of such a demon is far from optimal; lacking the dexterity of Maxwell's "gate keeper" (Leff and Rex, 2003; Maruyama *et al.*, 2008) it works only on average like an automaton.

D. Brownian motors

As detailed in Sec. II.B, a necessary condition for the rectification of symmetric signals, whether random or periodic in time, is the spatial asymmetry of the substrate. Rectification devices involving asymmetric substrates are termed *ratchets*. In most such devices, however, noise (no matter what its source, i.e., stochastic, chaotic, or thermal) plays a non-negligible or even dominant role. Under such conditions one speaks of Brownian motors (Bartussek and Hänggi, 1995; Hänggi and Bartussek, 1996; Reimann *et al.*, 1996; Astumian, 1997; Astumian and Hänggi, 2002; Hänggi *et al.*, 2002, 2005; Linke, 2002; Kay *et al.*, 2007). The label "Brownian motor" should not be abused to refer to all small ratchet-like devices. For instance, the rocked ratchets of Sec. II.D.1 work quite differently in the presence or absence

of noise, whereas the pulsated and correlation ratchets (sometimes also referred to as "stochastic" ratchets) of Secs. II.D.2 and II.D.3 work only in the presence of noise.

The hallmarks of genuine Brownian motors are listed in Sec. I. In this section we discuss in detail noise rectification and directed transport on asymmetric periodic substrates and potentials. We point out to the reader the following cautions: (i) Strict periodicity is not a requirement for the operation of a Brownian motor. The ratchet system may contain small amounts of disorder (Harms and Lipowsky, 1997; Popescu *et al.*, 2000; Kafri and Nelson, 2005; Martinez and Chacon, 2008) or even be nonperiodic (Marchesoni, 1997). (ii) Spatial asymmetry can also result as a collective effect, for instance, in extended systems consisting of interacting, symmetric dynamical components, introduced in Sec. V.

The archetypal model of ratchet substrates in one-dimension is the double-sine potential proposed by Bartussek *et al.* (1994),

$$V(x) = -V_0[\sin(2\pi x/L) + \tfrac{1}{4}\sin(4\pi x/L)], \tag{23}$$

or, in the rescaled units of Eq. (6), $V(x)=-\omega_0^2[\sin x + 1/4\sin(2x)]$. In Fig. 4, the barriers are skewed to the right with ratchet length $l_+ > l_-$. A Brownian particle with Langevin equation (1) moving on such a substrate is characterized by an asymmetric mobility function $\mu(F) \neq \mu(-F)$; as the particle mobility depends now not only on the amplitude, but also on the orientation of the drive F, symmetric substrate perturbations are expected to induce a net current in either direction.

Broadly speaking, ratchet devices fall into three categories depending on how the applied perturbation couples to the substrate asymmetry.

1. Rocked ratchets

Consider first, for simplicity, the Langevin equation (3) with the sinusoidal drive of Eq. (8). When applied to the reflection-symmetric sine potential of Eq. (5), $F(t)$ breaks instantaneously the symmetry of the potential by tilting it to the right for $F(t)>0$, and to the left for $F(t)<0$. However, due to the spatiotemporal symmetry of the process, $V(x)=V(-x)$ and $F(t)=F(-t)$, over one drive cycle $T_1=2\pi/\Omega_1$ the drifts to the right and left compensate one another: the net current is null. When placed in the double-sine potential of Eq. (23), instead, an overdamped particle is more easily moved to the right than to the left. Indeed, depinning occurs at $F=F_{3R}$ and $F=-F_{3L}$ for $F(t)$ oriented, respectively, to the right and left; moreover, from the asymmetry condition $l_+ > l_-$ the inequality $F_{3R} < F_{3L}$ follows immediately. The depinning thresholds for the potential in Eq. (23) in the rescaled units of Eq. (6) are $F_{3R}=3/4$ and $F_{3L}=3/2$.

If the forcing frequency Ω_1 is taken much smaller than all intrawell relaxation constants, $\omega_0^2 T_1 \gg 1$ and $T_1 \gg \langle t(L,0)\rangle$, then the net transport current can be computed in the adiabatic approximation by averaging the instantaneous velocity $\dot{x}(t)=\mu[F(t)]F(t)$ [see Eq. (7)], over one forcing cycle, that is (Bartussek *et al.*, 1994; Borromeo *et al.*, 2002),

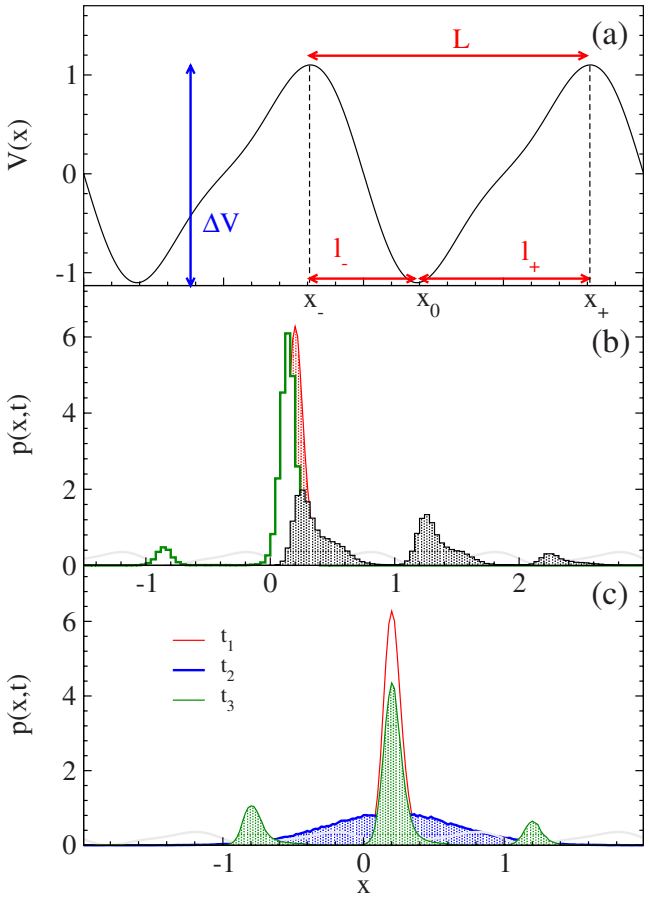

FIG. 4. (Color online) Ratchet mechanism. (a) Sketch of the potential in Eq. (23) with $L=1$ and $V_0=L/2\pi$. The three consecutive extremal points $x_-=-0.19$, $x_0=0.19$, and $x_+=0.81$ define a potential well; the barrier height is $\Delta V=V(x_\pm)-V(x_0) \simeq 0.35$ and its asymmetry is quantified by the difference l_+-l_- with $l_\pm=|x_\pm-x_0|$. The curvature of the potential at the bottom of the well is $\bar{\omega}_0^2=(3\sqrt{3}/2)\omega_0^2\simeq 10.1$. (b) Rocket ratchet. Probability density $p(x,t)$ for a Brownian particle initially centered around $x=0$ and then driven for $t=10$ by a dc force $A_0=-0.5$ and 0.5. The backward displacement is strongly suppressed, hence the positive natural orientation of this ratchet. (c) Pulsated ratchet. The ratchet potential is switched "on" and "off" periodically with $t^{\rm on}=1$, $t^{\rm off}=3$, and $T_2=t^{\rm on}+t^{\rm off}$ (see text). The particle, initially set at $x=x_0$, relaxes first in the starting well during $t^{\rm on}$ (curve 1, $t_1=t^{\rm on}$), then diffuses symmetrically driven only by noise for $t^{\rm off}$ (curve 2, $t_2=T_2$), and finally gets retrapped in the neighboring wells as the next cycle begins (curve 3, $t_3=T_2+t^{\rm on}$). As the left peak of $p(x,t_3)$ is more pronounced than the right peak, the natural orientation of this ratchet is negative. In the simulations of (b) and (c) the ratchet potential $V(x)$ is the same as in (a) (also drawn to guide the eye) and the intensity of the noise in Eq. (4) is $D=0.1\Delta V$. Courtesy of Marcello Borromeo.

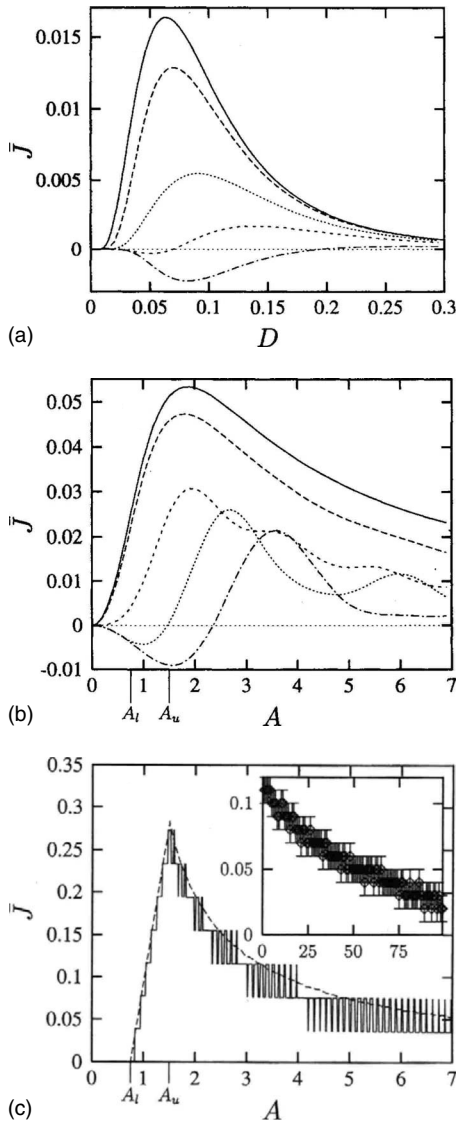

FIG. 5. Rocked ratchet. (a) Rectification current j vs the noise intensity D [see Eq. (4)] and (b), (c) vs ac modulation strength $A \equiv A_1$, for the ratchet potential in Eq. (23) with $L=1$. The relevant simulation parameters are (a) $A_1=0.5$ and $\Omega_1=0.01$, 1, 2.5, 4, and 7 (top to bottom); (b) $D=0.1$ and $\Omega_1=0.01$, 1, 4, 7, and 10 (top to bottom). In (a) and (b) the solid line for $\Omega_1=0.01$ coincides with the adiabatic limit in Eq. (24). (c) Deterministic regime with $D=0$, and $\Omega_1=0.01$ (dashed line) and $\Omega_1=0.25$ (solid line). The inset depicts the width of the nth plateau step vs n for $A>7.8$ (with error bars). This locking mechansim for the plateau width is governed by a devil's staircase. From Bartussek *et al.*, 1994.

$$j \equiv \frac{\langle \dot{x} \rangle}{L} = \frac{1}{T_1} \int_0^{T_1} \frac{\mathrm{sgn}[F(s)]}{\langle t[L, F(s)] \rangle} ds. \tag{24}$$

The adiabatic current in Eq. (24) is positive definite, as the natural ratchet direction is defined by the choice $F_{3R} < F_{3L}$. However, its range of validity is restricted to extremely low temperatures T and drive frequencies Ω_1. On raising Ω_1, the rectification current develops a more complicated dependence on the noise intensity D and the drive amplitude A_1, as proven by the numerical simulations reported in Figs. 5(a)–5(c). This is because, for forcing periods T_1 shorter than the mean first-passage time $\langle t(L,0) \rangle$, the driven particle oscillations span fewer substrate cells. A few properties of the rocked ratchet current in Fig. 5 are remarkable.

(i) At finite temperature, the maximum rectification effect occurs right in the adiabatic regime, $\Omega_1 \to 0$, and with natural orientation, panels; Figs. 5(a) and 5(b).

(ii) For $\Omega_1 > \omega_0$, the drive and interwell oscillations may combine to reverse the current orientation. Such current inversions are restricted to selected D and A_1 ranges, but never in the absence of noise; Figs. 5(a) and 5(b).

(iii) In the noiseless regime, $T \equiv 0$, the incommensuration between forced oscillation amplitude and substrate periodicity causes the quantized locking structure of Fig. 5(c). This structure disappears either in the limit $\Omega_1 \to 0$ [because the step height, i.e., $L\Omega_1/(2\pi)$, is proportional to Ω_1] or in the presence of noise, when due to randomness the finer steps for $A_1 > F_{3L}$ merge into the broad oscillations of Fig. 5(b).

(iv) As the temperature vanishes, the adiabatic current in Eq. (24) is suppressed for $A_1 < F_{3R}$ and enhanced elsewhere [see Fig. 8(a)]. For $F_{3R} < A_1 < F_{3L}$ the particle can only move to the right, so that j grows almost linearly with A_1, while for $A_1 > F_{3L}$ the particle can drift in both directions, thus causing j to decrease.

Rectifiers, like rocked ratchets, can work against an external dc drive. On adding a dc component A_0 to the sinusoidal force, namely, on applying the drive (9) instead of Eq. (8), we can determine the value of A_0, termed the stopping force, such that for a certain choice of the other perturbation parameters A_1, Ω_1, and D the net current vanishes.

Rocked ratchets with massive particles exhibit strong inertial effects also capable of reversing their current. A noiseless inertial rocked ratchet is naturally subject to developing chaotic dynamics; indeed, its current turns out to be extremely sensitive to the initial conditions (Jung *et al.*, 1996; Mateos, 2000, 2003; Borromeo *et al.*, 2002; Machura, Kostur, *et al.*, 2007). However, an appropriate noise level suffices to stabilize the rectification properties of an inertial ratchet and makes it a useful device with potential applications in science and technology (Machura, Kostur, Talkner, *et al.*, 2004; Marchesoni *et al.*, 2006a).

In the notation of Sec. II.A.1, slightly generalized to account for the asymmetry of the potential in Eq. (23), we define two additional pairs of thresholds, besides the depinning thresholds $F_{3R,L}$: the repinning thresholds $F_{1R,L}$ and the underdamped transition thresholds $F_{2R,L}$, with $F_{iR} < F_{iL}$ for $i=1,2,3$ (the subscript R,L denoting the orientation of the drive). Under the adiabatic condition $\Omega_1 \ll \gamma, \omega_0$, the following approximations have been obtained by Borromeo *et al.* (2002) and Marchesoni *et al.* (2006a):

(i) In the zero-temperature limit, $T \to 0$,

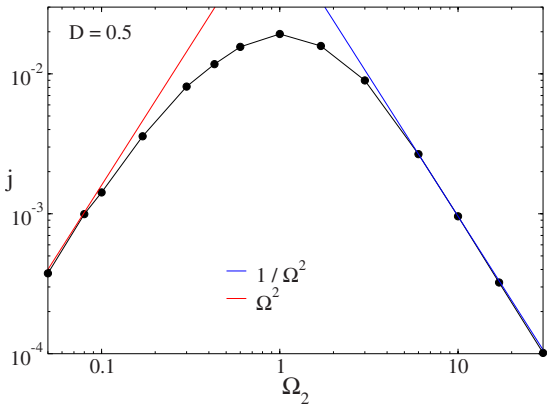

FIG. 6. (Color online) Pulsated ratchet. Rectification current $j=-\langle\dot{x}\rangle$ vs Ω_2 (dimensionless units), for the ratchet potential of Eq. (23) with $L=2\pi$ and $V_0=1$. Other simulation parameters are $A_2=0.8$ and $D=0.5$ The low-frequency Ω_2^2 and high-frequency Ω_2^{-2} asymptotic limits are denoted by straight lines. Courtesy of Marcello Borromeo.

$$j(A_1)=\begin{cases} j_R(A_1), & F_{2R}<A_1<F_{2L}, \\ j_R(A_1)-j_L(A_1), & A_1>F_{2L}, \end{cases} \tag{25}$$

and $j(A_1)=0$ for $A_1<F_{2R}$. The right and left current components are $j_{R,L}(A_1)=2\sqrt{A_1^2-F_{2R,L}^2}/\pi\gamma L$.

(ii) In the noiseless regime, $T\equiv 0$,

$$j(A_1)=\begin{cases} j_R(A_1), & F_{3R}<A_1<F_{3L}, \\ j_R(A_1)-j_L(A_1), & A_1>F_{3L}, \end{cases} \tag{26}$$

and $j(A_1)=0$ for $A_1<F_{3R}$. Here $j_{R,L}(A_1)=[\sqrt{A_1^2-F_{1R,L}^2}+\sqrt{A_1^2-F_{3R,L}^2}]/\pi\gamma L$. Note that $j(A_1)$ in Eq. (26) is discontinuous at the depinning thresholds $F_{3R,L}$ as expected for the response curve of any underdamped rocked ratchet operated in the deterministic regime (see Sec. II.A.1).

2. Pulsated ratchets

Consider now the overdamped process of Eq. (19) with $F_1(t)=0$ and $F_2(t)=A_2\,\mathrm{sgn}[\cos(\Omega_2 t+\phi_2)]$. As discussed in Sec. II.C.2, modulation of the amplitude of a symmetric potential $V(x)$ in the presence of an uncorrelated, time-symmetric perturbation $\xi(t)$ does not suffice to induce rectification. This state of affairs changes when $F_2(t)$ couples instead to an asymmetric substrate, like our reference ratchet potential (23). For the sake of simplicity, we set $A_2=1$, so that the effective substrate potential $[1+F_2(t)]V(x)$ appears to switch on and off at every half period $T_2/2=\pi/\Omega_2$. The interplay between time modulation and spatial asymmetry generates a nonzero drift current, which, at low (but not too low) frequencies, is oriented in the positive direction. Devices operated under similar conditions are termed pulsated ratchets.

Rectification by a pulsated ratchet can be explained qualitatively by looking at Fig. 4. The probability density of a particle initially placed at the bottom of a potential well (top) is mostly confined to that well, as long as $T_2/2$ is not exceedingly longer than the escape time $\langle t(L,0)\rangle$, which is the case at low temperatures. When, during the following half cycle, the substrate is switched off (middle), the particle, still subject to noise, diffuses freely with Einstein's constant D and, for $T_2\gg L^2/D$, its probability density approaches a Gaussian spanning many unit cells. By switching on again, the substrate cuts such a probability density into smaller peaks of different sizes, one for each well surrounding the initial one. For potential barriers skewed as in the figure, $l_+>l_-$, wells on the right are expected to be less (because of the larger diffusion length l_+) populated than wells on the left, hence there is a negative net current. As a consequence, the potential in Eq. (23) has positive natural orientation when rocked, and negative orientation when pulsated. The mechanism illustrated in Fig. 6 can work even in the presence of a dc force $F_1(t)=A_0$ pointing in the opposite direction, $A_0>0$. Such an upward-directed motion is clearly powered by the thermal fluctuations $\xi(t)$.

The directed particle current is bound to vanish in the adiabatic limit, $\Omega_2\to 0$, when thermal equilibrium is approached. A similar conclusion holds true for fast substrate modulations, $\Omega_2\gg\omega_0^2$ (in rescaled units). In perturbation analysis (Savel'ev, Marchesoni, and Nori, 2004b), one finds the noteworthy result that the current decays to zero in both asymptotic regimes remarkably fast, namely, as Ω_2^2 in the slow-modulation limit and Ω_2^{-2} in the fast-modulation limit. Moreover, for intermediate modulation frequencies, the current in a pulsated ratchet is generally not oriented in its natural direction; current inversions are possible when the forcing frequency matches some intrinsic relaxation rate of the process.

Finally, pulsated ratchets can be operated under very general amplitude modulations $F_2(t)$ as well. This ratchet effect proved robust with respect to the following: (i) Modifications of the potential shape (Reimann, 2002). (ii) Changes in the switching sequence. A generic discrete modulation signal $F_2(t)$ is characterized by different residence times, namely, t_{on} in the on state, $+A_2$, and t_{off} in the off state, $-A_2$. For periodic modulations, $t_{\mathrm{on}}+t_{\mathrm{off}}=T_2$ defines the so-called duty cycle of the device (Bug and Berne, 1987; Ajdari and Prost, 1992). For random modulations, instead, t_{on} and t_{off} must be interpreted as the average residence times in the corresponding on or off state (Astumian and Bier, 1994; Faucheux *et al.*, 1995). In both cases the modulation is asymmetric for $t_{\mathrm{on}}\neq t_{\mathrm{off}}$. (iii) Replacement of pulsated with flashing substrates. The substrate is made to switch, either periodically or randomly in time, among two or more discrete configurations, which do not result from the amplitude modulation of a unique substrate profile (Gorman *et al.*, 1996; Chen, 1997; Borromeo and Marchesoni, 1998; Lee *et al.*, 2004). The rectification process is controlled by the spatial asymmetry of the single-substrate configurations, by the temporal asymmetry of the switching sequence, or by a combination of both. (iv) Modulation of the temperature (Bao, 1999; Reimann *et al.*, 1996). Modulation of the intensity of the ambient noise $\xi(t)$ or its coupling to the device corresponds to

introduction of the time-dependent temperature $T(t)=[1+F_2(t)]T$ for an appropriate control signal $F_2(t)$ with amplitude smaller than 1. Pulsation of the potential amplitude V_0 or the temperature T yields similar rectification effects, since the net current of a pulsated ratchet is controlled by the barrier-to-noise ratio. (v) The addition of constant or spatially modulated damping terms [Luchsinger (2000); Suzuki and Munakata (2003); see also Reimann (2002)]. Inertial effects make the rectification mechanism sensitive to the particle mass, so that selective transport and segregation of mixed species becomes possible (Derènyi and Vicsek, 1995; Derènyi and Ajdari, 1996).

3. Correlation ratchets

To better understand the role of asymmetry in the rectification of a nonequilibrium process, we consider now an overdamped Brownian particle with Langevin equation (3) diffusing in the ratchet potential of Eq. (23) subject to a zero-mean, colored Gaussian noise $F \equiv \eta(t)$, with

$$\langle \eta(t)\,\eta(0)\rangle = (Q/\tau)\exp(-|t|/\tau). \tag{27}$$

The substrate asymmetry is capable *per se* of rectifying the correlated fluctuation $\eta(t)$, even in the absence of external modulations or thermal noise. The early prediction of this transport effect, based on simple perturbation arguments (Magnasco, 1993; Bartussek *et al.*, 1994; Doering *et al.*, 1994; Millonas and Dykman, 1994; Luczka *et al.*, 1995), kindled a widespread interest in the thermodynamics of molecular motors. A more sophisticated path-integral analysis (Bartussek *et al.*, 1996) led later to the following low-noise estimates of the correlation ratchet current:

(i) In the weak-color limit, $\omega_0^2\tau \ll 1$,

$$j(\tau) = j_+(\tau) - j_-(\tau), \tag{28}$$

where $j_\pm(\tau)=r_K \exp[-\tau^2 Q c_\pm/(D+Q)^2]$ and r_K is the equilibrium Kramers rate for the particle to exit a potential well through one side, $r_K = \bar{\omega}_0\omega_\pm \exp[-\Delta V/(D+Q)]/(2\pi)$. Here x_0 and $x_\pm$ are the extremal points of $V(x)$ defined in Fig. 4(a); $\bar{\omega}_0^2=V''(x_0)$, $\omega_\pm^2=|V''(x_\pm)|$, and $c_\pm=\int_{x_0}^{x_\pm}[V''(x)]V'(x)dx$.

(ii) In the strong-color limit, $\tau\to\infty$,

$$j(\tau) = j_0\{1-\exp[-QL(l_+-l_-)/2D^2\tau]\}, \tag{29}$$

where j_0 is a positive definite constant. Equation (28) can be regarded as the difference of two exit currents $j_\pm(\tau)$, respectively, through x_+ (forward) and x_- (backward), in the presence of colored noise (Millonas and Dykman, 1994).

The orientation of the current of a correlation ratchet is extremely sensitive to the substrate geometry. In the strong-color limit, the condition $l_+-l_->0$ between the two ratchet lengths guarantees that the current is positive, no matter what the choice of $V(x)$; correlation ratchets work in the natural direction of the corresponding rocked ratchet.

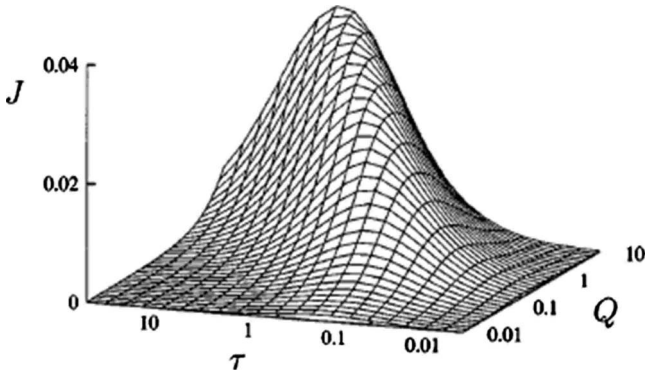

FIG. 7. Correlation ratchet. Rectification current j vs τ and Q for $D=0.1$. The parameters of the ratchet potential, Eq. (23), are as in Fig. 4. More data can be found in Bartussek *et al.*, 1996.

In the weak-color limit, the current in Eq. (28) has the same sign as the difference $c_- - c_+ = \int_0^L [V''(x)]V'(x)dx$, which in turn depends on the detailed profile of $V(x)$, regardless of $\mathrm{sgn}[l_+ - l_-]$. Numerical simulation of correlation ratchets with the potential given by Eq. (23) confirmed that, consistently with the inequality $c_- - c_+ > 0$, $j(\tau)$ is positive definite, as illustrated in Fig. 7; as $j(\tau\to 0)=j(\tau\to\infty)=0$, optimal rectification is achieved for an intermediate noise correlation time, $\omega_0^2\tau \sim 1$. Modification of the potential profile, e.g., by adding an appropriate higher-order Fourier component without changing $l_+ - l_-$, suffices to reverse the sign of $c_- - c_+$ and thus introduce at least one current inversion (Bartussek *et al.*, 1996).

Correlation ratchets have the potential for technological applications to "noise harvesting," rather than to nanoparticle transport. The low current output and its extreme sensitivity to the substrate geometry and the particle mass (Marchesoni, 1998; Lindner *et al.*, 1999) makes the design and operation of correlation ratchets as mass rectifiers questionable. However, the asymmetry-induced rectification of nonequilibrium fluctuations, no matter how efficient and hard to control, can be exploited by a small device to extract from its environment and store the power it needs to operate.

4. Further asymmetry effects

The rectification mechanisms introduced in Sec. II.C apply to any periodic substrate, independently of its spatial symmetry. In the presence of spatial asymmetry, the relevant drift currents get modified as follows.

a. Current offsets

At variance with Secs. II.C.1 and II.C.2, two ac drives applied to an asymmetric device are expected to induce a net current $j_{\mathrm{av}}=\langle \dot{x}\rangle_{\mathrm{av}}$ also for incommensurate frequencies Ω_1 and Ω_2. This is a ratchet effect that in most experiments is handled as a simple current offset. This conclusion is apparent, for instance, in the case of low-frequency rectangular input waves, where the device

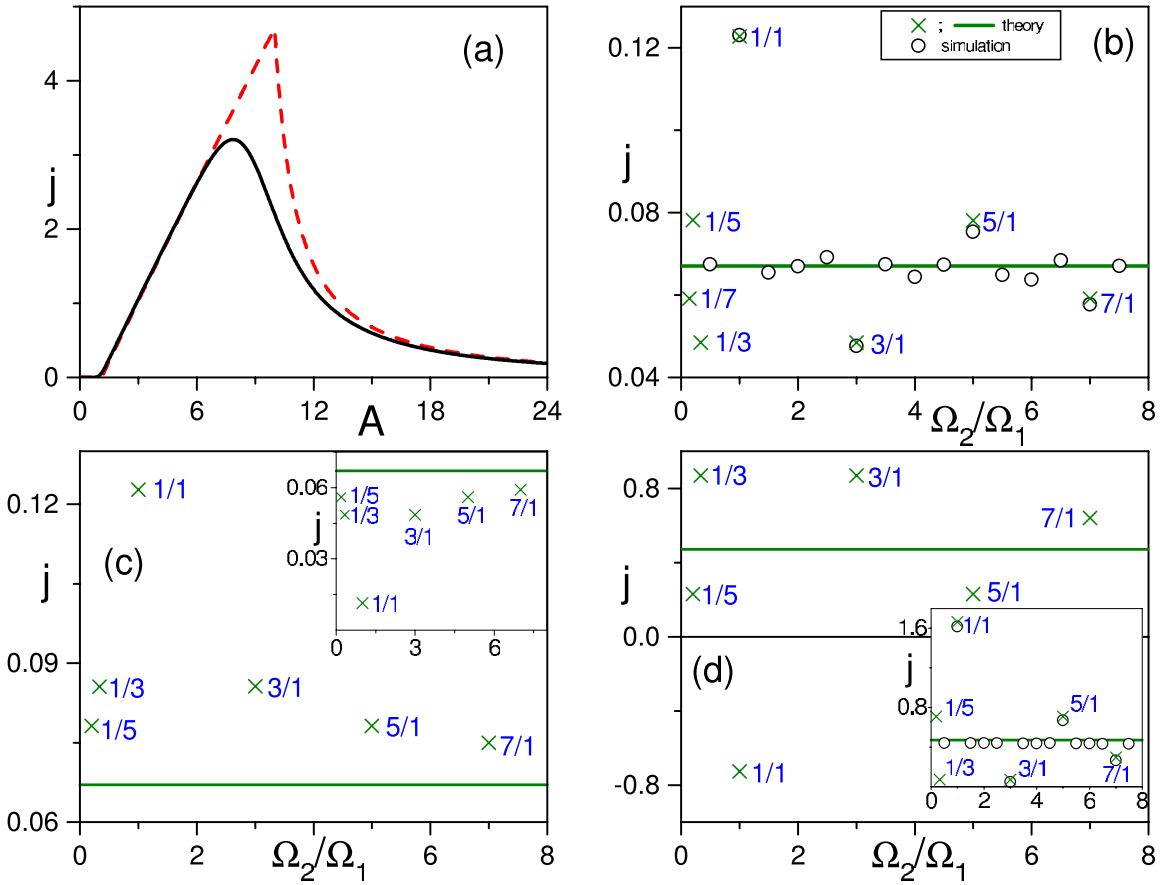

FIG. 8. (Color online) Net current in a piecewise linear potential with amplitude ΔV, driven by two rectangular wave forms, Eq. (18): (a) one-frequency rocked ratchet; (b),(c) harmonic mixing of Sec. II.C.1; (d) gating mechanism, Eq. (19). The ratchet potential is $V(x)=x\Delta V/L_2$ for $-L_2<x<0$ and $V(x)=x\Delta V/L_1$ for $0<x<L_1$, with $L_1=0.9$ and $L=1$; $\Delta V=1$ in (a)–(c) and $\Delta V=2$ in (d). (a) Response curve $j(A)\equiv\langle\dot{x}\rangle/L$ to a low-frequency rectangular force with amplitude A at zero temperature $D=0$ (dashed curve), and low temperature $D/\Delta V=0.05$ (solid curve). (b) Numerical simulations for a doubly rocked ratchet with $\phi_1=\phi_2=\pi$ and $\Omega_1=0.01$ (open circles) vs adiabatic approximation, Eqs. (21) and (30) (line and crosses). The offset $j_{\rm av}$, Eq. (30), is indicated by the line; the spikes of Eq. (21) at some selected integer-valued odd harmonics are marked with crosses (×). (c) Adiabatic approximation for $\phi_1=\phi_2=3\pi/2$ (main panel) and $\phi_1=3\pi/2$, $\phi_2=\pi/2$ (inset). In both cases $A_1=3$, $A_2=2$, $D=0.6$. (d) Numerical simulations vs adiabatic approximation, Eqs. (21) and (31), for a rocked-pulsated ratchet with $A_1=4$, $A_2=0.5$, and $\Omega_1=0.01$; noise level $D=0.4$. Main panel: $\phi_1=\phi_2=\pi$ (adiabatic approximation); inset: simulation (open circles) vs the fully adiabatic approximation (×) for $\phi_1=\pi$ and $\phi_2=0$. From Borromeo and Marchesoni, 2005b.

output current can be expressed as a linear combination of two known ratchet currents (Savel'ev, Marchesoni, Hänggi, *et al.*, 2004a, 2004b):

(i) Harmonic mixing current (Sec. II.C.1). When the drive is a double rectangular wave, Eq. (18), $j_{\rm av}$ can be regarded as the incoherent superposition of currents from two rocked ratchets driven by rectangular waves with amplitudes A_1+A_2 and $|A_1-A_2|$, respectively, i.e.,

$$j_{\rm av}=\tfrac{1}{2}[j_0(|A_1-A_2|)+j_0(A_1+A_2)]. \tag{30}$$

(ii) Gating current (Sec. II.C.2). The rocked-pulsated device of Eq. (19) can be regarded as the incoherent superposition of two ratchets with potentials $V_\pm(x)=(1\pm A_2)V(x)$, respectively, both rocked with amplitude A_1; hence

$$j_{\rm av}=\tfrac{1}{2}[j_+(A_1)+j_-(A_1)]. \tag{31}$$

In Eqs. (30) and (31) $j_{0,\pm}(A)$ are the net currents of Eq. (24) for a rocked ratchet driven by a rectangular wave with amplitude A and vanishing frequency, the subscripts 0, ± referring to the regular, high- and low-amplitude potential configurations, $V(x)$ and $V_\pm(x)$.

b. Asymmetry induced mixing

As anticipated in Sec. II.C.1, a double rectangular wave is not capable of rectifying a Brownian particle in a symmetric potential, that is, $\langle\dot{x}\rangle=0$ also under harmonic mixing conditions, $\Omega_2/\Omega_1=m/n$ with m,n coprime integers and $m+n$ odd. This is no longer the case if $V(x)$ is asymmetric. The nonzero odd moments of the process $x(t)$, determined by the substrate asymmetry, generate additional harmonic couplings of the "odd" harmonics of the drive, i.e., for $\Omega_2/\Omega_1=(2m-1)/(2n-1)$ with $2m$

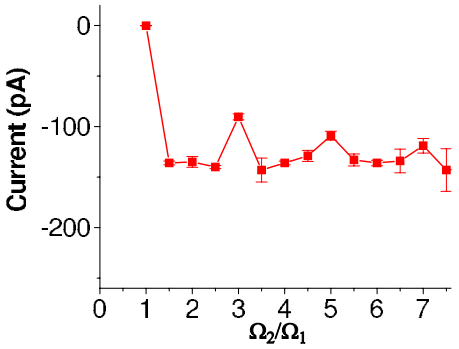

FIG. 9. (Color online) Net current through a single conical nanopore for the sum of two voltage signals applied across the pore, $0.5\,\mathrm{sgn}[\sin(\Omega_1 t)]+0.5\,\mathrm{sgn}[\sin(\Omega_2 t+\pi)]$, with different Ω_2/Ω_1. The measurements were taken in a 0.1M KCl solution at pH 8.0. For further details, see Kalman *et al.*, 2007.

-1 and $2n-1$ coprime, as shown in Fig. 8. The total rectification current, including both the incommensurate term of Eq. (30) and this new harmonic mixing spike, was calculated analytically by Savel'ev, Marchesoni, Hänggi, *et al.* (2004a, 2004b):

$$j = j_{\mathrm{av}} - \frac{(-1)^{m+n} p(\Delta_{n,m})}{(2m-1)(2n-1)} j_{\mathrm{odd}}, \tag{32}$$

where $p(\Delta_{n,m})$ is given by Eq. (21) and $j_{\mathrm{odd}}=\frac{1}{2}[j_0(|A_1-A_2|)-j_0(A_1+A_2)]$.

The competition between current offset, item (a), and asymmetry-induced spikes, item (b), may cause surprising current reversals for special values of the driving frequencies, as observed in several experimental setups (cf. Secs. III, IV, and VII.B). Moreover, replacement of the rectangular wave form, Eq. (18), with a more conventional linear superposition of two sinusoids of the same frequency, Eq. (16), leads to an even more complicated interplay of nonlinearity and asymmetry-induced harmonic mixing (Savel'ev, Marchesoni, Hänggi, *et al.*, 2004a). A special limit of the biharmonically driven rocked ratchet is discussed in Sec. II.E.2.

A demonstration of the combination of harmonic mixing and asymmetry effects in the context of particle transport at the nanoscale has been reported by Kalman *et al.* (2007), who drove dilute ions through conical nanopores by applying a biharmonic rectangular voltage. Harmonic mixing and gating currents could be separated, as predicted by the theory, and the resulting commensuration effects are displayed in Fig. 9.

E. Efficiency and control issues

The analysis of Sec. II.D suggests that the output of a real ratchet device is hard to control experimentally, let alone to predict. As a matter of fact, if we use a ratchet to rectify an assigned signal, the only tunable variables are the temperature T, the damping constant γ (or the mass m), and the substrate profile $V(x)$. Under certain experimental circumstances these quantities may prove not directly accessible for this purpose or inconvenient to change. This is why control of particle transport in small devices sometimes requires the introduction of auxiliary signals or auxiliary particle species (Sec. V.C), or even the use of a feedback control scheme to optimize the Brownian motor current (Feito and Cao, 2007; Craig, Kuwada, *et al.*, 2008; Craig, Long, *et al.*, 2008; Son *et al.*, 2008).

1. Optimization

The most common definition of efficiency for a loaded Brownian motor is

$$\eta_0 = \langle \dot{x} \rangle A_0 / \langle P \rangle_{\mathrm{in}}, \tag{33}$$

where $\langle \dot{x} \rangle A_0$ is the average mechanical work done per unit of time against a working load A_0 and $\langle P \rangle_{\mathrm{in}}$ is the average net power pumped into the system by the external drives, no matter how applied. The quantity η_0 has been interpreted in terms of macroscopic thermodynamics by Sekimoto (1998) [for further developments on issues of energetics and efficiency, see also Parrondo and de Cisneros (2002)], and references therein. In their scheme, a ratchet operates like a Carnot cycle, where the lower temperature is determined by the thermal noise, Eqs. (2) and (4), and the higher temperature is related to the magnitude of the external modulation. Since the Brownian motor operates far from thermal equilibrium, the efficiency is typically smaller than the limiting efficiency of a reversible Carnot cycle.

The ensuing question as to whether a ratchet can be operated at the maximal Carnot efficiency spurred an intense debate [for a review, see Sec. 6.9 in Reimann (2002)]. The issue has been clarified by an analysis performed within the framework of linear irreversible thermodynamics by Van den Broeck (2007): The key to obtaining maximal Carnot efficiency for a Brownian motor is zero overall entropy production. This can be achieved by the use of architectural constraints for which the (linear) Onsager matrix has a determinant equal to zero, implying vanishing (linear) irreversible heat fluxes. Maximizing efficiency subject to "maximum-output power" (Van den Broeck, 2005) also leads to the same condition of a vanishing determinant of the Onsager matrix (i.e., perfect coupling), yielding the Curzon-Ahlborn (1975) limit, which in turn at small temperature difference yields half the Carnot efficiency. For the archetype Smoluchowski-Feynman Brownian motor device (Smoluchowski, 1912; Feynman *et al.*, 1963) the efficiency at maximum power has been evaluated by Tu (2008) for more general coupling schemes: Interestingly enough, the typical upper bound set by Curzon and Ahlborn (1975) may well be surpassed.

In spite of the combined efforts of theorists and experimenters, as of today the question remains unanswered. At present, ratchet devices operating under controllable experimental conditions hardly achieve an efficiency η_0 larger than a few percent.

On the other hand, the definition (33) of efficiency is not always adequate to determine the optimal performance of a Brownian motor. First, η_0 assumes that work

is being done against a load A_0, which is not always the case. For example, one clearly finds a vanishing efficiency whenever no load A_0 is present. Second, the only transport quantifier used in Eq. (33) is the drift velocity $\langle v\rangle$, whereas the fluctuations of $\dot{x}(t)=v(t)$, i.e., the variance $\sigma_v^2=\langle v^2\rangle-\langle v\rangle^2$, are also of practical importance. Note that we use $v(t)$ to denote the particle velocity in Eq. (6) as a proper stochastic process. If $\sigma_v>\langle v\rangle$, and even more so if $\sigma_v\gg\langle v\rangle$, the Brownian motor can possibly move for some time against its drift direction $\langle v\rangle$.

A load-independent rectification efficiency η_r has been introduced by Suzuki and Munakata (2003) and then generalized by Machura, Kostur, Talkner, *et al.* (2004). They computed η_r as the ratio of the dissipated power associated with the directed motion of the motor against both the friction and the load, and the "total" input power in the presence of the time-periodic forcing. The result assumes the explicit form

$$\eta_r=\langle v\rangle(A_0+\langle v\rangle)/|\langle v^2\rangle+\langle v\rangle A_0-D_0|, \tag{34}$$

where D_0 is the free diffusion coefficient of Sec. II.A.3. This definition holds evidently also for $A_0=0$, while numerical evidence indicates that $\langle v^2\rangle\geqslant D_0$, consistently with the inequality $\eta_r\leqslant 1$. Note that the definition (34) assumes that $x(t)$ is a damped process with finite γ (no matter how large). In this way η_r accounts explicitly for the power dissipated as velocity fluctuations during the rectification process; in particular, it increases upon decreasing σ_v. Machura, Kostur, Talkner, *et al.* (2004) noticed that, for a rocked ratchet, σ_v exhibits pronounced peaks in correspondence with the rectification thresholds $F_{3R,L}$ (large damping) and $F_{2R,L}$ (small damping), where the diffusion coefficient also has a maximum (Sec. II.A.3). That led to the general conclusion that transport by a Brownian motor can be optimized by operating away from activation thresholds, in regimes of large net currents, where velocity fluctuations are intrinsically small.

2. Vibrated ratchets

Besides the exceptions presented in Sec. IV, transport control in a rocked ratchet cannot be obtained experimentally by deforming the substrate potential "on demand." As shown by Borromeo and Marchesoni (2005a), this goal can more easily be achieved by means of an external tunable signal. Let $V(x)$ be assigned a fixed profile, say, the standard double sine in Eq. (23). The ratchet current can be still varied by injecting an additional control signal with frequency Ω_2, that is, by replacing the harmonic drive in Eq. (8) with the biharmonic drive in Eq. (16); in the adiabatic regime $\Omega_2\gg\Omega_1$ the system response is very different than in Sec. II.D.4. A rocked ratchet operated under such conditions is termed *vibrational* ratchet.

Following the perturbation approach of Blechman (2000), Landa and McClintock (2000), and Baltanás *et al.*, (2003) the variable $x(t)$ in Eq. (3) can be separated as $x(t)\to x(t)+\psi(t)$: in the remainder of this section $x(t)$ will

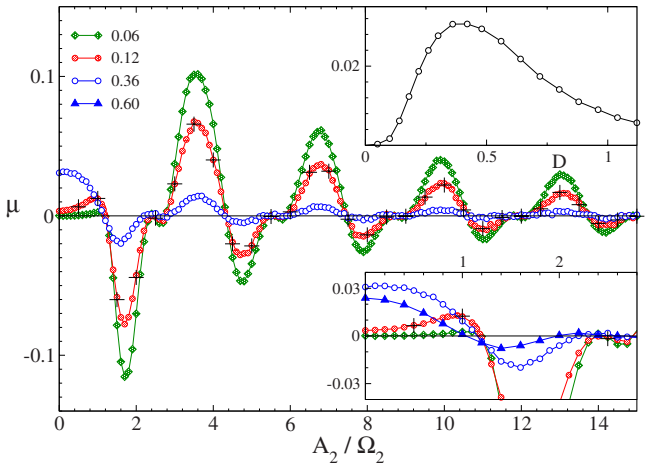

FIG. 10. (Color online) Mobility μ vs A_2/Ω_2 for a vibrated ratchet with $A_1=0.5$, $\Omega_1=0.01$, $\phi_1=\phi_2=0$, and different values of the noise intensity D (see legend, main panel). All simulation data have been obtained for $\Omega_2=10$, but the black crosses where we set $D=0.12$ and $\Omega_2=20$. Bottom inset: simulation data for μ as in the main panel with an additional curve at $D=0.6$. Top inset: μ vs D for $A_2=0$, $A_1=0.5$, and $\Omega_1=0.01$; circles: simulation data; solid curve: adiabatic formula (11.44) in Risken (1984). From Borromeo and Marchesoni, 2005a.

represent a slowly time-modulated stochastic process and $\psi(t)$ the particle free spatial oscillation $\psi(t)=\psi_0\sin(\Omega_2 t+\phi_2)$, with $\psi_0=A_2/\Omega_2$. On averaging out $\psi(t)$ over time, the Langevin equation for the slow reduced spatial variable $x(t)$ can be written as

$$\dot{x}=-\bar{V}'(x)+A_1\cos(\Omega_1 t+\phi_1)+\xi(t), \tag{35}$$

where

$$\bar{V}(x)=-V_0[J_0(\psi_0)\sin x+\tfrac{1}{4}J_0(2\psi_0)\sin 2x] \tag{36}$$

and $J_0(x)$ is the Bessel function of zeroth order. The symmetry of the effective vibrated potential (35) is restored if one of its Fourier components vanishes, namely, for $A_2/\Omega_2=\frac{1}{2}j_1, j_1, \frac{1}{2}j_2, \frac{1}{2}j_3, j_2, \frac{1}{2}j_4, \frac{1}{2}j_5, j_3, \ldots$, where $j_1=2.405$, $j_2=5.520$, $j_3=8.654$, $j_4=11.79$, $j_5=14.93\ldots$, are the ordered zeros of the function $J_0(x)$; correspondingly, the ratchet is expected to vanish, as confirmed by the simulation data displayed in Fig. 10.

Not all zeros of this sequence mark an inversion of the ratchet current. For instance, for $A_2/\Omega_2<\frac{1}{2}j_1$ the current is oriented in the natural direction of the effective potential, Eq. (36); for $\frac{1}{2}j_1<A_2/\Omega_2<j_1$, the coefficient of $\sin 2x$ changes sign and so does the ratchet natural orientation, or polarity; on further increasing A_2/Ω_2 larger than j_1, the sign of both Fourier coefficients in Eq. (36) become reversed: this is equivalent to turning $V(x)$ upside down (besides slightly remodulating its profile), so that the polarity of $\bar{V}(x)$ stays negative. Following this line of reasoning one predicts double zeros (i.e., no current inversions) at $\psi_0=j_1, j_2, j_3, j_4, \ldots$.

This control technique can be easily applied to the transport of massive Brownian particles in both symmet-

ric (Borromeo and Marchesoni, 2007a)—see inset of Fig. 10—and asymmetric devices (Borromeo and Marchesoni, 2007). Likewise, the use of a delay in a feedback control signal (Feito and Cao, 2007, 2008: Craig, Kuwada, *et al.*, 2008; Craig, Long, *et al.*, 2008; Son *et al.*, 2008) can, via synchronization mechanisms, efficiently improve the performance of Brownian motor currents; a scheme that can also be implemented readily in experimental flashing ratchets (Craig, Kuwada, *et al.*, 2008). In fact, an experimental implementation of a feedback controlled flashing ratchet mechanism has been realized with an optical line trap: It has been observed that the use of feedback increases the ratchet velocity by up to an order of magnitude (Lopez, Kuwada, *et al.*, 2008), in agreement with theory.

III. TRANSPORT IN NANOPORES

Membranes in biology encase cells and their organelles and allow the compartmentalization of cellular processes, thereby operating far from thermal equilibrium, a condition that is essential to life. Membranes separate two phases by creating an active or passive barrier to the transport of matter between them. As a first classification, membranes can be divided into biological and artificial membranes. The latter term is applied to all membranes made by man with natural, possibly modified, materials and with synthetic materials (synthetic membranes). Synthetic membranes can be further divided into organic (made with polymers) and inorganic membranes (made with alumina, metals, etc.).

Transport across a membrane occurs through channels or pores (Berezhkovskii *et al.*, 2003; Kolomeisky, 2007). In several cases, the membrane transport properties must be regarded as a collective effect, where the function of an individual channel is influenced by the presence of (possibly diverse) neighboring channels. This is the case, for instance, of ion pumps (Läuger, 1991; Im and Roux, 2002) in cellular membranes (Sec. III.A) or for coupled ion channels that experience a common transmembrane voltage. Single-molecule techniques, however, allow for the study and characterization of rectification properties of individual entities, such as single-ion channels. Nowadays, synthetic membranes with assigned pore density and patterns are made commercially available. Moreover, by means of increasingly sophisticated growth methods, irradiation (Fleischer *et al.*, 1975), and nanofabrication techniques (Li *et al.*, 2001; Storm *et al.*, 2003; Dekker, 2007; Healy *et al.*, 2007), the cross sections of membrane pores can be modulated along their axis. As a result, transport in artificial ion channels fabricated from asymmetric single pores of the most diverse geometries have become accessible to experiments (Siwy and Fuliński, 2004; Healy *et al.*, 2007); see also Sec. III.B.

In this section we focus on devices where the size of the transported particles is comparable to the pore cross section. Transport in these devices can be analyzed in terms of the one-particle 1D mechanisms illustrated in Sec. II. Larger pores, commonly used to channel fluids (liquid or gaseous) or colloidal particles suspended in a fluid, are considered in Sec. VI in the context of microfluidic devices.

A. Ion pumps

As remarked, biology teaches us useful lessons that can guide us in the design of artificial Brownian motors. Biological membranes are known to form lipophilic barriers and have embedded a diverse range of units which facilitate the selective movement of various ionic and polar segments or the pumping of protons and electrons across channel-like membrane openings. These biological nanodevices typically make use of electrochemical gradients that enable them to pump a species against its concentration gradient at the expense of yet another gradient. Ultimately, such devices convert nondirectional chemical energy, say, from the hydrolysis of adenosine triphosphate (ATP), into directed transport of charged species against electrochemical gradients.

Although many details of the underlying mechanism are far from being understood, these machines apparently make use of mechanisms that characterize the physics of Brownian motors (Astumian, 2007). A characteristic feature is that changes in the binding affinity at selective sites in the transmembrane region must be coupled to conformational changes which, in turn, control motion into the desired direction. Thus, in contrast to rocked or pulsated ratchets, where the particle-potential interaction acts globally along the whole periodic substrate landscape, the transport mechanism at work here can be better described as an "information" ratchet (Astumian and Derényi, 1998; Parrondo and de Cisneros, 2002). Indeed, the effective potential bottlenecks to transduction of Brownian motion become modified locally according to the actual location of the transported unit; as a result, information is transferred from the unit to the potential landscape. For example, this scheme can be used to model the pumping of Ca^{2+} ions in Ca^{2+}-ATPase (Xu *et al.*, 2002). Related schemes have also been invoked in the theoretical and experimental demonstration of pumping of Na^+ and K^+ ions via pulsed electric field fluctuations in Na- and K-ATPase (Xie *et al.*, 1994; Freund and Schimansky-Geier, 1999; Tsong, 2002) or for the operation of a catalytic wheel with help of a ratchetlike, electroconformational coupling model (Rozenbaum *et al.*, 2004).

Yet another mechanism can be utilized to pump electrons in biomolecules. It involves nonadiabatic electron tunneling in combination with asymmetric, but nonbiased, nonequilibrium fluctuations, as proposed by Goychuk (2006). The nonequilibrium fluctuations originate from either random binding of negatively charged ATP or externally applied asymmetric, but nonbiased, electric stochastic fields. Likewise, unbiased nonequilibrum two-state fluctuations (telegraphic noise) can induce directional motion across an asymmetric biological nanopore, as numerically investigated for an aquaglyceroporin channel, where water and glycerol are transported by

means of a rocked ratchet mechanism (Kosztin and Schulten, 2004).

Finally, we stress that in such realistic complex biological channels the physical implications of an externally applied control are often difficult to predict. This is due to the multifaceted consequences any control action may have in terms of chemical variations, conformational changes, polarization effects, and the like. Moreover, unlike single-molecule-type experiments, single-channel recordings are not easily accessible when dealing with biological molecules. Nanopores of lesser complexity are thus synthetic nanopores which can be fabricated by the use of bottom-down nanoscience techniques—the theme we review next.

B. Artificial nanopores

With the recent advances of track-etching (Fleischer *et al.*, 1975) and silicon technologies (Li *et al.*, 2001; Storm *et al.*, 2003; Dekker, 2007), charge transport in a single nanopore became experimentally accessible. This is a substantial leap forward with respect to ion pump and zeolite transport experiments, where experimental data are taken over a relatively high channel density. Fabricated nanopores in polymer films and silicon materials are investigated in view of their potential applications as biomimetic systems, that is, for modeling biological channels, and as biosensors.

Siwy and co-workers (Siwy and Fuliński, 2002; Siwy *et al.*, 2005; Constantin and Siwy, 2007; Vlassiouk and Siwy, 2007) have prepared a nanofluidic diode, which had been predicted to rectify ion current as a bipolar semiconductor diode rectifies electron current (Daiguji *et al.*, 2005). This diode is based on a single conically shaped nanopore track-etched in a polymer film with openings of several nanometer and 1 μm, respectively (see Fig. 11). The surface charge of the pore is patterned so that two regions of the pore with positive and negative surface charges create a sharp barrier called the transition zone. This nanofluidic diode is bipolar in character since both positively and negatively charged ions contribute to the measured current. Majumdar and co-workers (Karnik *et al.*, 2007) fabricated a similar nanofluidic diode with a sharp barrier between a positively charged and a neutral side of the pore. The presence of only one type of surface charge causes the latter device to be unipolar.

Ion rectification was achieved by applying a longitudinal ac voltage (Fig. 11); the system thus operates as a one-cell 1D rocked ratchet (Sec. II.D.1), where the spatial asymmetry is determined by the interaction of a single ion with the inhomogeneous charge distribution on the pore walls. The rectification power of the pore is defined as the ratio of the ionic currents recorded for positive and negative driving voltages, i.e., $\eta(V) = |I(V)|/|I(-V)|$. Of course, due to their asymmetric geometry, conical pores can rectify diffusing ions also for uniform wall-charge distributions (Siwy *et al.*, 2005); however, the corresponding η factor would be at least one order of magnitude smaller than reported here.

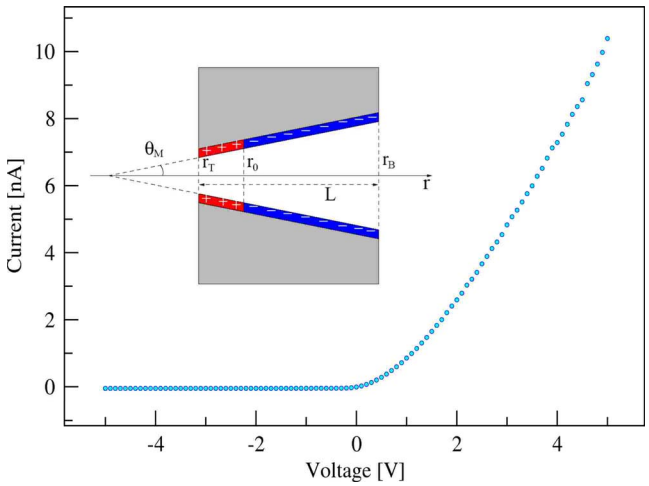

FIG. 11. (Color online) Ion current recorded experimentally by Constantin and Siwy (2007) at 0.1M KCl, pH=5.5, through a single conical nanopore with end diameters 5 and 1000 nm, respectively. The pore rectification power is η=217 at 5 V. Inset: Geometry of a conical nanopore with schematic representation of surface charge distribution creating a bipolar nanofluidic diode. Figure provided by Zuzanna Siwy.

As a serious limitation of the present design, it is not possible to control the rectification power of a given conical nanopore without introducing changes to its built-in electrochemical potential. An alternate approach has been proposed by Kalman *et al.* (2007), where two superposed rectangular voltage signals of zero mean were used to control the net ion current through a nanopore of preassigned geometry. By changing the amplitude, frequency, and relative phase of these signals they used the gating effect of Sec. II.C.2 to gain control over the orientation and the magnitude of ion flow through the pore. Their experimental data were found in excellent agreement with the theoretical prediction of Eq. (32). The magnitude of ion current variation achieved by asymmetric signal mixing was comparable with the incommensurate current offset Eq. (30), which means that the nanopore diode could be operated without regard for the details of its intrinsic rectification power.

We conclude this section on artificial nanopores by anticipating that asymmetric micropores etched in silicon membranes also work as microfluidic ratchet pumps for suspended colloidal particles (Kettner *et al.*, 2000; Müller, 2003). For instance, entropic effects on the rectification efficiency of the conical nanopores of Siwy and co-workers have been analyzed by Kosinska *et al.* (2008). However, in-pore diffusion in a liquid suspension requires a fully 3D analysis of the pumping mechanism, which sets the basis for the fabrication of more complicated ionic devices (Stein *et al.*, 2004; van der Heyden *et al.*, 2004). This category of device is reviewed in Sec. VI.

C. Chain translocation

The opposite limit of composite objects passing through a much narrower opening is often called "trans-

location." Using the experimental setup in Fig. 12(a), Kasianowicz *et al.* (1996) first measured the blockage currents of single-stranded RNA and DNA electrophoretically driven through a transmembrane pore. Recent developments of this technique demonstrated single-nucleotide resolution for DNA hairpins (Vercoutere *et al.*, 2003; Gerland *et al.*, 2004; Ashkenasy *et al.*, 2005), thus raising the prospect of creation of nanopore sensors capable of reading the nucleotide sequence directly from a DNA or RNA strand [see Healy (2007); Movileanu (2008); Zwolak and Di Ventra (2008)]. Nowadays, translocation mechanisms are investigated in both protein channels [mainly the bacterial α-hemolysin pore (Kasianowicz *et al.*, 1996)] and synthetic pores. Both these approaches have advantages and disadvantages (Dekker, 2007; Healy, 2007). Protein channels can be engineered with almost angstrom precision, but the lipid membrane in which they may be incorporated is very mechanically unstable. Synthetic pores, on the other hand, offer robustness to the system, which allows us to better characterize the physical aspects of translocation phenomena.

As a main difference with ion transport, the translocation of a long polymer molecule in a 1D device involves entropic effects, which become important when the opening cross section grows comparable with the radius of gyration R_0 of the polymer. These effects were predicted by Arvanitidou and Hoagland (1991) to account for the conformation changes of a chain in moving past a conduit constriction, and finally observed by Han *et al.* (1991) and Han and Craighead (2000) in an artificial channel. As a model pore-constriction system, they fabricated a channel consisting of a periodic sequence of regions of two different depths, as shown in Fig. 12(b). The thick regions were 1 mm deep, i.e., comparable with the R_0 of the double-stranded DNA molecules they used in their experiment, whereas the depth of the thin region, 90 nm, was much smaller than R_0.

The thick regions act like "entropic traps," as the DNA molecules are entropically prevented from entering the thin regions. For the same reason, a chain caught between two traps tends to fall back into the trap that contains most of it. In the presence of an external electric field, escape from a trap is initiated by the introduction of a small portion of DNA into an adjacent thin region, just enough to overcome the activation barrier for escape. This initiation process is local in nature, and the energy barrier does not depend on the total length of the trapped DNA molecule. Once a DNA molecule is in the transition state (once a proper length of "beachhead" is formed), it readily escapes the entropic trap, regardless of the length of the remaining molecule in the trap. Quite counterintuitively, Han and co-workers found that escape of DNA occours faster in longer entropic traps than in shorter ones.

A theoretical interpretation of these results was given by Park and Sung (1999), who treated the dynamics of a flexible polymer surmounting a 1D potential barrier as a multidimensional Kramers activation process (Hänggi *et al.*, 1990). To determine the activation free energy, Park and Sung computed the free energy of the polymer at the transition state. For a small-curvature barrier, the polymer retains its random coil conformation during the whole translocation process, giving rise to essentially the same dynamics as that of a Brownian particle. For a large-curvature barrier, on the other hand, a conformational transition (coil-stretch transition) occurs at the onset of the barrier crossing, which significantly lowers the activation free energy and so enhances the barrier crossing rate. As the chain length varies, the rate shows a minimum at a certain chain length due to the competition between the potential barrier and the free energy decrease by chain stretching. Synthetic nanopores can thus be used as Coulter counterdevices to selectively detect single DNA molecules, resolving their length and diameter.

Spatial asymmetry can rectify translocation through synthetic and biological pores alike. This is the case, for instance, of a hydrophobic polymer translocating across a curved bilayer membrane. Extensive simulation (Baumgärtner and Skolnick, 1995) showed that the polymer crosses spontaneously and almost irreversibly from the side of lower to that of higher curvature, so as to maximize its conformational entropy ("entropy" ratchets; Sec. V.A.1). Moreover, in protein translocation through a biomembrane, unlike that through the chemical artificial channels, structure of the pores can come into play by helping rectify the thermal fluctuations of the stretched molecule: When specific predetermined segments of the protein cross the membrane, chemicals acting as chaperons bind on the segments to prevent their backward diffusion (Hartl, 1996; Jülicher *et al.*, 1997; Nigg, 1997). The ensuing chemical asymmetry then competes with the entropic asymmetry to determine the translocation current.

D. Toward a next generation of mass rectifiers

1. Zeolites

Zeolites are three-dimensional, nanoporous, crystalline solids (either natural or synthetic) with well-defined structures that contain aluminum, silicon, and oxygen in their regular framework. The silicon and aluminum atoms are tetrahedrally connected to each other through shared oxygen atoms; this defines a regular framework of voids and channels of discrete size, which is accessible through nanopores of well-defined molecular dimensions. The negative electric charge of the zeolite framework is compensated by (inorganic or even organic) cations or by protons (in the acidic form of the zeolites). The ions are not a part of the zeolite framework, and they stand in the channels. The combination of many properties—such as the uniform cross section of their pores, the ion exchange properties, the ability to develop internal acidity, high thermal stability, high internal surface area—makes zeolites unique among inorganic oxides and also leads to unique activity and selectivity. As a result, zeolites can separate molecules based on size, shape, polarity, and degree of unsatura-

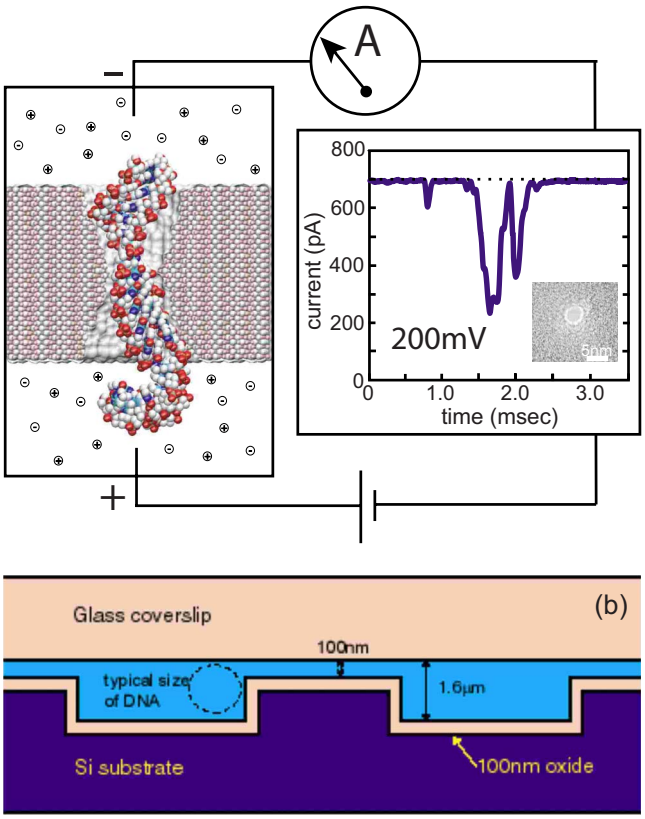

FIG. 12. (Color online) DNA translocation. (a) Electric detection of individual DNA molecules with a nanopore. A constant voltage bias induces a steady-state ionic current through a single nanopore (left panel, from simulation); adding DNA to the negatively biased compartment causes transient reductions of the ionic current (right panel, from experiment). This reduced conductance is associated with the translocation of DNA through the pore, which partially blocks the ionic current. From Aksimentiev *et al.*, 2004. (b) Schematic diagram of the entropic trap in Han *et al.*, 1999.

tion, among others properties (Kärger and Ruthven, 1992; Kärger, 2008b).

Nuclear magnetic resonance (NMR) provides direct access to the density and mobility of molecules in zeolites. By implementing a time-dependent NMR technique, termed pulsed field gradient NMR, Kärger and co-workers [see Kärger (2008a)] investigated the problem of particle diffusion in a narrow zeolite nanopore. For instance, they observed that, owing to the constrained pore geometry (0.73 nm across), the mean square displacement of CF_4 molecules (0.47 nm in diameter) diffusing in the zeolite $AlPO_4$-5 increases linearly with the square root of the observation time rather than with the observation time itself. That was an early experimental demonstration of the single-file diffusion mechanism introduced in Sec. II.A.4. In the meantime, however, real zeolite crystals have been repeatedly found to deviate notably from their ideal textbook structure (Schemmert *et al.*, 1999), so that their pore cross sections ought to be regarded as longitudinally corrugated. To what extent this may affect particle diffusion is still a matter of ongoing research (Kärger *et al.*, 2005; Taloni and Marchesoni, 2006).

Most zeolite structure types exhibit 3D pore networks. The most studied example is a synthetic zeolite of type MFI (Zeolite Socony Mobil-five). Their pore network is formed by mutually intersecting straight (in the crystallographic y direction) and sinusoidal (in the crystallographic x direction) channels. Although there is no corresponding third channel system, molecular propagation has also been observed in the z direction. Experimental data are consistent with a simple law of *correlated* diffusion anisotropy (Fenzke and Kärger, 1993) $a_z^2/D_z = a_x^2/D_x + a_y^2/D_y$, where a_i and D_i, with $i=x,y,z$, denote, respectively, the lattice and the diffusion constants in the i direction. This means that the molecular "memory" is shorter than the mean travel time between two adjacent network intersections.

With the advent of synthetic zeolites and zeolitic membranes, researchers are fascinated by the option that the existence of different channel types within one and the same material may be used for an enhancement of the performance of catalytic chemical reactions. As the diffusion streams of the reactant and product molecules tend to interfere with each other, rerouting them through different channels may notably speed up a catalytic reactor; hence, the idea of reactivity enhancement by "molecular traffic control" (Derouane and Gabelica, 1980; Neugebauer *et al.*, 2000).

2. Nanotubes

Another interesting category of artificial nanopore is the carbon nanotubes (Dresselhaus *et al.*, 1996). Single-walled carbon nanotubes are cylindrical molecules of about 1 nm in diameter and 1–100 μm in length. They consist of carbon atoms only, and can essentially be thought of as a layer of graphite rolled up into a cylinder. Multiple layers of graphite rolled in on themselves are said to form a multiwall carbon nanotube. The electronic properties of nanotubes depend strongly on the tube diameter as well as on the helicity of the hexagonal carbon lattice along the tube (chirality). For example, a slight change in the pitch of the helicity can transform the tube from a metal into a large-gap semiconductor, hence their potential use as quantum wires in nanocircuits (Dekker, 1999; Collins and Avouris, 2000). An even wider range of geometries and applications became available recently with the synthesis of various oxide nanotubes (Rêmskar, 2004). With their hollow cores and large aspect ratios, nanotubes are excellent conduits for nanoscale amounts of material. Depending on the filling material, experimenters have thus realized nanoscale magnets, hydrogen accumulators, thermometers, and switches.

Nanotubes also provide an artificial substrate for controllable, reversible, atomic-scale mass transport. Regan *et al.* (2004) attached indium nanocrystals to a multiwall carbon nanotube and placed it between electrodes set up in the sample chamber of an electron microscope. Applying a voltage to the tubes, they observed that the

metallic particles at one end of the tube gradually disappeared, while the number at the other end grew. While the details of the underlying driving mechanism (thermomigration versus electromigration) remain unclear, they concluded that the voltage dictates the directionality of the nanoscale mass conveyor. Experimenters even succeeded in synthesizing carbon nanotubes encapsulating metallic atoms and characterizing the electromechanical properties of such nanochannels [see, e.g., Gao and Bando (2002)]. In the near future, carbon nanotubes will also be combined to form molecular "gears," whose feasibility has been proven so far only by simulation (Drexler, 1992). A conceptual example is provided by a double-walled carbon nanotube consisting of two coaxial single-walled nanotubes with different chiralities, immersed in an isothermal bath. In the presence of a varying axial electrical voltage, this system would exhibit a unidirectional ratchetlike average rotation as a function of the chirality difference between its constituents (Marchesoni, 1996).

Nanotubes have also been used to realize prototypes of thermal diodes for phonon transport (Chang *et al.*, 2006). With this concept in mind, one can further devise a phonon Brownian motor aimed to ratchet a net heat flux from cold to hot, as numerically demonstrated by Li *et al.* (2008). This class of device has the potential to allow an efficient control of heat fluxes at the nanoscales.

In spite of the recent advances in nanotechnology, (inner or outer) transport along nanotubes is still controlled by external gradients. Nevertheless, nanotube-based ratchets, though not immediately available, are likely to represent one of the next frontiers in artificial Brownian motor research. Moreover, synthetic nanotubes are potential building blocks for nanofluidic devices also (Holt *et al.*, 2006), as discussed in Sec. VI.

IV. COLD ATOMS IN OPTICAL LATTICES

Optical lattices are periodic potentials for atoms created by the interference of two or more laser fields (Jessen and Deutsch, 1996; Grynberg and Robilliard, 2001). In near-resonant optical lattices the laser fields produce simultaneously a periodic potential for the atoms and a cooling mechanism. The optical potential for an atom in an optical lattice is given by the light shift, or ac Stark shift, of the atomic energy level that acts as the ground state of an assigned optical transition. The simplest case is represented by the $J_g=1/2\rightarrow J_e=3/2$ atomic transition in a 1D configuration.

Consider two counterpropagating laser fields, detuned below the atomic resonance, with orthogonal linear polarizations and the same intensity and wavelength λ. Their interference results in a spatial gradient with polarization ellipticity of period $\lambda/2$. This in turn produces a periodic potential for the atom. For instance, the atomic hyperfine ground states $|g,\pm\rangle=|J_g=1/2,M=\pm 1/2\rangle$ experience periodic potentials in phase opposition along the direction x of light propagation, namely,

$$V_{\pm}(x) = V_0(-2 \pm \cos kx)/2, \tag{37}$$

where $k=2\pi/\lambda$ and the depth of the potential wells V_0 scales as I_L/Δ, with I_L the total laser intensity and Δ the detuning from atomic resonance. As the laser fields are near resonance with the atomic transition $J_g=1/2\rightarrow J_e=3/2$, the interaction with the light fields also leads to stochastic transitions between the Zeeman sublevels $|g,\pm\rangle$ of the ground state. The rate of this transition can be quantified by the photon-atom scattering rate Γ' which scales as I_L/Δ^2. It is therefore possible to vary independently the optical lattice depth V_0 and Γ' by changing simultaneously I_L and Δ.

The stochastic transitions between ground states also lead to damping and fluctuations. The damping mechanism, named Sisyphus cooling, originates from the combined action of light shifts and optical pumping, which transfers, through cycles of absorption and spontaneous emission involving the excited state J_e, atoms from one ground state sublevel to the other one. Moreover, the stochastic transitions between the two potentials $V_{\pm}(x)$ also generate fluctuations of the instantaneous force experienced by the atom. In conclusion, the equilibrium between cooling and heating mechanisms determines a stationary diffusive dynamics of the atoms, a process confined to the symmetric ground-state optical lattice $V_{\pm}(x)$.

Random amplitude pulsations of one symmetric potential, Eq. (37), do not suffice to produce rectification. The only missing element needed to reproduce the rocked setups of Secs. II.C and II.D is the additive ac force $F(t)$. In order to generate a time-dependent homogeneous force, one of the lattice beams is phase modulated, and we indicate by $\phi(t)$ its time-dependent phase. In the laboratory reference frame the phase modulation of one of the lattice beams results in the generation of a moving optical lattice $V_{\pm}(x-\phi(t)/2k)$, reminiscent of the periodic sieves by Borromeo and Marchesoni (2007a). In the accelerated reference frame $x\rightarrow x-\phi(t)/2k$, the optical potential would be stationary; however, an atom of mass m experiences also an inertial force in the z direction proportional to the acceleration of the moving frame, namely, $F(t)=(m/2k)\ddot{\phi}(t)$. This is the homogeneous ac drive needed to rock a cold atom ratchet.

The harmonic mixing and rocking ratchet setups described above were used by Renzoni and co-workers (Schiavoni *et al.*, 2003; Gommers *et al.*, 2005, 2006, 2007, 2008) to investigate experimentally the relationship between symmetry and transport in 1D atom traps. We discuss here separately the experimental results for two different cases: (i) a biharmonic driving including two harmonics at frequencies Ω_0 and $2\Omega_0$, and (ii) a multifrequency driving obtained by combining signals at three different frequencies.

A. Biharmonic driving

Schiavoni *et al.* (2003) and Gommers *et al.* (2005) generated a biharmonic drive, Eq. (16), with $\Omega_2=2\Omega_1$ and

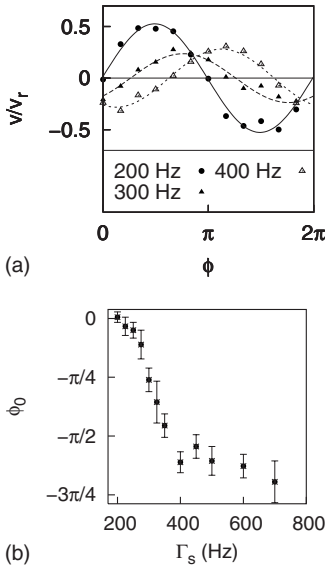

FIG. 13. Cold atoms in an optical lattice. (a) Average atomic velocity as a function of the phase ϕ_2 for different values of $\Gamma_s=[\omega_v/(2\pi)]^2/\Delta$ (a quantity proportional to the scattering rate Γ'). The data are labeled by the lattice detuning Δ, as the vibrational frequency at the bottom of the wells was kept constant, $\omega_v/2\pi=170$ kHz; the forcing frequency is $\Omega_1/2\pi=100$ kHz. The lines are the best fit of the data with the function $v/v_r=A_\Delta \sin(\phi-\phi_0)$, where $v_r=\hbar k/m$ is the so-called atom recoil velocity. (b) Experimental results for the phase shift ϕ_0 as a function of Γ_s. From Gommers *et al.*, 2005.

$\phi_1=0$, and searched for a harmonic mixing current proportional to $\sin(\phi_2-\phi_0)$. At variance with Eq. (17), an additional phase lag ϕ_0 was introduced to account for the finite atom dissipation. Indeed, by generalizing our argument of Sec. II.C.1, one can easily prove that increase in the damping makes ϕ_0 drop from 0 down to $-\pi/2$. In the experiment, the atom dissipation could be tuned continuously, without changing the optical potential constant V_0, by varying simultaneously I_L and Δ at a constant I_L/Δ ratio; thus harmonic mixing was experimentally accessible in limiting regimes of both zero and infinite damping.

The experimental results of Fig. 13 for cesium atoms cooled in the microkelvin range clearly demonstrate the mechanism of harmonic mixing at work. In fact, the net atom velocity plotted in panel (a) is well fitted by $v/v_r=A_\Delta \sin(\phi_2-\phi_0)$, where the dependence of ϕ_0 on Γ' is as in panel (b), and A_Δ is a characteristic function of the system (Gommers *et al.*, 2005). For the smallest scattering rate examined in the experiment, no current was generated at $\phi_2=l\pi$, with l integer, as expected from Eq. (17). On the other hand, the magnitude of the phase shift ϕ_0 increases with increasing scattering rate, thus causing current generation for $\phi_2=l\pi$. Besides confirming the notion of harmonic mixing, the experimental results of Schiavoni *et al.* (2003) and Gommers *et al.* (2005) suggest that symmetry breaking can be controlled by dissipation. Closely related results have been reported by Ustinov *et al.* (2004) in their attempt to control fluxon ratcheting in Josephson junctions by means of harmonic mixing.

B. Multifrequency driving

Recent experiments with multifrequency driving (Gommers *et al.*, 2006, 2007) aimed to investigate the transition from periodic to quasiperiodic driving, and to examine how the analysis of Sec. II.C is modified in this transition. The multifrequency driving was obtained by adding a sinusoidal component to the ac drive employed in the previous section, i.e.,

$$F(t)=A_1\cos(\Omega_1 t)+A_2\cos(2\Omega_1+\phi_2)+A_3\cos(\Omega_3 t+\phi_3). \tag{38}$$

For irrational Ω_3/Ω_1 the driving is quasiperiodic. Clearly, in a real experiment Ω_3/Ω_1 is always a rational number, which can be written as p/q, with p and q two coprime positive integers. However, as the duration of the experiment is finite, by choosing p and q sufficiently large it is possible to obtain a driving that is effectively quasiperiodic on the time scale of the experiment.

Consider first the case of periodic driving, with rational Ω_3/Ω_1. Adding a third harmonic with phase constant $\phi_3\neq 0$ in Eq. (38) breaks the time symmetry of $F(t)$ so that directed transport is allowed for $\phi_0=0$ and $\phi_2=l\pi$. In other words, for $\phi_3\neq 0$, the third driving component leads to an additional phase shift of the current as a function of ϕ_2. As a result, the current will retain its sinusoidal phase dependence $\sin(\phi_2-\phi_0)$ as above, with the difference that now ϕ_0 accounts for the phase shifts produced both by dissipation and by the added driving component. Following the discussion in Sec. II.D.4, one concludes that in the quasiperiodic regime the third-order harmonic at frequency Ω_3 is not relevant to characterize the time symmetry of the forcing signal, which is entirely determined by the biharmonic terms at frequency Ω_1 and $2\Omega_2$.

In later experiments (Gommers *et al.*, 2006, 2007), the transition to quasiperiodicity was investigated by studying the atomic current as a function of ϕ_2 for different p/q. By increasing p and q the driving was made more and more quasiperiodic on the finite duration of the experiment, with the quantity pq an easily accessible measure of the degree of quasiperiodicity. The data for the average atomic current were fitted with the function $v/v_{\max}=\sin(\phi_2-\phi_0)$ and the resulting values for ϕ_0 were plotted as a function of pq. For small values of pq, i.e., for periodic driving, the added component at frequency Ω_3 leads to a shift which strongly depends on the actual value of pq. For larger values of pq, i.e., approaching quasiperiodicity, the phase shift ϕ_0 tends to a constant value independent of ϕ_3, which coincides with the purely dissipative phase shift measured in the biharmonic driving case of Sec. IV.A. The experimental results confirm that, in the quasiperiodic limit, the only relevant symmetries are those determined by the periodic biharmonic driving and dissipation.

C. More cold atom devices

Cold atoms in optical traps proved to be a playground for rectification experiments.

(i) Gating effect. For instance, Gommers *et al.* (2008) modified the experimental setup described above to demonstrate experimentally a gating ratchet with cold rubidium atoms in a driven near-resonant optical lattice. As suggested in Sec. II.C.2, a single-harmonic periodic modulation of the optical potential depth with frequency Ω_2 was applied, together with a single-harmonic rocking force with frequency Ω_1. The modulation of the optical potential depth V_0 was obtained by modulating the intensity I_L of the laser beams. This also resulted in an unavoidable modulation of the optical pumping rate, which affected only the fitting phase shift ϕ_0. Directed motion was observed for rational values of Ω_2/Ω_1, a result due to the breaking of the symmetries of the system.

(ii) Pulsated ratchets. Although a *bona fide* rocked ratchet for cold atoms in an optical lattice has not been realized [see, e.g., Ritt *et al.* (2006)], a variation of the 1D optical lattice described above allowed an early demonstration of a randomly pulsated ratchet. Mennerat-Robilliard *et al.* (1999) set the polarizations of the laser beams at an angle $\theta \neq \pi/2$ and applied a weak Zeeman magnetic field orthogonal to the optical lattice. The effect of the magnetic field consisted in removing the degeneracy of the ground states by adding a $\lambda/2$ wavelength component to both potentials in Eq. (37), which thus acquired different asymmetric profiles. As a consequence, the random optical transitions between the modified potentials $V_{\pm}(x)$ turned out to propel trapped cold rubidium atoms in the vertical direction, with a sign that depended on θ and the orientation of the magnetic field.

In Sec. II.D.2 we reported that rectification can occur on symmetric 1D substrates that shift instantaneously back and forth in space with a fixed amplitude, namely, on substrates that are subjected to a time-discrete phase modulation (periodic or random). In this case, breaking the supersymmetry condition (14) requires appropriate asymmetric space-dependent switching rates (Gorman *et al.*, 1996). Based on this rectification scheme, Sjölund *et al.* (2006) realized a simple flashing ratchet for cold atoms. It consisted again of a millikelvin cold gas of cesium atoms switching between two symmetric ground-state optical lattices, coupled via optical pumping. In the presence of induced friction, although small, and for appropriate laser detunings and intensities of the laser beams, the degeneracy of the ground states was removed by making one ground state, say V_+, long lived and the other one, V_-, short lived. If we further consider that the two optical lattices were shifted one relative to the other, $V_-(x)=V_+(x-x_0)$, then we conclude that the switching rates between potentials were state and position dependent with $k_{-\to+}(x) \gg k_{+\to-}(x)$. In this setup, the atoms execute stationary time-asymmetric sequences of random jumps between V_+ and V_-. During the time spent in the short-lived lattice V_-, they experience a potential with an incline that depends on x_0. Thus their diffusion is strongly enhanced in one specific direction, and correspondingly reduced in the opposite direction. In the experiment, the spatial shift x_0 and the transition rates between the two optical lattices could be adjusted at will. A directed motion with constant velocity was observed in the absence of additional forcing terms, i.e., for $F(t)=0$, except for specific system parameters, where symmetry was restored. Moreover, they showed that their device, when operated in three dimensions (Ellmann *et al.*, 2003), can generate directed motion in any direction.

V. COLLECTIVE TRANSPORT

The studies on rectification mechanisms reviewed in Sec. II were conducted mostly for a single particle; however, often systems contain many identical particles, and the collective interactions between them may significantly influence the transport of particle aggregates (Aghababaie *et al.*, 1999). For example, interactions among coupled Brownian motors can give rise to novel cooperative phenomena like anomalous hysteresis and zero-bias absolute negative resistance (Reimann *et al.*, 1999). The interactions among individual motors plays a particular important role for the occurrence of unidirectional transport in biological systems; see, e.g., Sec. IX in the review by Reimann (2002).

In this section we restrict ourselves to the properties of 1D and 2D systems of pointlike interacting particles, although an extension to 3D systems is straightforward. Let the pair interaction potential $\mathcal{W}(r)$ be a function of the pair relative coordinates $\mathbf{r}=(x,y)$, characterized by an appropriate parameter g, quantifying the strength of the repelling ($g>0$) or attracting force ($g<0$), and by a constant λ, defining the pair interaction length. An appropriate choice of $\mathcal{W}(r)$, with $g>0$, can be used to model hard-core particles with diameter λ (Savel'ev *et al.*, 2003, 2004a). We term the pair interaction long range if λ is larger than the average interparticle distance, and short range in the opposite regime. In the absence of perturbations due to the substrate or the external drives, long-range repelling particles rearrange themselves to form a triangular Abrikosov (1957) lattice. When placed on a disordered substrate or forced through a constrained geometry, such an ideal lattice breaks up into lattice fragments punctuated by pointlike defects and dislocations and separated by faulty boundaries. In the presence of a drive, such boundaries act like 1D easy-flow paths, or rivers, for the movable particles. This process, often referred to as "plastic" flow, has been analyzed numerically by Reichhardt *et al.* (1998).

Rectification of interacting particles occurs as a combined effect of the configuration of the device and the geometry of its microscopic constituents. In this context the dimensionality of the underlying dynamics is also important: (i) transport in some 2D geometries can often be reduced to the 1D mechanisms illustrated in Sec. II (reducible 2D geometries); (ii) under certain circum-

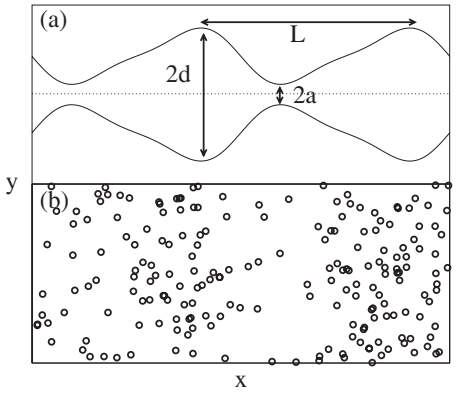

FIG. 14. 1D reducible asymmetric geometries. (a) Channel with standard asymmetric profile $y(x)=y_0-y_1[\sin(2\pi x/L)+(1/4)\sin(4\pi x/L)]$; the parameters y_1 and y_0 control the width $2d$ and the bottleneck $2a$. (b) Disordered pattern of circular defects generated with periodic distribution $y(x)$ along the x axis.

stances, however, a *bona fide* 2D rectification may occur at a nonzero angle with the driving force (irreducible 2D geometries). Finally, we remark that particle interaction can be exploited to rectify particles of one species by acting on particles of another species, alone, by either an appropriate drive or a specially tailored substrate geometry.

A. Asymmetric 1D geometries

We consider now two examples of 2D reducible geometries where the transport of massless repelling particles, subjected to an external ac drive, occurs as a collective effect, namely, under conditions incompatible with the rectification of a single particle. In particular, we show that collective effects make transport of interacting particles possible even in the absence of an *ad hoc* ratchet substrate.

1. Boundary effects

Consider the asymmetric channel in Fig. 14(a) filled with n repelling particles per unit cell. The corresponding particle density is $\rho=n/a_l$, where a_l is the area of the channel unit cell. The walls are rigid and particle-wall collisions are taken elastic and relatively short range (interaction length not much larger than λ). The profiles $\pm y(x)$ of the upper (+) and lower (−) walls are modeled by an appropriate double-sine function; $2d$ and $2a$ denote, respectively, the width of the channel and of its bottlenecks. Due to the repulsive interactions, the particles are pressed against the walls which corresponds to an effective asymmetric spatial modulation. As a consequence, when driven by an ac force, the particles are more likely to flow to the left than to the right. The ensuing rectification mechanism is reminiscent of a 1D rocked ratchet with an inverted potential (23). Numerical simulations, besides supporting this prediction, clearly indicate an optimal or resonant, temperature regime in which the particle drift is maximized. This observation can be explained by noticing that, at low temperatures, the ac drive causes a moving particle to migrate to the center of the channel where it no longer interacts with the boundaries; while at high temperatures the driving force becomes irrelevant and thus the particle is no longer pushed through the channel bottlenecks periodically in time. The first simulation evidence of this phenomenon was produced by Wambaugh *et al.* (1999). Their results obtained for the special case of magnetic vortex channeling are discussed in Sec. VII.A.

At high enough particle densities ρ, the net current in the channel is expected to be suppressed, as the repelling particles end up clogging the bottlenecks and thus hampering collective longitudinal oscillations. In the opposite limit of, say, $n=1$, the arguments above seem to rule out rectification, as a single oscillating particle would be confined in the inner channel of radius a. However, this conclusion holds only in the absence of thermal fluctuations, $T=0$. At finite T, reducing the diffusion in a 2D channel to a 1D process implies defining an effective diffusion constant (Sec. II.A.3) $D(x)/D_0=[1+y'(x)^2]^{-1/3}$ equivalent to a periodic asymmetric modulation of the temperature (Reguera *et al.*, 2006) [a Seebeck ratchet in the notation of Reimann (2002)]. A particle crossing a channel bottleneck perceives a lower effective temperature on the left, where the wall is steeper, than on the right, so that it gets sucked forward; the opposite happens in correspondence to the largest channel cross sections. As long as $\int dx/D(x)\neq 0$, the oscillating motion of a single particle can indeed be rectified, with a sign that depends on the details of the wall profile (Ai and Liu, 2006). No matter how weak, such a mechanism, termed an entropic ratchet (Slater *et al.*, 1997), supports the conclusion of Wambaugh *et al.* (1999) that rectification in a channel occurs only at finite T, as a certain amount of noise is needed for the particle to explore the asymmetric geometric of the device. Moreover, the argument above hints at the occurrence of an optimal channel density ρ, as detected in real superconducting devices (Sec. VII.A).

2. Asymmetric patterns of symmetric traps

Olson *et al.* (2001) proposed a new type of 2D ratchet system which utilizes gradients of pointlike disorder, rather than a uniformly varying substrate potential. Consider a 2D sample containing a periodically graduated density of point defects, as sketched in Fig. 14(b). Each defect is depicted as a circular microhole, which acts as a symmetric short-range particle trap of finite depth. In real experiments, such defects can actually be created by either controlled irradiation techniques or direct-write electron-beam lithography (Kwok *et al.*, 2002). The defect density $\rho_l(x)$ was chosen to be uniform along the vertical axis, and to follow the typical double-sine asymmetric profile of Eq. (23) along the horizontal axis. We now inject into the sample repelling massless particles with average density ρ and interaction length λ. The defect radius controls particle pinning by defects and was taken much smaller than λ. For a sufficiently

high particle-to-defect density ratio, the particles fill most of the pinning sites and create an effective repulsive potential. If we further assume long-range particle pair interactions $\mathcal{W}(r)$, such a 2D potential becomes insensitive to the details of the defect distribution; it retains only the periodic horizontal modulation of $\rho_l(x)$, thus resulting in a mean-field ratchet potential $V(x)$, as in Eq. (23). The effective amplitude V_0 is a function of at least three length scales: the interaction constant, the average particle distance, and the average defect spacing. A certain fraction of particles does not become pinned at individual defects but, subjected to an applied ac drive, can move in the interstitial regions between pinning sites. Although the moving interstitials do not directly interact with the short-ranged defects, they feel the long-range interaction of the particles trapped at the pinning sites and described by the mean-field potential $V(x)$. As a consequence, a horizontally applied ac drive can induce a longitudinal particle transport, as proven by Olson *et al.* (2001) by means of numerical simulation.

Two conditions are instrumental to the onset of a rectification current: (i) a finite temperature, $T>0$, and (ii) a defect filling fraction close to or larger than 1, both conditions required for interstitial particles to get and stay unpinned. As in Sec. V.A.1, condition (i) implies the existence of an optimal rectification temperature. The dependence on the forcing frequency and amplitude are as discussed in Sec. II.D.1. These ideas have been implemented to control transport of colloids and charge carriers in experimental setups where point defect gradients could be engineered at will (cf. Secs. VI.A, VII.B, and VIII.C).

B. 2D lattices of asymmetric traps

Examples of substrates sustaining transverse rectification are asymmetric potential barriers, height $q>0$, or wells, depth $q<0$, either isolated or arranged into 1D chains and 2D lattices. Similar lateral displacement devices, also known as bumper arrays, have been proposed to separate particles by exploiting their mass and size dispersion (Savel'ev *et al.*, 2005; Heller and Bruus, 2008). Consider, for instance, pyramidal potential barriers or wells with isosceles triangular cross section. This geometry, sketched in Fig. 15, is a generalization of the experimental setup by Villegas *et al.* (2003).

The substrates discussed here combine two types of asymmetry: the triangular shape of their building blocks and the asymmetry associated with the pyramidal structure of each block. The latter asymmetry affects the motion of the particles only if the drive is strong enough to push them across the barriers or wells. Savel'ev *et al.* (2005) numerically simulated the dynamics of a gas of *repelling* massive particles driven across 1D or 2D lattices of barriers or wells for different parameters of the substrate lattice (Fig. 15, bottom panel), the drive $\mathbf{F}(t)$, and the particle pair potential $\mathcal{W}(r)$. Although Savel'ev *et al.* (2005) showed that inertial effects often enhance transverse rectification, we restrict our presentation to the case of massless particles, certainly the most relevant for technological applications. We consider next two distinct operating regimes.

(i) Deterministic setups. An ac force applied along the y axis, i.e., parallel to the symmetry axis of the pyramid cross section, is known to induce a longitudinal particle drift in the drive direction [for more detail see Zhu *et al.* (2004) and Sec. VII]. Indeed, driving a (distorted) lattice of repelling particles along the crystallographic axis of the substrate, oriented parallel to the symmetry axis of the substrate blocks, makes the system reducible to a mean-field 1D dynamics in that direction, along the line of Sec. V.A. Due to the pyramidal shape of its building block, the reduced 1D substrate is spatially asymmetric, which explains the reported longitudinal particle flows.

(ii) Diffusive setups. Under appropriate conditions dc or ac forces applied perpendicularly to the symmetry axis may induce a transverse particle drift in the y direction. For all geometries considered, the net velocity of a gas of noninteracting overdamped particles driven perpendicularly to the symmetry axis vanishes for $T\to 0$. Indeed, sooner or later each particle gets captured in a horizontal lane between two triangle rows and then keeps oscillating back and forth in it forever. At finite temperature fluctuations tend to push the particle out of its lane, thus inducing the net transverse currents reported in the earlier literature (Duke and Austin, 1998; Bier *et al.*, 2000; Huang *et al.*, 2004). More remarkably, Savel'ev *et al.* (2005) reported that the interaction among particles not only contributes to transverse rectification but actually plays a dominant role if the interaction length λ or the particle density is large enough. In particular, the particle-particle interaction was shown to control transverse rectification for both weak short-range and strong long-range interparticle forces [see Fig. 15(a)]. Therefore transverse rectifications of interacting colloidal particles (short range) and magnetic vortices (long range) are expected to differ appreciably (see Secs. VI.A and VII).

To illustrate the key mechanism of transverse rectification, we consider only rectification by pyramidal barriers, $q>0$, subjected to the dc force $F(t)=A_0$. For a detailed analysis, see Savel'ev *et al.* (2005). Consider first the geometry in Figs. 15(b)–15(e) (bottom panel), where the pyramids are stacked up in a close row ($\Delta_y=0$). The particle interactions have a strong impact on the equilibrium particle distribution; a transition from an ordered latticelike to a disordered liquidlike phase is displayed in frames (b)–(e). Nevertheless, the transverse currents $\langle v_y\rangle$ show a qualitatively similar A_0 dependence for both weak short-range and strong long-range interactions; only the decaying tail is longer for the latter. The region of the linear growth of $\langle v_y\rangle$ for the case of weak short-range interaction corresponds to the regime when a constant fraction of particles (less than 1/2 because of the geometry of the system) is rectified into the y direction. This regime applies for increasing A_0 until particles start crossing over the triangles [frames (d) and (e)]. These results can be easily generalized to describe transverse

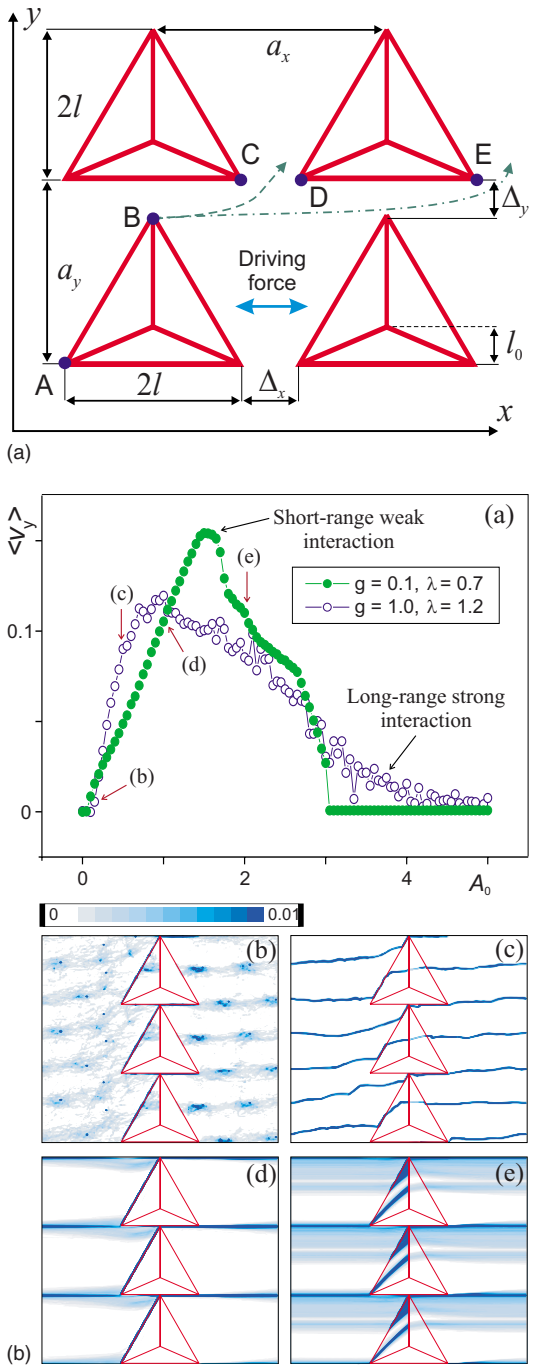

FIG. 15. (Color online) 2D sieves for magnetic vortices. Top panel: asymmetric 2D arrays of potential energy barriers and wells, top view. The parameters l; l_0; a_x; a_y; Δ_x; Δ_y define the geometry of the array. The dashed and dash-dotted arrows represent trajectories perturbed by thermal noise or particle-particle repulsion. Bottom panel: (a) Transverse net velocity $\langle v_y \rangle$ vs A_0 for *massless* interacting particles dc driven through a gapless triangular chain: $a_y=2$, $a_x=6$, $l=1$, $\Delta_x=4$, $\Delta_y=0$, and $T=0$. The repulsive potential $\mathcal{W}(r)$ is a wedge function with $g=1$ and half-width $\lambda=0.05$. Solid circles are for weak short-range interacting particles, while open circles are for strong long-range interacting particles. Particle distributions for strong long-range (b), (c) and weak short-range (d), (e) interactions for the A_0 values indicated by arrows in (a). The results in (a)–(e) coincide with those obtainable for low-frequency ac drives, as shown in Savel'ev *et al.* (2005).

rectification in any 2D lattice of triangular-shaped barriers or wells. Moreover, the orientation of the transverse net current is independent of the sign of A_0, so that the above description can be readily extended to low-frequency ac drives.

Savel'ev *et al.* (2005) also simulated the case of a 2D array of pyramids (top panel of Fig. 15), where a gap between triangles along the y axis, $\Delta_y>0$, turned out to make the net current sensitive to the particle-particle interaction length λ. In the limit of low T, if λ is smaller than a certain threshold value $\lambda^c \sim \Delta_y$, then the net current vanishes; if λ exceeds λ^c, then the current rapidly increases. This effect has been advocated to separate particles according to their interaction length. More precisely, particles having an interaction length smaller than λ^c would pass through the array or sieve of barriers separated by Δ_y. In contrast, particles with a longer interaction length $\lambda>\lambda^c$ would be sifted sideways. On connecting several such sieves with different gaps Δ_y, one can construct a device capable of separating the different fractions of a particle mixture.

The overall conclusions of Savel'ev *et al.* (2005) do not change when barriers are replaced with wells of the same shape, nor for lattices of asymmetric pins of different aspect ratios and geometries (Duke and Austin, 1998; Ertas, 1998; Bier *et al.*, 2000; Zau, Marchesoni, Moshchalkov, *et al.*, 2003; Zau *et al.*, 2004; Huang *et al.*, 2004; Chepelianskii and Shepelyansky, 2005). This effect had been anticipated to some extent by Lorke *et al.* (1998), who investigated the magnetotransport properties of a square lattice of triangular antidots of the type shown in Fig. 15. Antidot lattices are 2D electron gases with appropriately placed submicron voids. They fabricated their lattices by electron beam lithography on shallow high-electron-mobility transistor structures, grown on semi-insulating gallium-arsenide substrates. In particular, they reported evidence that, under far-infrared irradiation, electron sloshing between the antidot rows lead to a net electric current along the symmetry axis of the antidots. Significant transverse effects were observed in the presence of an orthogonal magnetic field. Moreover, in most applications to the electrophoresis of macromolecules, the particles moving through these sieves are suspended in the fluid where they diffuse, thus involving additional microfluidic effects (Sec. VI).

C. Binary mixtures

We address now the problem of induction and control of the net transport of passive particles (target or A particles), namely, particles that are little sensitive to the applied drives and/or substrates. Savel'ev *et al.* (2003, 2004) proposed to employ auxiliary B particles that (i) interact with the target species and (ii) are easy to drive by means of external forces. By driving the auxiliary particles one can regulate the motion of otherwise passive particles through experimentally accessible means.

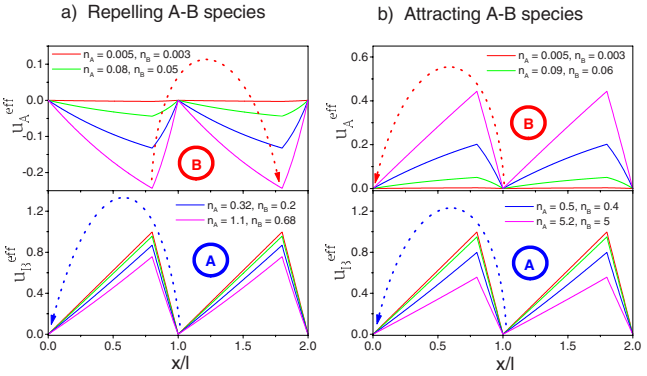

FIG. 16. (Color online) Spatial dependence of the effective potentials $V_A^{\mathrm{eff}}(x)$ and $V_B^{\mathrm{eff}}(x)$ at different densities of the A and B particles. In both panels, particles of the same type repel one another; the interaction between particles of different species is repulsive in (a) and attractive in (b). There is no substrate for the A particles, $V_A(x)=0$, whereas the ratchet potential $V_B(x)$ is piecewise linear: $V_B(0<x<l_+)=x/l_+$, $V_B(l_+<x<l)=(1-x)/l_-$, with $l_-=0.2$ and $l_+=0.8$. The other coupling parameters are $g_{AA}=g_{BB}=|g_{AB}|=1$ and $T=1$. From Savel'ev *et al.*, 2005.

Savel'ev and co-workers considered a mixture of two species of pointlike overdamped Brownian particles A and B at temperature T, diffusing on the 1D periodic substrates described by potentials $V_A(x)$ and $V_B(x)$, respectively. Particles of type A interact pairwise with one another as well as with the B particles via the potentials $\mathcal{W}_{AA}$ and $\mathcal{W}_{AB}$ $(=\mathcal{W}_{BA})$, while $\mathcal{W}_{BB}$ describes the interaction of the B pairs. The pair interaction is quantified by the tunable strengths g_{ij}, with $i,j=A,B$, whereas the interaction constants λ_{ij} play no significant role as long as they are conveniently small.

To illustrate the rectification mechanisms in a binary mixture, we review the case of a pulsated device with oscillating temperature, i.e., a temperature ratchet studied originally by Reimann *et al.* (1996); see also Sec. II.D.2. The model can be made simpler with two assumptions: (i) One subsystem (say, the auxiliary B particles) is subject to an asymmetric ratchet potential $V_B(x)$, while the other one (the target A particles) is not, $V_A(x)=0$. This may happen, for instance, in a mixture of neutral and charged particles with the ratchet potential produced by an electrical field. (ii) The interaction among particles of the same type is repulsive, i.e., $g_{AA}>0$, $g_{BB}>0$.

Under these operating conditions, the B particles condense naturally at the minima of the asymmetric substrate potential [see Figs. 16(a) and 16(b), bottom panels]. In addition, if the B particles repel the A particles, $g_{AB}>0$, then the latter will accumulate in regions where the density of the B particles is minimum, that is, near the maxima of the substrate potential $V_B(x)$. Vice versa, for attractive AB interactions, $g_{AB}<0$, the B particles concentrate around the minima of $V_B(x)$. Therefore the target A particles feel an effective potential $V_A^{\mathrm{eff}}(x)$ which has opposite spatial asymmetry with respect to $V_B^{\mathrm{eff}}(x)$ for $g_{AB}>0$, and has the same asymmetry for $g_{AB}<0$ [see Figs. 16(a) and 16(b), top panels]. Note that, for low occupation numbers n_A and n_B, the bare potential $V_B(x)$ is only marginally affected by particle interaction, i.e., $V_B^{\mathrm{eff}}(x)\simeq V_B(x)$. During the lower-$T$ half cycle, all particles are confined more tightly around the minima of the relevant effective potential, while, during the higher-T half cycle, the particles of both species diffuse more easily out of the $V_A^{\mathrm{eff}}(x)$ and $V_B^{\mathrm{eff}}(x)$ potential wells. As the asymmetry of the ratchet potentials $V_A^{\mathrm{eff}}(x)$ and $V_B^{\mathrm{eff}}(x)$ for repelling A and B particles is opposite, so is the orientation of their currents. On the contrary, two attracting A and B species drift in the same direction. This implies that the transport of the two particle species can be effectively and separately controlled by regulating their numbers n_A and n_B per unit cell, without the need of tuning their substrate.

As $g_{AA},g_{BB}>0$, the potential wells of $V_A^{\mathrm{eff}}(x)$ $[V_B^{\mathrm{eff}}(x)]$ tend to flatten out when the corresponding density n_B $[n_A]$ increases. This results in the decay of the associated ratchet current $\langle v_B\rangle$ $(\langle v_B\rangle)$. In contrast, the ratchet asymmetry and current of one species may be enhanced by increasing the density of the other mixture component. For instance, in the case of AB attractive forces, the A particles tend to concentrate in the regions of higher B densities, that is, around the minima of V_B, thus attracting even more B particles and making the $V_B^{\mathrm{eff}}(x)$ potential wells deeper. In short, one can enhance the transport of the "target" particles by adding a certain amount of auxiliary particles. All these properties have been reproduced analytically in the framework of the nonlinear Fokker-Planck formalism (Savel'ev *et al.*, 2003, 2004b).

The influence of the interspecies interaction on the transport of a binary mixture has been investigated in Savel'ev *et al.* (2004a), where dc and ac external forces were applied at constant temperature, to the particles either of one species only or of both simultaneously. Their main results can be summarized as follows: (i) with increasing intensity of an applied dc driving force, there is a dynamical phase transition from a "clustered" motion of A and B particles to a regime of weakly coupled motion (Marchesoni *et al.*, 2006b); (ii) by applying a time-asymmetric zero-mean drive to the B species only, one can obtain a net current for both the A and B species, even in the absence of a substrate; (iii) when two symmetric ac signals act independently on the A and B particles, and only the particles of one species feel an asymmetric substrate, then the two species can be delivered in the same or opposite direction by tuning the relative signal phase (for both attractive and repulsive AB interactions). Superconducting devices based on these two-species transport mechanisms have been realized experimentally in recent years (Sec. VII.C).

VI. MICROFLUIDICS

Microfluidics (Squires and Quake, 2005) is playing an ever-growing role in controlling transport of particles, or

even whole extended phases, on the microscale and nanoscale. The ability to manipulate the dynamics of liquids is crucial in various applications such as for lab-on-a-chip technology. The Brownian motor concept has recently been invoked in different contexts to face this challenge. In this regard we remark that the inertial forces of small suspended particles are typically quite small (Purcell, 1977). Pointlike particles can then be considered to be advectively transported by the fluid velocity field at the particle's actual position. Then, for an incompressible liquid, the particle dynamics is volume conserving, and consequently no dynamical attractors emerge (Kostur *et al.*, 2006). However, for extended particles the local velocity of a surface point need not coincide with the fluid velocity which would act at this point in the absence of the particle. Notably, for extended objects with internal degrees of freedom the volume of the state space is no longer conserved by the dynamics, thus giving rise to attractors for stationary flow fields (Kostur *et al.*, 2006). Of course, Brownian diffusion provides an additional transport mechanism that must also be taken into account.

We remark here that, in spite of the intrinsic hydrodynamical effects, microfluidic devices do not fall into the category of collective ratchets as defined in Sec. V, because here *transported* objects are not required to interact with one another. The suspension fluid still plays a central role: (a) it powers particle transport, and (b) it determines how the particle dynamics is coupled to the asymmetric geometry of the substrate. Genuine collective ratchets are discussed in Sec. VII.

A. Transporting colloids

Many physical examples and technological applications involve particles or molecules in solution that undergo a directed net motion in response to the action of a ratchet. There, the ratchet does not induce a mean flow of the solvent itself. For instance, colloidal particles or macromolecules, suspended in solution, move when exposed to a sawtooth electric potential that is successively turned on and off (Rousselet *et al.*, 1994). Electrolytic effects can be avoided by shuttling microsized Brownian polystyrene particles by optically trapping them with repeatedly applied on-off cycles in an optical tweezer, thus mimicking a flashing Brownian motor (Faucheux and Libchaber, 1995; Faucheux *et al.*, 1995; Marquet *et al.*, 2002). As a function of the cycle frequency one can even detect flux reversal of diffusing colloidal spheres in an optical three-state thermal Brownian motor (Lee *et al.*, 2004). This modus operandi of a Brownian motor can therefore be put to work to pump or separate charged species such as fragments of DNA. A micromachined silicon-chip device that transports rhodamine-labeled fragments of DNA in water has been demonstrated with a flashing on-off Brownian motor scheme by Bader *et al.* (1999). Yet other devices are based on ideas and experimental realizations of entropic ratchets (Slater *et al.*, 1997; Duke and Austin, 1998; Ertas, 1998; Chou *et al.*, 1999; van Oudenaarden and Boxer, 1999; Tessier and Slater, 2002) which make use of asymmetry within geometric sieve devices to transport and separate polyelectrolytes.

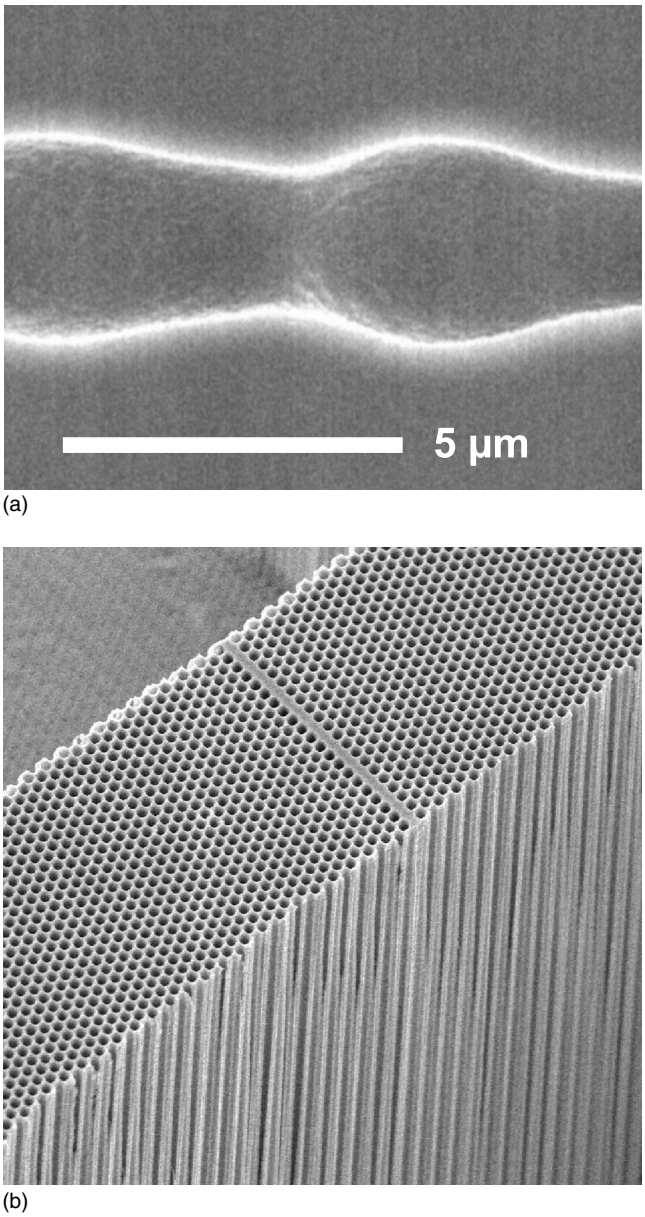

FIG. 17. Artificial porous sieves. (a) Scanning-electron-microscope picture of a single pore with ratchet longitudinal profile. The length of one period is 8.4 μm. The maximum pore diameter is 4.8 μm and the minimum pore diameter is 2.5 μm. (b) Scanning-electron-microscope picture of a silicon wafer pierced by practically identical pores about 1.5 mm apart and 1 mm in diameter. This illustrates the enormous potential for particle separation of a parallel 3D ratchet architecture. Figure provided by Frank Müller.

A similar concept is employed to selectively filter mesoscopic particles through a microfabricated macroporous silicon membrane (Fig. 17), containing a parallel array of etched asymmetrical bottlenecklike pores (Kettner *et al.*, 2000; Müller *et al.*, 2000; Matthias and Müller, 2003). The working principle and predicted particle flow for this microfluidic Browinan motor device

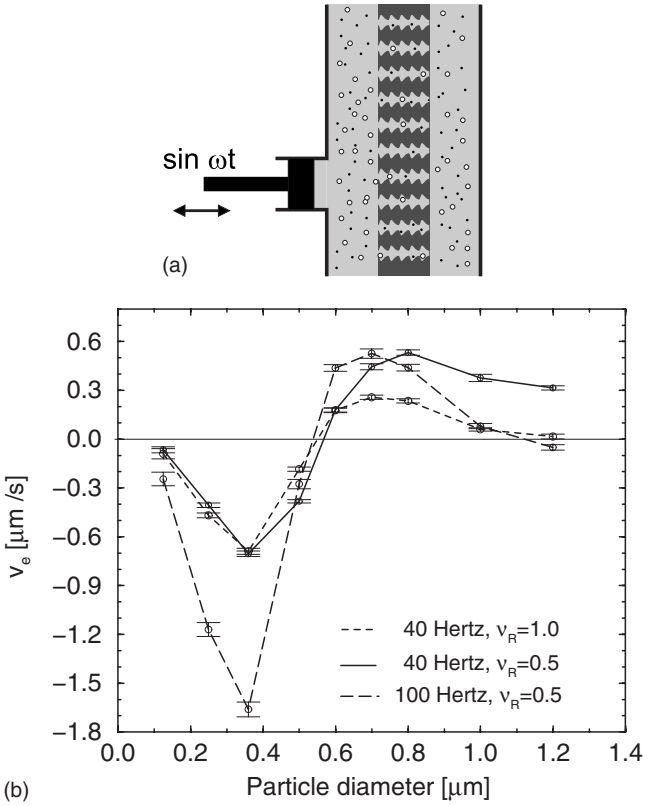

FIG. 18. Microfluidic drift ratchet of Kettner *et al.* (2000). Top panel: A macroporous silicon wafer is connected at both ends to basins. The pores with their ratchet-shaped profile are sketched in dark gray. The basins and pores are filled with liquid; microparticles of two different species are represented. The fluid is pumped back and forth by the piston on the left. Figure provided by Christiane Kettner. Bottom panel: Theoretically predicted net particle current v_e vs the particle diameter for different driving frequencies and viscosities (relative to water) ν_R. Note in particular the very sharp velocity reversal around 0.5 μm. The results are for a pore of infinite length consisting of periodic units with a pore length of $L=6$ μm, a maximum pore diameter of 4 μm, and a minimum pore diameter of 1.6 μm; see Fig. 17(a). For further details see Kettner *et al.* (2000).

are shown in Fig. 18. A fluid such as water containing immersed, suspended polystyrene particles is pumped back and forth with no net bias through the 3D array of asymmetric pores of Fig. 17. Such an artificial Brownian motor is thus kept far away from equilibrium by the periodically varying pressure across the membrane. Due to the asymmetry of the pores, the fluid develops asymmetric flow patterns (Kettner *et al.*, 2000), thus providing a ratchetlike 3D force profile in which a Brownian particle of finite size can (i) undergo Brownian diffusion into liquid layers of differing speed, and/or (ii) become reflected asymmetrically from the pore walls. Both mechanisms will then result in a driven nonequilibrium net flow of particles. Note that the direction of the net flow cannot be easily guessed *a priori*. Indeed, the direction of the Brownian motor current is determined by the interplay of the Navier-Stokes flow in this engineered geometry and hydrodynamic thermal fluctuations.

A detailed quantitative interpretation of the experimental data is plagued by several complications such as the influence of hydrodynamic interactions and, possibly, electric response effects due to residual charge accumulation near the boundaries. A most striking feature of this setup, however, is the distinct dependence of current reversals on particle size. The sharply peaked current-size characteristics curves of this directed flow, that is, the theoretical flow versus size prediction in Fig. 18 and the experimental current-pressure characteristics in Fig. 19, suggest a highly selective particle separation efficiency (Kettner *et al.*, 2000). This microfluidic artificial Brownian device has been implemented in experiments with suspended polystyrene spheres of well-defined diameters (100, 320, 530, and 1000 nm) by Matthias and Müller (2003): Their experimental findings are in good qualitative agrement with the theory as shown in Fig. 19.

Remarkably, this device has advantageous 3D scaling properties: A massively parallel architecture composed of about 1.7×10^6 pores illustrated in Fig. 17 is capable of directing and separating suspended microparticles very efficiently. For this reason, this type of device has clear potential for biomedical separation applications and therapy use.

The separation and sorting of cellular or colloidal particles is definitely a topic attracting wide interest in different areas of biology, physical chemistry and soft matter physics. The powerful toolbox of optical manipulation (Grier, 2003; Dholakia *et al.*, 2007) uses the optical forces exerted on colloids by focused laser beams to move and control objects ranging in size from tens of nanometers to microns. If the optical forces are sufficiently strong to rule transport, the stochastic Brownian forces play only a minor role, so that transport occurs as a deterministic process with an efficiency close to unity, a circumstance known as (optical) peristalsis (Koss and Grier, 2003; Bleil *et al.*, 2007). Such a scheme can then be implemented to experimentally realize ratchet cellular automata capable of performing logical operations with interacting objects. All together, in combination with this new optical technology, colloids provide ideal model systems to investigate statistical problems near and far away from thermal equilibrium (Babic and Bechinger, 2005; Babic *et al.* 2005).

B. Transporting condensed phases

Most present applications use ratchet concepts to transport or filter discrete objects, like colloidal particles or macromolecules. However, ratchets may also serve to induce macroscopic transport of a continuous phase using local gradients only. One such realization, strongly related to the above cases of particle transport in a "resting" liquid phase, is the Brownian motion of magnetic particles in ferrofluids subjected to an oscillating magnetic field (Engel and Reimann, 2004). In contrast to the cases reported above, here the motion is also transmitted to the solvent by viscous coupling.

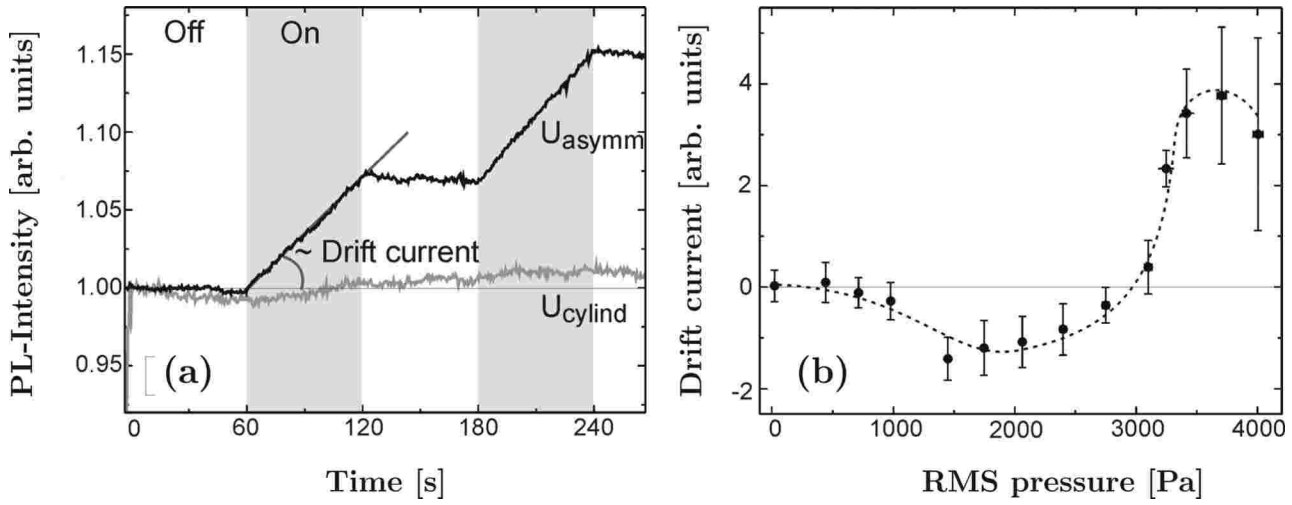

FIG. 19. Operating a microfluidic drift ratchet. Parallel Brownian motors in a macroporous silicon membrane containing approximately 1.7×10^6 asymmetric pores with 17 etched modulations each (see Fig. 17, top panel). (a) When the pressure oscillations of the water are switched on, the measured photoluminescence signal and thus the number of particles in the basin located to the right (see top panel of Fig. 18) increases linearly in time, corresponding to a finite transport velocity. In contrast, for symmetric cylindrical-shaped pores no net drift is observed. (b) The experimentally observed net transport behavior strongly depends on the amplitude of the applied pressure and qualitatively shows the theoretically predicted current inversion (Kettner *et al.*, 2000). The pressure oscillations are toggled on and off each 60 s. Other experimental parameters are as follows: the suspended luminescent polystyrene spheres in water are 0.32 μm across, the frequency of the pressure oscillations is 40 Hz, and the root mean square (rms) of the applied pressure during the "on" phase is 2000 Pa. A control experiment using straight cylindrical pores with a diameter of 2.4 μm showed no directed Brownian motor transport. Image: Max-Planck-Institute of Microstructure Physics, Halle, Germany.

Another class of system does not require colloidal particles to drive the motion of the liquid phase. In a first example, a secondary large scale mean flow is triggered in Marangoni-Bénard convection over a solid substrate with asymmetric grooves (Stroock *et al.*, 2003). The direction and strength of the mean flow can be controlled by changing the thickness of the liquid layer and the temperature gradient across the layer.

Yet another intriguing situation involves self-propelled Leidenfrost drops placed on a hot surface also with a ratchetlike grooved profile (Fig. 20). The locally asymmetric geometry of the support induces a directed drop motion. This effect has been observed for many liquids and in wide temperature ranges within the film boiling (Leidenfrost) regime (Linke *et al.*, 2006; Quéré and Ajdari, 2006).

Moreover, microdrops confined to the gap between asymmetrically structured plates move when drop shape or wetting properties are changed periodically, for instance by vibrating the substrate, applying an on-off electric field across the gap or a low-frequency zero-mean electric field along the gap (Gorre *et al.*, 1996; Buguin *et al.*, 2002). In a related experiment, the motion of drops on a global wettability gradient was strongly enhanced when a periodic force was applied (Daniel *et al.*, 2004). In that work the ratchet aspect was determined by the intrinsically asymmetric shape of the drops and the hysteresis of their contact angle on the gradient substrate.

The theory for particle transport operated by Brownian motors is presently well developed (Hänggi and Bartussek, 1996; Astumian, 1997; Jülicher *et al.*, 1997; Astumian and Hänggi, 2002; Reimann and Hänggi, 2002; Hänggi *et al.*, 2005). In clear contrast, models for ratchet-driven transport of a continuous phase are rather scarce, although the concept is thought to be important for emerging microfluidic applications (Squires and Quake, 2005).

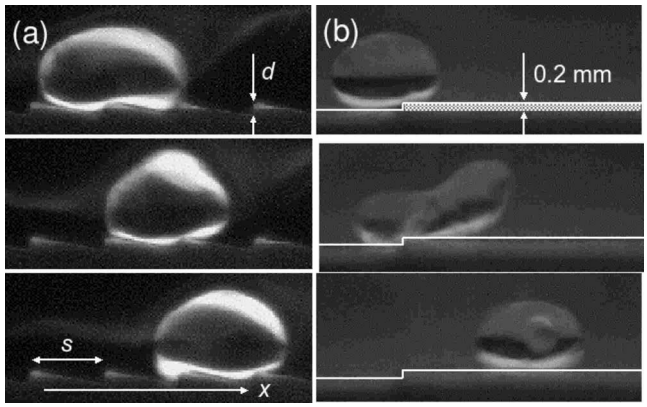

FIG. 20. Self-propelled droplets. (a) Video sequence (time interval 32 ms) demonstrating droplet motion perpendicular to a thermal gradient. A droplet of the refrigerant tetrafluorethane (R134a; boiling point $T_b=26.1\,^\circ$C) was placed on a room-temperature, horizontally leveled, brass surface with a ratchet-like grooved profile ($d=0.3$ mm, $s=1.5$ mm). (b) Droplet of liquid nitrogen on a flat surface moving with a small initial velocity toward a piece of tape (shaded). Figure provided by Heiner Linke.

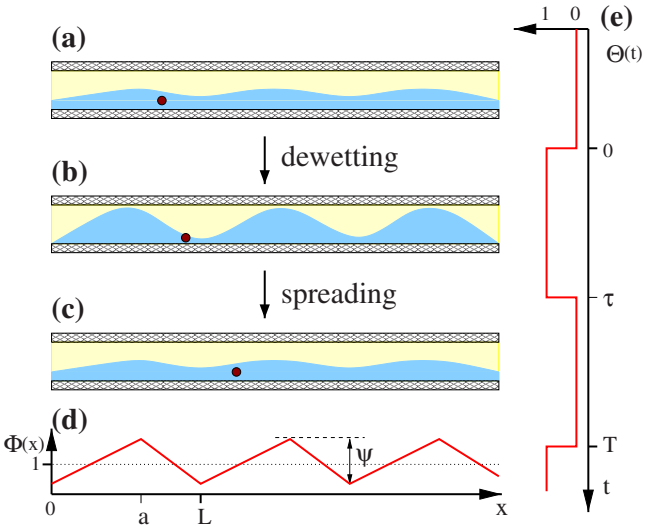

FIG. 21. (Color online) Fluidic ratchet. (a)–(c) Illustration of the working principle of a fluidic ratchet based on dewetting-spreading cycles. (d) The spatial asymmetric periodic interaction profile $\Phi(x)$ responsible for the wettability pattern and (e) the time dependence $\Theta(t)$ of the switching in relation to the dewetting and spreading phases (a)–(c). The filled circle indicates a fluid element that gets transported during one ratchet cycle although the evolution of the interface profile is exactly time periodic. For further details and resulting directed flow pattern, see John *et al.* (2008).

In recent work, a model for the flow of two immiscible layered liquids confined between two walls and driven by a flashing wettability ratchet has been put forward by John and Thiele (2007) and John *et al.* (2008). Here one employs the general concept of wettability comprising all effective interactions between the liquid-liquid free interface and the solid walls. Notably, any interaction that is applicable in a time-periodic, spatially periodic (but locally asymmetric) fashion is capable of driving a flow, i.e., will result in directed transport. There exist several possibilities for experimental realizations of spatially inhomogeneous and time-switching interactions. A practical setup consists of thin films of dielectric liquids in a capacitor with a periodic, locally asymmetric voltage profile, that can be periodically switched on and off. A spatially homogeneous electric field would destabilize the interface between two dielectric liquids. Therefore an on-off ratchet with a constant lateral force can result in the dewetting-spreading cycle sketched in Fig. 21. The process underlying this motor scheme may be termed "electro dewetting."

C. Granular flows

The concept of ratchet physics found an early application in the field of granular matter (Jaeger *et al.*, 1996). Indeed, to explain the vertical grain size segregation under vibration, the so-called *Brazil-nut* effect (Rosato *et al.*, 1987), Bug and Berne (1987) initially investigated directed diffusion in sawtoothlike inclined grooves. In the meantime, this problem spurred several computer simulations aimed at exploring granular ratchets. Another unusual phenomenon, observed both experimentally and in computer simulations, is horizontal size segregation. It involves the occurrence of horizontal flows of granular layers that are vibrated vertically on plates whose surface profile consists of sawtoothlike grooves (Derényi and Vicsek, 1995; Rapaport, 2002).

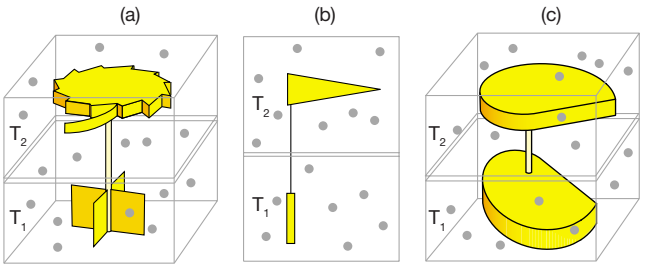

FIG. 22. (Color online) Taming thermal motion. (a) A schematic representation of the Smoluchowski-Feynman rachet device, which is able to rectify thermal Brownian motion of gases held at two different temperatures (Feynman *et al.*, 1963). An idealized version suitable for computer studies is presented in (b) with the ratchet replaced by a triangular unit and the pawl replaced by a rigidly joined blade residing in the lower gas compartment. (c) A 3D rotational construction. Figure provided by C. Van den Broeck.

The spontaneous anelastic clustering of a vibrofluidized granular gas has been employed, for instance, to generate phenomena such as granular fountains (convection rolls) and ratchet transport in compartmentalized containers, where symmetry-breaking flow patterns emerge perpendicular to the direction of the energy input (Eggers, 1999; Brey *et al.*, 2001; Farkas *et al.*, 2002; van der Meer *et al.*, 2004). Granular systems exhibit a rich scenario of intriguing collective transport phenomena, which have been tested and validated both computationally and experimentally (van der Meer *et al.*, 2007).

All these systems are kept away from thermal equilibrium by vertical vibrations, while the presence of random perturbations plays a role as a source of complexity, due to the intrinsically chaotic nature of granular dynamics. Closer in spirit to the present review are, however, those devised granular Brownian motors which are truly capable of putting thermal Brownian motion at work (Cleuren and Van den Broeck, 2007; Costantini *et al.*, 2007, 2008). In those setups, an asymmetric object of mass m (Fig. 22) is free to slide, without rotation, in a given direction. Its motion with velocity v is induced by *dissipative* collisions with a dilute gas of surrounding particles of average temperature T. On each collision, only a certain fraction (called the restitution coefficient) of the total kinetic energy of the object-particle system is conserved. At variance with the case of elastic collisions, here isotropy, implying $\langle v\rangle=0$, and energy equipartition, implying $\langle v^2\rangle=kT/m$, do not apply: Dissipation is responsible for breaking the time-reversal symmetry. As a result one finds that the asymmetric object undergoes a directed random walk with nonzero average velocity, which can be modeled in terms of an effective biased

Langevin dynamics for the velocity variable v. Such a Langevin dynamics assumes the form of an Ornstein-Uhlenbeck process (Hänggi and Thomas, 1982; Risken, 1984) governed by an effective Stokesian friction and an effective external force, both depending on the restitution coefficient (Cleuren and Van den Broeck, 2007; Costantini *et al.*, 2007). The directed motion of the object is accompanied by a continuous flow of heat from the gas to the object, in order to balance the dissipation of the collisional processes; as a consequence, the average temperature of the asymmetric object is lower than the gas temperature.

Ever since the formulation of the second law of thermodynamics there have been debates about its validity at the small scales. In this context the ratchet gadget by Smoluchowski (1912) and later popularized by Feynman *et al.* (1963) points at the heart of a controversy, which concerns the very working principle of Brownian motors: To be consistent with this law, no rectification of thermal fluctuations can take place at thermal equilibrium, at which all dynamics is intrinsically governed by the principle of detailed balance. A steadily working Brownian motor necessarily requires a combination of asymmetry and nonequilibrium, such as a temperature gradient. This point has been convincingly elucidated in recent molecular dynamics studies by Van den Broeck and collaborators (Van den Broeck *et al.*, 2004, 2005; Van den Broeck and Kawai, 2006), who stylized a Maxwell demon operating far away from equilibrium (Fig. 22). Several computer versions of Smoluchowski-Feynman ratchets operating in a dilute gas of colliding granular particles have thus been confirmed to generate directed transport in the presence of a finite temperature difference. With the possibility of today's observation and manipulation of physical, chemical, and biological objects at the nanoscale and mesoscale, such devices no longer represent a theorist's thought experiment, but are rather becoming a physical reality. It is right on these length scales that thermal fluctuations cannot be ignored, as they combine with nonequilibrium forces to yield constructive transport.

VII. SUPERCONDUCTING DEVICES

Magnetic vortices in type-II superconducting devices provide a flexible and experimentally accessible playground for testing our stochastic transport models. In recent years an impressive effort has been directed toward the design and operation of a new generation of vortex devices with potential applications to terahertz (THz) technology (Hechtfischer *et al.*, 1997; Zitzmann *et al.*, 2002), fluxon circuitry (Shalóm and Pastoriza, 2005), and quantum computation (You and Nori, 2005), to mention but a few. We anticipate that magnetic vortices are inherently quantum objects that, under most experimental conditions, behave like (massless, pointlike) classical particles. Genuine quantum effects in the vortex transport are discussed in Sec. VIII.

A magnetic field applied to a type-II superconducting film, with intensity H comprised between the critical values H_{c1} and H_{c2}, penetrates into the sample producing supercurrent vortices, termed Abrikosov vortices (Abrikosov, 1957; Blatter *et al.*, 1994). The supercurrent circulates around the normal (i.e., nonsuperconducting) core of the vortex; the core has a size of the order of the superconducting coherence length ξ (parameter of a Ginzburg-Landau theory); the supercurrents decay on a distance λ (London penetration depth) from the core. In the following we assume that $\lambda \gg \xi$. The circulating supercurrents produce magnetic vortices, each characterized by a total flux equal to a single flux quantum $\Phi_0 = hc/2e$ (hence the name fluxon for magnetic vortex) and a radially decaying magnetic field

$$B(r) = B_0 K_0(r/\lambda), \tag{39}$$

where $K_0(x)$ is a modified Bessel function of zeroth order and $B_0 = \Phi_0/(2\pi\lambda^2)$. Far from the vortex core, $r \gg \lambda$, the field decays exponentially $B(r)/B_0 = \sqrt{\lambda\pi/2r}e^{-r/\lambda}$, whereas, approaching the vortex center, it diverges logarithmically for $\xi < r \ll \lambda$, $B(r)/B_0 = \ln(\lambda/r)$, and then saturates at $B(0) = B_0 \ln(\lambda/\xi)$ inside the core, $r < \xi$. As a consequence, the coupling between vortex supercurrents and magnetic fields determines a long-range repulsive vortex-vortex interaction.

Due to mutual repulsion, fluxons form a lattice (also called the Abrikosov vortex lattice, usually triangular, possibly with defects and dislocations) with average vortex density ρ approximately equal to H/Φ_0. A local density $\mathbf{I}$ of either a transport current or a magnetization current or both exerts on each fluxon a Lorentz force $\mathbf{F}_L = \Phi_0 \mathbf{I} \times \mathbf{H}/cH$.

The distribution and microscopic properties of pinning centers can qualitatively influence the thermodynamic and vortex transport properties of the superconducting sample. Pinning forces created by isolated defects in the material oppose the motion of the fluxons, thus determining a critical (or threshold) current, below which the vortex motion is suppressed. Many kinds of artificial pinning centers have been proposed and developed to increase the critical current, ranging from the dispersal of small nonsuperconducting second phases to creation of defects by irradiation (Altshuler and Johansen, 2004). A novel approach to the problem came with advances in lithography, which allowed for regular structuring and modulation of the sample properties over a large surface area (Harada *et al.*, 1996). Long-range correlation in the position of the pinning centers resulted in the interplay between the length scales characterizing the pin lattice and the vortex lattice. Indeed, the magnitude of the commensuration effects is readily controlled by tuning the intensity of the magnetic field H: at the first matching field $H_1 = \Phi_0/a_l$, pin and vortex lattices are exactly commensurate, with one fluxon per pin lattice cell of area a_l; at the nth matching field $H(n) = nH_1$, each pin lattice cell is occupied by $n = \rho a_l$ fluxons; for irrational H/H_1, pin and vortex lattices are incommensurate. Commensuration effects are responsible for a variety of dynamical superconducting states

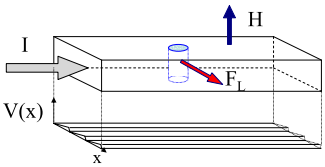

FIG. 23. (Color online) Diagram of a superconductor in the presence of an external magnetic field H. A direct current with density I flowing along the y direction (indicated by the large arrow) induces a Lorentz force F_L that moves the vortex in the x direction (upper panel). The superconductor is patterned with a pinning potential (lower panel). The potential is periodic and asymmetric along the x direction, and is invariant under translation along y; the potential $V(x)$ is an effective ratchet potential (see Sec. II.D).

of relevance to the problem of vortex rectification (Reichhardt *et al.*, 1998).

As a first attempt to design a vortex ratchet, Lee *et al.* (1999) showed that an ac electric current applied to a superconductor patterned with the asymmetric pinning potential shown in Fig. 23 can induce vortex transport whose direction is determined only by the asymmetry of the pattern. The fluxons were treated as zero-mass pointlike particles moving on a sawtooth potential along the x axis, according to the scheme of Sec. II.D.1. They demonstrated theoretically that, for an appropriate choice of the pinning potential, such a rocked ratchet can be used to manipulate single vortices in superconducting samples under realistic conditions. The rectification mechanisms of an extended overdamped string, like a fluxon, on a ratchet potential had been anticipated by Marchesoni and co-workers (Marchesoni, 1996; Costantini *et al.*, 2002). Brownian motor ratcheting of single oscillating fluxons have been observed experimentally in asymmetrically etched Nb strips (Plourde *et al.*, 2000), on planar patterns of columnar defect (Kwok *et al.* 2002), and in asymmetric linear arrays of underdamped Josephson junctions (Lee, 2003), and in an annular Josephson junction (Ustinov *et al.*, 2004), to mention just a few recent experiments.

A. Fluxon channels

A more viable approach to achieve controllable stochastic transport of fluxons in superconducting devices consists of exploiting collective boundary effects as suggested in Sec. V.A.1. Fluxon rectification in asymmetric channels has been investigated by Wambaugh *et al.* (1999) by means of a molecular dynamics (MD) code, originally developed to study magnetic systems with random and correlated pinning (Reichhardt *et al.*, 1998). They simulated a thin slice of a zero-field-cooled, type-II superconducting slab, taken orthogonal to the magnetic vortex lines generated by a tunable external magnetic field of intensity H. When regarded as fairly rigid field structures, magnetic vortices formed a confined 2D gas of zero-mass repelling particles with density $\rho = H/\Phi_0$. The simulated sample had very strong, effectively infinite pinning except for the "zero pinning" central

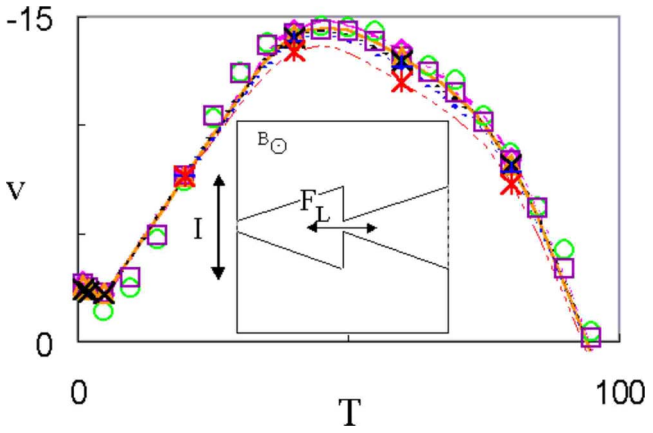

FIG. 24. (Color online) Rectified average fluxon velocity $\langle v \rangle$ (in units of λ/τ) vs T for the sawtooth channel geometry in the inset (width, 7λ, bottleneck, λ). The magnetic field H is directed out of the figure. A vertically applied alternating current square wave drives the fluxons back and forth horizontally along the channel with period $\tau = 100$ MD steps. The number of fluxons per unit cell is 1 (circles), 25 (diamonds), 50 (squares), 75 (triangles), 100 (×), 150 (+), 250 (∗). From Wambaugh *et al.*, 1999.

sawtooth-shaped channel, sketched in the inset of Fig. 24. In the channel fluxons moved subject to fluxon-fluxon repulsions, an externally applied ac driving Lorentz force, forces due to thermal fluctuations, and strong damping. The fluxons outside the channel could not move, thus impeding the movable fluxons in the middle from crossing the channel walls. As a consequence, the interaction length of the fluxon-wall collisions was the same as of the fluxon-fluxon collisions. The net fluxon velocity $\langle v \rangle$ vs temperature shown in Fig. 24 is negative and exhibits an apparent resonant behavior, vs both T and H (i.e., the fluxon density ρ), as anticipated in Sec. V.A.1.

These conclusions have been corroborated experimentally by Togawa *et al.* (2005) and Yu *et al.* (2007). The more recent work fabricated triangular channels from bilayer films of amorphous niobium germanium, an extremely weak-pinning superconductor, and niobium nitride (NbN), with relatively strong pinning. A reactive ion etching process removed NbN from regions as narrow as 100 nm, defined with electron-beam lithography, to produce weak-pinning channels for vortices to move through easily. In contrast, vortices trapped in the NbN banks outside of the channels remain strongly pinned. The vortex motion through such asymmetric channels exhibited interesting asymmetries in both the static depinning and the dynamic flux flow. The vortex ratchet effect thus revealed a even richer dependence on magnetic field and driving force amplitude than anticipated by the simplified model simulated by Wambaugh *et al.* (1999).

Devices like that simulated in Fig. 24 serve as excellent fluxon rectifiers. By coupling two or more such devices, one can design fluxon lenses, to regulate the fluxon concentration in chosen regions of a sample, and

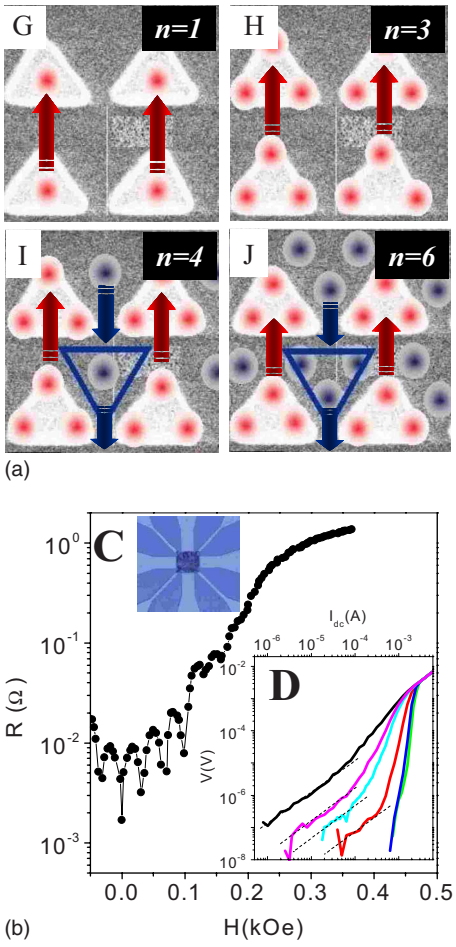

FIG. 25. (Color online) Experimental implementation of a 2D sieve for magnetic vortices. (a) Sketch of the positions of the vortices for several matching fields $H(n)$, i.e., for n vortices per unit cell. Vortices pinned on the triangles (no more than three per unit cell) and interstitial vortices are shown. The pinning substrate is a square lattice with constant 750 nm; the triangular pinning sites have been grown on a Si support, are 40 nm thick with side about 600 nm long. (b) dc magnetoresistance $R(H)$ vs H. The temperature is $T=0.98T_c$ and the injected dc current density is $I_{dc}=12.5$ kA cm^{-2}. The upper inset shows a micrograph of the measuring bridge, which is 40 μm wide. The darker central area of the inset is the (90×90)-μm^2 array of magnetic triangles. The lower inset shows the characteristics curves $V_{dc}-I_{dc}$ at the matching magnetic fields $H(n)=nH_1$ with $H_1=32$ Oe and $n=1$, 3, 4, 6, 8, and 10 (top to bottom). The $V(I_{dc})$ curves change abruptly at magnetic fields from $n=3$ to 4, because an Ohmic regime appears at low currents. This is a clear signature of the presence of interstitial vortices. From Villegas *et al.*, 2003.

eventually channel networks or circuits for fluxons in superconducting films.

Fluxon channeling was observed first experimentally in an effective 1D vortex rectifier by Villegas *et al.* (2003). Their device has the pedagogical merit of showing all collective transport effects summarized in Sec. V at work. A 100-μm-thick niobiun film was grown on an array of nanoscale triangular pinning potentials oriented as in Fig. 25(a), with bases lined up along the x axis and vertices pointing in the y direction. Magnetoresistance $R(H)$ experiments were done with a magnetic field H applied perpendicular to the substrate in a liquid helium system. The dc magnetoresistance curves in the bottom panel of Fig. 25 exhibit commensurability effects in which dissipation minima develop as a consequence of the geometrical matching between the vortex lattice and the underlying periodic structure. At these matching fields, the vortex lattice motion slows down, and $R(H)$ minima appear at the equally spaced values $H(n)=nH_1$, with $H_1=32$ Oe. The $R(H)$ minima are sharp at the $n=1,2,3$ matching fields, but shallow and not well defined for higher n. This effect is a consequence of the appearance of interstitial vortices at increasing H beyond H_3, three being the maximum number of vortices contained in each triangle.

In order to interpret the experimental results, one separates all vortices in two groups: (i) pinned vortices, which move from one triangular-shaped pinning trap to another one and thus are directly affected by an effective 1D rocked ratchet substrate with positive polarity in the y direction; and (ii) interstitial vortices, which are channeled in-between triangles and do not directly interact with the pinning traps (Savel'ev *et al.*, 2003; Zhu, Marchesoni, Moshchalkov, *et al.*, 2003). However, as is apparent in the top panel of Fig. 25 and discussed in Sec. V.C, pinned vortices, being strongly coupled to the substrate potential, determine a weaker mean-field potential that acts on the interstitials with opposite asymmetry (Savel'ev *et al.*, 2003). As a consequence, when all fluxons are subjected to the same ac drive force, the fluxon-fluxon repulsion pushes the interstitials in the direction opposite to the pinned vortices (for an animation see http://dml.riken.go.jp/vortex).

The effects of this mechanism are illustrated in Fig. 26. At constant temperature (close to T_c to avoid random pinning) and H multiple of H_1, an ac current density $I(t)=I_{ac}\sin(\Omega t)$ was injected along the x axis. This yields a sinusoidal Lorentz force with amplitude F_L acting on the vortices along the y axis. Despite the zero time average of such Lorentz force, a nonzero dc voltage drop V_{dc} in the x direction was measured, thus proving that the vortices actually drift in the y direction. Note that, due to the peculiar substrate symmetry, an ac current $I(t)$ oscillating along the y axis can rectify the fluxon motion only parallel to it (transverse rectification, Sec. VII.B). The amplitude of the dc voltage signal decreases with increasing H because the effective pinning is suppressed by the intervortex repulsion. Moreover, when $n>3$ (corresponding to more than three vortices per unit cell), a reversed V_{dc} signal begins to develop with a maximum occurring at a lower Lorentz force F_L than the positive dc maxima: The interstitials, which feel a weak inverted ratchet potential with respect to the pinned vortices, dominate the rectification process. This current reversal effect is enhanced when further increasing the magnetic field [Figs. 26(c) and 26(d)] and finally, at very high magnetic fields, close to the normal state, the voltage reversal, although suppressed in magnitude,

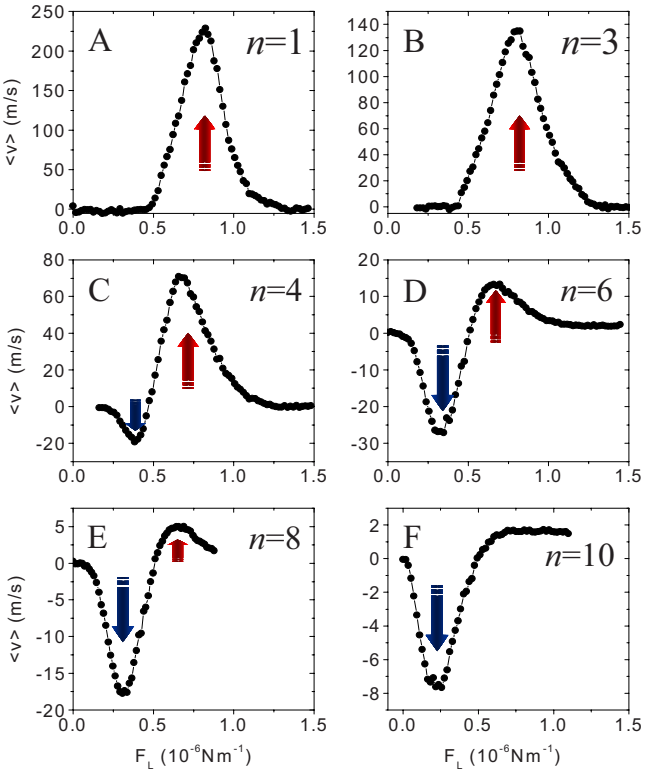

FIG. 26. (Color online) Vortex current in a 2D sieve. (a)–(f) Net velocity $\langle v \rangle$ of vortices vs the amplitude F_L of the ac Lorentz force for $\Omega = 10$ kHz and different matching magnetic fields $H(n)$; other parameter values are as in Fig. 25. Arrows show the direction of the net flow, dominated, respectively, by the pinned and the interstitial vortices [see Fig. 25(a)]. From Villegas *et al.*, 2003.

spans over the entire F_L range [Fig. 26(f)].

Moshchalkov and co-workers (Silva *et al.*, 2006; de Vondel *et al.*, 2007) also demonstrated longitudinal fluxon rectification. Silva *et al.* (2006) observed multiple current reversals in regular square lattices of asymmetric double-well traps periodically driven along an easy direction, as in the simulations by Zhu and co-workers (Zhu, Marchesoni, Moshchalkov, *et al.*, 2003; Zhu, Marchesoni, and Nori, 2003). More interestingly, de Vondel *et al.* (2007) detected inverted fluxon currents in large triangular arrays, similar to those reviewed here, but at magnetic fields (or fluxon densities) so high that a collective ratchet mechanism would not be plausible. They attributed their finding to a new intra-antidot rectification mechanism controlled by the magnetic flux quantization condition synchronously satisfied at the edge of each asymmetric antidot. Finally, Silva *et al.* (2007) detected vortex rectification also as a dipole-induced effect in reducible symmetric arrays of micromagnets.

B. Fluxon rectification in 2D arrays

The rectification of a fluxon lattice, no matter how distorted or disordered, is an inherently 2D process. Following the theoretical and numerical investigations reviewed in Sec. V.B, a number of experimental groups [Crisan *et al.* (2005); Menghini *et al.* (2007); Van Look *et al.* (2002) to mention a few] prototyped devices aimed at controlling vortex ratcheting in both directions parallel (longitudinal rectifiers) and perpendicular (transverse rectifiers) to an applied ac Lorentz force.

Longitudinal transport in a 2D array of asymmetric pinning traps has been experimentally obtained, for instance, by de Vondel *et al.* (2005), who reported that, under appropriate operating conditions, fluxon rectification can be enhanced for F_L amplitudes comprised between two critical pinning forces of the underlying asymmetric substrate. The shape of the net dc voltage drop $V_{\rm dc}$ as a function of the drive amplitude indicated that their vortex ratchet behaved differently from standard overdamped models. Rather, as the repinning force necessary to stop vortex motion is considerably smaller than the depinning force, their device resembles the behavior of the inertial ratchets of Sec. II.D.1. More recently, Shalóm and Pastoriza (2005) reported longitudinal fluxon rectification in square arrays of Josephson junctions, where the coupling energies had been periodically modulated along one symmetry axis. Similarly, longitudinal fluxon rectification has also been observed in square arrays of magnetic dots with size-graded period (Gillijns *et al.*, 2007). Both are experimental implementations of the asymmetric patterns of symmetric traps introduced in Sec. V.A.2. Finally, Ooi *et al.* (2007) trapped symmetric fluxon lattices in a triangular dot lattice that they had photolithographed on a thin $Bi_2Sr_2CaCu_2O_{8+\delta}$ (Bi2212) single-crystal film, by setting the applied magnetic field at the lowest multiples of H_1. By subjecting the fluxon lattice to a biharmonic Lorentz force oriented along the crystallographic axes of the dot lattice, they obtained demonstration of harmonic mixing on a symmetric substrate. However, the results of these experiments can be easily explained also in terms of simple 1D models.

Transverse transport, instead, requires genuinely irreducible 2D geometries. When designing and operating a device capable of transverse rectification, experimenters can vary the orientation of the pinning lattice axes, the symmetry axes of the individual traps (if any), and the direction of the injected current (i.e., of the Lorentz force). Many have explored by numerical simulation the geometries best suited for the experimental implementation of this concept (Zhu *et al.*, 2001; Reichhardt and Reichhardt, 2005). The most recent realizations of transverse fluxon rectifiers fall into two main categories.

1. Symmetric arrays of asymmetric traps

Gonzalez *et al.* (2007) modified the experimental setup of Villegas *et al.* (2003) to investigate the rectification mechanisms presented in Secs. V.A and V.B. They confirmed the numerical simulations by Savel'ev *et al.* (2005), who had predicted that the same device can exhibit either longitudinal or transverse output current depending on orientation of the ac drive with respect to the pinning lattice axes. In the longitudinal ratchet con-

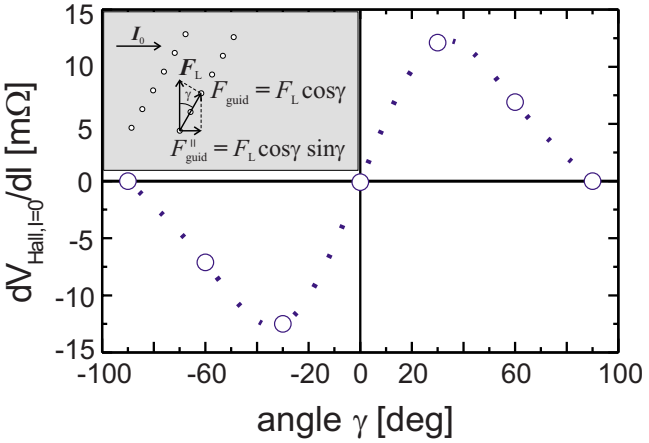

FIG. 27. (Color online) Angular dependence of R_H measured on a circular shaped 90-nm-thick sample at $T=30$ K, $H=143$ mT, and with dc current $I_{dc}=10$ mA. Inset: Portion of a 20 μm$\times$10 μm rectangular lattice of circular antidots with radius of 1 μm; I_{dc} is horizontally oriented from left to right corresponding to a Lorentz force F_L pointing upward. The angular dependence is fitted by the sinusoidal law $\sin 2\gamma$, as sketched in the inset. From Wördenweber *et al.*, 2004.

figuration a sinusoidal driving current $I(t)$ was applied perpendicular to the triangle reflection symmetry axis (x axis) and the output voltage signal V_{dc} was recorded in the same direction. We recall that the Lorentz-force-induced vortex motion, parallel to the triangle reflection symmetry axis (y axis), corresponds to a voltage drop in the direction of the injected current. To observe an optimal transverse rectification effect, the axes of the current injection and the voltage drop were inverted. The asymmetry of the traps with respect to the direction of the Lorentz force is responsible for the observed fluxon drift in the y direction.

The number n of vortices per lattice cell was controlled by varying the intensity of the magnetic field orthogonal to the device, $H=nH_1$. On increasing n, the voltage associated with the longitudinal ratchet current changes sign and gets amplified, as is to be expected due to the presence of the $n-3$ interstitials per unit cell (Sec. VII.A). The H dependence of the transverse fluxon rectification is very different: (i) the transverse net current shows no inversions; (ii) increase in the number of interstitials suppresses transverse rectification.

2. Asymmetric arrays of symmetric traps

Controlled transport of vortices through rows of antidots was measured by Wördenweber *et al.* (2004) via standard four-probe Hall-type experiments (Altshuler and Johansen, 2004). (100–150)-nm-thick $YBa_2Cu_3O_2$ films were deposited on CeO_2 buffered sapphire and then covered with a 50-nm-thick Au layer. Asymmetric lattices of symmetric antidots in the shope of circular microholes were patterned via optical lithography and ion beam etching. The inset of Fig. 27 shows a typical antidot lattice. A tunable dc current I_{dc} was then injected so that the corresponding Lorentz force $\mathbf{F}_L$ was at an angle γ with respect to the orientation of the antidot rows.

Reference measurements on samples without antidots as well as temperature-dependent measurements of the Hall resistance R_H for different angles γ clearly indicate that, for $T<83$ K and low dc drive current, the Hall resistance is dominated by the directed vortex motion along the antidot rows. Under these circumstances, R_H quantifies the fluxon current in the direction of the dc current I_{dc} (with negative Hall voltage), or, equivalently, *transverse* to the drive force $\mathbf{F}_L$. In view of the symmetry of the traps, for currents perpendicular to the antidot rows, no transverse fluxon current was observed; as shown in Fig. 27, changing the sign of γ led to inversion of the transverse current. Most notably, the detected drift was not restricted by a current threshold, that is, fluxons seemed not to jump from antidot to antidot, like individual vortices in a defective superconductor sample (Sec. V.A.2), but rather to obey an Ohmic behavior. The absence of an activation threshold was explained by Wördenweber *et al.* (2004) by invoking a combination of (i) finite-size effects, as the area where vortices can be nucleated is severely restricted by the device geometry; and (ii) screening effects, as trapped fluxons induce spatially nonuniform current distributions around neighboring antidots. Due to current screening, the antidot rows serve as easy-flow (i.e., thresholdless) paths for the driven vortices, which thus acquire a transverse velocity proportional to $\sin 2\gamma$ (see Fig. 27).

At higher temperatures and stronger drives, this effect becomes negligible and no transverse rectification was detected (Wördenweber *et al.*, 2004). Moreover, on replacing I_{dc} with a symmetric ac drive $I_{ac}(t)$, no net current is expected, either longitudinal or transversal.

C. Anisotropic fluxon rectifiers

Transport control in a binary mixture can be achieved in samples with no ratchet substrate. As reported in Sec. V.C, when one component of the binary mixture is driven, the moving particles drag along the other nondriven component, interacting with it. A time-asymmetric ac drive produces rectification of both components of the binary mixture, which can be tuned by means of the ac drive parameters. The device acts like a ratchet, but it has no ratchet substrate.

Savel'ev and Nori (2002) proposed to implement this new ratchet concept in a layered superconductor. In this class of materials, a magnetic field, tilted away from the high-symmetry crystalline c axis, penetrates the sample as two perpendicular vortex arrays (Ooi *et al.*, 1999; Grigorenko *et al.*, 2001; Matsuda *et al.*, 2001), known as "crossing" vortex lattices (Koshelev, 1999). One vortex sublattice consists of stacks of pancake vortices (PVs) aligned along the c axis, whereas the other is formed by Josephson vortices (JVs) confined between CuO_2 layers (Fig. 28). A weak attractive PV-JV interaction has been experimentally observed (Grigorenko *et al.*, 2001). The JVs are usually very weakly pinned and can be easily

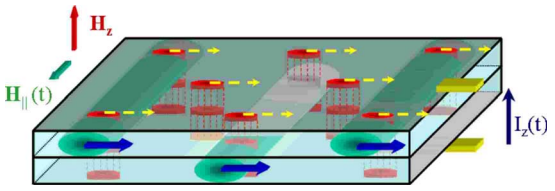

FIG. 28. (Color online) Vortex lensing mechanisms. Subjected to a superposition of dc and time asymmetric ac in-plane magnetic fields, $H_{\parallel}(t)=H_{\parallel}^{\mathrm{dc}}+H_{\parallel}^{\mathrm{ac}}(t)$, the JVs (horizontal cylinders) are asymmetrically pushed in and out of the sample. If the ac component of $H_{\parallel}(t)$ increases slowly, the PV stacks (pancakes) remain trapped by the JVs, and both move together toward the center of the lens. If, on the way back, $H_{\parallel}^{\mathrm{ac}}(t)$ decreases rapidly, the JVs leave the PVs behind them. Courtesy of Sergey Savel'ev.

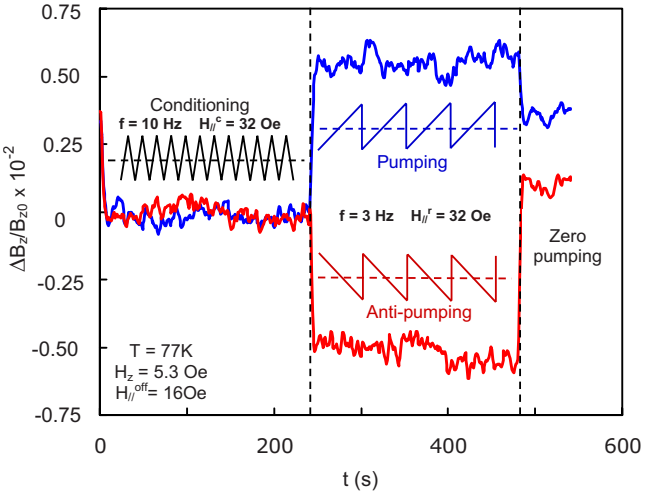

FIG. 29. (Color online) Vortex lens operation. The curves show the measured percentage change of the magnetic induction (PV density) at the sample center, when an initial conditioning signal is applied, followed by pumping and antipumping time-asymmetric drives. The conditioned PV density increases (decreases) during several cycles of the pumping (antipumping) drive and then saturates. As soon as the drive is switched off, the PV density starts to relax from the nonequilibrium pumping (antipumping) state toward an equilibrium state. Courtesy of Sergey Savel'ev.

driven either by changing the in-plane magnetic field $H_{\parallel}$ or by applying an electrical current I_z flowing along the c axis.

Time-asymmetrically-driven JVs can drag along the PVs, thus causing a net motion of the PVs, as illustrated in Fig. 28. The simplest possible operating mode consists of slowly increasing the in-plane field $H_{\parallel}$ from 0 to $H_{\parallel}^{\max}$ for a fixed value of the out-of-plane magnetic field H_z. The increasing in-plane field slowly drives the JVs from the edges to the middle of the sample. In turn, the JVs drag the PVs along with them toward the sample center. As a result, asymmetric cycling causes either pumping (focusing) or antipumping (defocusing) of the PVs at the center of the lens.

Cole *et al.* (2006) performed a vortex lensing experiment on an as-grown single Bi2212 crystal. The changes in magnetic induction, arising from PV lensing and antilensing, were detected using one centrally placed element of a micro-Hall probe array (Altshuler and Johansen, 2004). In order to realize the asymmetric ac driven mode for the vortex lens, the following steps sketched in Fig. 29 were carried out: (i) The sample was cooled in fixed H_z at $H_{\parallel}=0$; (ii) a "conditioning" triangular wave was run for 4 min to equilibrate the PV system; (iii) a time-asymmetric, zero-mean ac drive was switched on for 4 min (for an animation see http://dml.riken.go.jp). The magnetic induction B_z was then monitored in real time starting from step (ii) at the centrally located Hall element and then related to the local PV density. The measured efficiency of this vortex lens, displayed in Fig. 29, is quite low. However, the same experiment, when performed on a symmetric pinning substrate, yields a much higher efficiency, as proven by Cole *et al.* (2006) for a film of Bi2212 patterned with a square array of circular antidots.

The two main advantages of this class of vortex devices over the earlier proposals reviewed in Secs. VII.A and VII.B are (i) the possibility to guide particles with no tailored spatial asymmetry and (ii) the tuning of the vortex motion by simply changing the parameters of the externally applied drive. The first feature allows expensive and cumbersome nanofabrication processing to be avoided; the second property becomes important if the transport properties of a device must be frequently varied, something which is generally hard to achieve in standard ratchet devices.

VIII. QUANTUM DEVICES

In the foregoing sections, we focused on directed transport within the realm of classical dynamical laws and classical statistical fluctuations. Totally new scenarios open up when we try to consistently incorporate quantum mechanical laws in the operation of an artificial Brownian motor. The quantum nature of fluctuations and quantum evolution laws, as governed by quantum statistical mechanics, allow for unexpected transport mechanisms. In particular, quantum mechanics provides the doorway to new features such as underbarrier (-threshold) tunneling, above-barrier reflection, and the interplay of coherent (i.e., with oscillatory relaxation) and incoherent (i.e., with overdamped relaxation) quantum transport. Last but not least, quantum mechanics generates the possibility for nonclassical correlations, including entanglement among quantum states in the presence of coupling.

A. Quantum dissipative Brownian transport

To set the stage and in order to elucidate the complexity involving directed quantum Brownian transport, we consider a 1D quantum particle of coordinate q and mass m, moving in a typically time-dependent rachetlike potential landscape $V_R(q,t)$. The particle is bilinearly coupled with strength c_i to a set of N harmonic oscilla-

tors x_i, with $i=1,\ldots,N$. The latter set of oscillators models the heat bath, with the oscillators prepared in a canonical state with density matrix $\hat{\rho}_{\rm bath}$, corresponding to an isolated, bare bath Hamiltonian, and a temperature kT. Accordingly, the total dynamics is governed by the Hamiltonian

$$H = \frac{p^2}{2m} + V_R(q,t) + \sum_{i=1}^{N}\left(\frac{p_i^2}{2m_i} + \frac{m_i}{2}\omega_i^2 x_i^2 - qc_i x_i + q^2\frac{c_i^2}{2m_i\omega_i^2}\right). \tag{40}$$

The last term, which depends only on the system coordinate, represents a potential renormalization term which is needed to ensure that the potential $V_R(q,t)$ coincides with the bare ratchet potential in the presence of coupling to the bath degrees of freedom. This Hamiltonian has been studied since the early 1960s for systems that are weakly coupled to their environment. Only in the 1980s was it realized by Caldeira and Leggett (1983, 1984) that this model is also applicable to strongly damped systems and may be employed to describe, for example, dissipative tunneling in solid state and chemical physics (Hänggi *et al.*, 1990).

One may convince oneself that the Hamiltonian in Eq. (40) indeed models dissipation. Making use of the solution of the Heisenberg equations of motion for the external degrees of freedom, one derives a reduced system operator-valued equation of motion, the so-called inertial generalized quantum Langevin equation, that is,

$$m\ddot{q}(t) + m\int_{t_0}^{t} ds\ \gamma(t-s)\dot{q}(s) + \frac{\partial V_R(q,t)}{\partial q} = \eta(t) - m\gamma(t-t_0)q(t_0). \tag{41}$$

The friction kernel is given by

$$\gamma(t) = \gamma(-t) = \frac{1}{m}\sum_{i=1}^{N}\frac{c_i^2}{m_i\omega_i^2}\cos(\omega_i t), \tag{42}$$

and the quantum Brownian force operator reads

$$\eta(t) = \sum_{i=1}^{N} c_i\left(x_i(t_0)\cos[\omega_i(t-t_0)] + \frac{p_i(t_0)}{m_i\omega_i}\sin[\omega_i(t-t_0)]\right). \tag{43}$$

The random force $\eta(t)$ is a stationary Gaussian operator noise with correlation functions

$$\langle\eta(t)\rangle_{\hat{\rho}_{\rm bath}} = 0, \tag{44}$$

$$S_{\eta\eta}(t-s) = \frac{1}{2}\langle\eta(t)\eta(s) + \eta(s)\eta(t)\rangle_{\hat{\rho}_{\rm bath}} = \frac{\hbar}{2}\sum_{i=1}^{N}\frac{c_i^2}{m_i\omega_i}\cos[\omega_i(t-s)]\coth\left(\frac{\hbar\omega_i}{2kT}\right). \tag{45}$$

Moreover, being an operator-valued noise, the η commutators do not vanish, i.e.,

$$[\eta(t),\eta(s)] = -i\hbar\sum_{i=1}^{N}\frac{c_i^2}{m_i\omega_i}\sin[\omega_i(t-s)]. \tag{46}$$

This complex structure for driven quantum Brownian motion in a potential landscape follows the fact that a consistent description of quantum dissipation necessarily requires the study of the dynamics in the full Hilbert space of the system plus environment. This is in clear contrast to the classical models, where the Langevin dynamics is directly formulated in the system state space (Hänggi and Ingold, 2005). Caution applies in making approximations to this structure, even if done semiclassically. The interplay of quantum noise with the commutator structure is necessary to avoid inconsistencies with the thermodynamic laws, such as a spurious finite directed current in an equilibrium quantum ratchet, i.e., even in absence of rocking, i.e., for $V_R(q,t)=V_R(q)$ (Machura, Kostur, *et al.*, 2004; Hänggi and Ingold, 2005). Simplifications are possible only under specific circumstances as in the case of very strong friction, when quantum corrections can consistently be accounted for by a semiclassical quantum Smoluchowski equation operating on the state space of the classical system only (Ankerhold *et al.*, 2001; Machura, Kostur, *et al.*, 2004; Machura, Luczka, *et al.*, 2007). The situation is presently less settled for weakly damped quantum Brownian motors (Carlo *et al.*, 2005; Denisov *et al.*, 2009) and for systems at high temperatures, where approximate reduced descriptions are often in conflict with the laws of thermodynamics; this is true in particular for the second law, central to this review (Hänggi and Ingold, 2005; Zueco and Garcia-Palacios, 2005).

An alternative approach to the quantum Langevin description, which in addition allows powerful computational methods, is based on the real-time path integral technique. Starting from the quantum statistical representation of the density operator evolution of the total dynamics of a system coupled to its environment(s), one traces over the bath degrees of freedom to end up with a path integral representation for the reduced density operator, the so-called influence functional, which consistently incorporates quantum dissipation (see, for instance, Hänggi *et al.*, 1990; Grifoni and Hänggi, 1998; Hänggi and Ingold, 2005; Kohler *et al.*, 2005).

B. Josephson Brownian motors

In the following we consider the role of quantum effects in artificial Brownian motors made of coupled Josephson junctions.

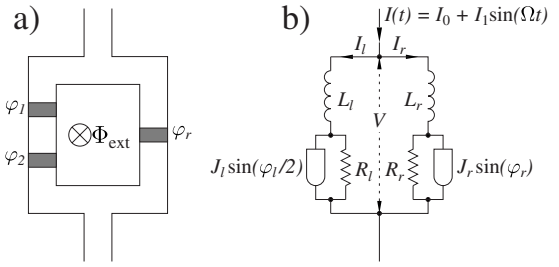

FIG. 30. SQUID rocked ratchet. (a) Schematic picture of an asymmetric SQUID with three junctions threaded by an external magnetic flux. (b) Equivalent electric circuit: the two junctions in series of the left branch behave like a single junction with φ replaced by $\varphi/2$. For further details, see Zapata *et al.*, 1996.

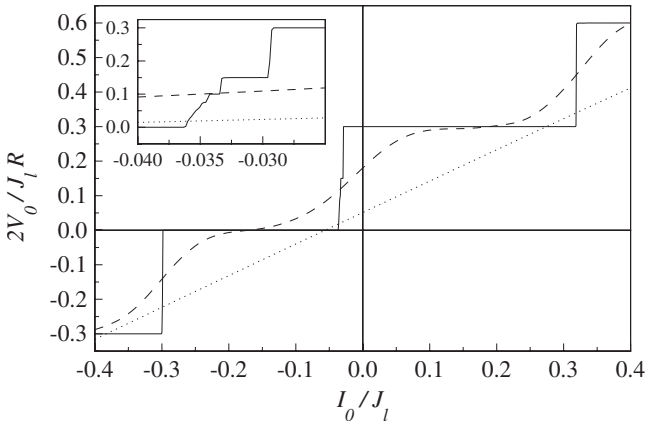

FIG. 31. Theoretically evaluated dc current-voltage [Josephson relation $V_0=(\hbar/2e)\langle\dot{\varphi}(t)\rangle$] characteristics for the SQUID ratchet of Fig. 30. Simulation parameters: (nonadiabatic) rocking frequency $\omega=2\hbar\Omega/eRJ_l=0.3$, ac drive amplitude $A=I_0/J_l=1.7$, and different noise levels $D=ek_BT/\hbar J_l=0$ (solid), 0.01 (dashed), and 0.5 (dotted). Inset: Magnified plot showing characteristic steps at fractional values of ω for $D=0$. Here R and J_l denote the resistance and the critical current amplitude of the two identical Josephson junctions placed in the left branch of the device (cf. Fig. 30).

1. Classical regime

Our first case refers to the limit when quantum coherence and tunneling events, such as photon-assisted tunneling, can safely be neglected, which is often the case at sufficiently high temperatures. In this regime the description of Josephson quantum systems can well be approximated by an effective Fokker-Planck dynamics in the context of the Stewart-McCumber model (Barone and Paternò, 1982), which includes effective parameters containing $\hbar$. An artificial Brownian motor then can be experimentally realized, for instance, with the asymmetric superconducting quantum interference device (SQUID) illustrated in Fig. 30 (Zapata *et al.*, 1996). In the overdamped regime, where capacitative effects can be ignored, such a device maps precisely onto the rocked ratchet of Sec. II.D.1. Under such operating conditions, the phase of the device is a classical variable which can be adequately described by the aforementioned "resistively shunted junction" model. Thermal Brownian motion at temperature T is included by adding Nyquist noise. The behavior of the rachet voltage so induced is displayed in Fig. 31 for a nonadiabatically rocked SQUID ratchet (Zapata *et al.*, 1996).

The results for this ratchet setup have been experimentally validated by use of high-temperature superconducting dc SQUIDs by the Tübingen group (Weiss *et al.*, 2000; Sterch *et al.*, 2002, 2005). In the meantime, several variants of this scheme have been studied, both theoretically and experimentally, including fluxon ratchets of various designs (Zapata *et al.*, 1998; Carapella and Costabile, 2001; Falo *et al.*, 2002; Lee, 2003; Berger, 2004; Beck *et al.*, 2005; Shalóm and Pastoriza, 2005); cf. also Sec. VII. Moreover, transport of fluxons in an extended, annular Josephson junction has also been demonstrated by Ustinov *et al.* (2004) as a harmonic mixing effect.

2. Quantum regime

To tackle true quantum effects, including quantum tunneling phenomena, we must resort to the theoretical scheme outlined in Sec. VIII.A. A first theoretical study of quantum ratchets was pioneered by Reimann *et al.* (1997) (see also Reimann and Hänggi, 1998). For a regime with several (quasi)bound states below a potential barrier one can evaluate the ratchet tunneling dynamics in terms of an effective action for the extremal bounce solution (in combination with a fluctuation analysis around this bounce solution) to obtain the corresponding tunneling rates. In Fig. 32 the result of such a quantum calculation is compared with the classical result for an adiabatically rocked quantum particle of mass m and coordinate q dwelling in a ratchet potential $V_R(q)$. Note that, within a quantum Brownian motor scheme, the role of mass m, i.e., the inertia, does enter the analysis explicitly. The most distinctive quantum signature is a striking current reversal which emerges solely as a consequence of quantum tunneling under adiabatic rocking conditions. Moreover, in contrast to the classical result, the directed current no longer vanishes as T tends to zero and additional resonancelike features show up.

Such a dependence of the current versus decreasing temperature in a quantum Brownian motor has been corroborated experimentally for vortices moving in a quasi-1D Josephson junction array with ratchet potential profile specially tailored so as to allow several bands below the barrier (Majer *et al.*, 2003). The experimental setup of this quantum ratchet device is displayed in Fig. 33. The experimental findings are in good agreement with the theoretical analysis by Grifoni *et al.* (2002).

C. Quantum dot ratchets

Another ideal resource to observe the interplay of (i) quantum Brownian motion, (ii) quantum dissipation, and (iii) nonequilibrium driving are semiconductor engineered quantum rectifiers. Composed of arrays of asymmetric quantum rectifiers (Linke *et al.*, 1998), these de-

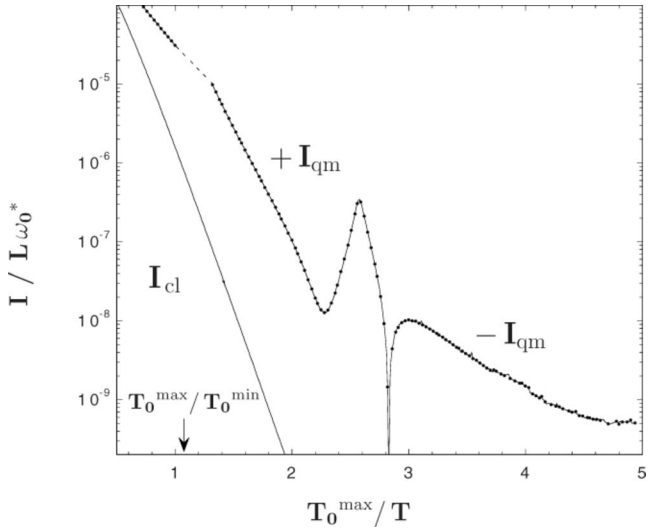

FIG. 32. The classical Brownian motor current $I_{\rm cl}$ occurring in a dichotomously rocked ratchet potential, Eq. (23), of period L, compared with the corresponding quantum Brownian motor current $I_{\rm qm}$ vs dimensionless inverse temperature T. The current is measured in units of $(L\omega_0^*)$ with $\omega_0^* = [4\pi^2 V_0/(L^2 m)]^{1/2}$ and the temperature is measured in units of the (maximal) crossover temperature $T_0^{\rm max}$ occurring in the rocked potential landscape. Notably, in contrast to an adiabatically rocked classical Brownian motor, the quantum current changes sign near $T_0^{\rm max}/T = 2.8$ which is a manifestation of true quantum tunneling. For more details see Reimann and Hänggi, 1998.

vices operate on geometric and dynamical length scales ranging between a few nanometers and microns. This class of devices allowed the first experimental validation of the distinctive features of quantum rectifiers, namely, tunneling-enhanced rachet current and tunneling-induced current reversals, by Linke and collaborators (Linke *et al.*, 1999, 2002). Their central results are illustrated in Fig. 34.

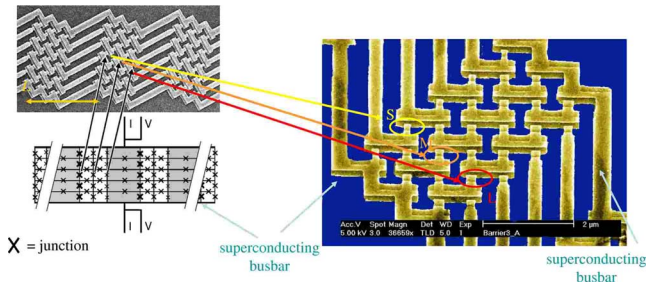

FIG. 33. (Color online) Asymmetric Josephson junction array. Top left: Scanning electron picture (with enlargement on the right) of a strongly asymmetric array of a long, narrow network of Josephson junctions arranged in a rectangular lattice. This arrangement determines the potential shape felt by vortices. Bottom left: Schematic layout. The Josephson junctions are represented by crosses, each network cell being delimited by four junctions. All arrays have a length of 303 cells and a width of 5 cells, placed between solid superconducting electrodes. The vortices assume a lower energy in cells with larger area and smaller junctions. Figure provided by Milena Grifoni.

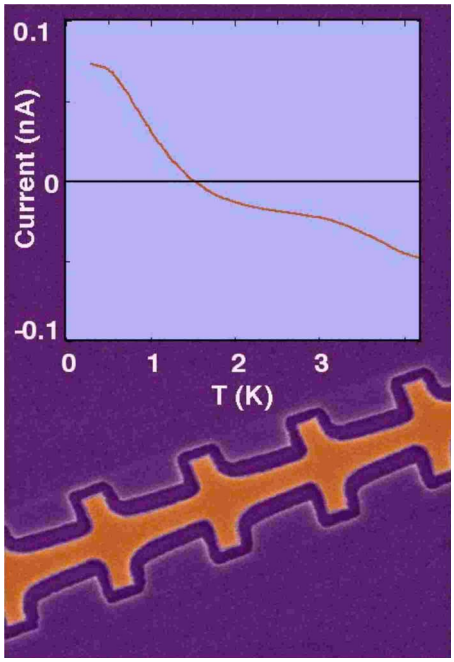

FIG. 34. (Color online) In an experimental quantum Brownian motor driven by an adiabatic square-wave zero-mean rocking voltage, quantum tunneling can contribute to the electron current. Due to the underlying asymmetric potential structure, the two opposite components of the time-averaged-driven current differ in magnitude, yielding a net quantum ratchet current (Reimann *et al.*, 1997; Linke *et al.*, 1999). The magnitudes can be individually controlled by tuning the temperature. This in turn causes a tunneling-induced current reversal (occurring near 1.5 K in the top graph) that can be exploited to direct electrons along *a priori* designed routes (Linke *et al.*, 1999). Below the current vs T graph is a scanning electron micrograph of the relevant quantum device. Figure provided by Heiner Linke.

Their quantum Brownian motor consisted of a 2D gas of electrons moving at the interface of a fabricated, ratchet-tailored GaAs/AlGaAs heterostructure. Its operating regime was achieved by adiabatically switching on and off a square-wave source-drain periodic voltage of frequency 190 Hz and amplitude of about 1 mV. We recall that, for an adiabatically rocked classical ratchet of Sec. II.D.1, noise-induced transport exhibits no current reversals, but things change drastically when quantum tunneling enters into the dynamics. A true benchmark for the quantum behavior of an adiabatically rocked Brownian motor is then the occurrence of a tunneling-induced reversal at low temperatures (Reimann *et al.*, 1997). This characteristic feature was first experimentally verified with an electron quantum rocked ratchet by Linke *et al.* (1999). Moreover, the current reversal reported in the top panel of Fig. 34 indicates the existence of parameter configurations where the current of a quantum Brownian motor vanishes. In correspondence to such configurations, one can imagine operating the device as a quantum refrigerator to separate "cold" from "hot" electrons in the absence of currents (Linke *et al.*, 2002). At higher temperatures this

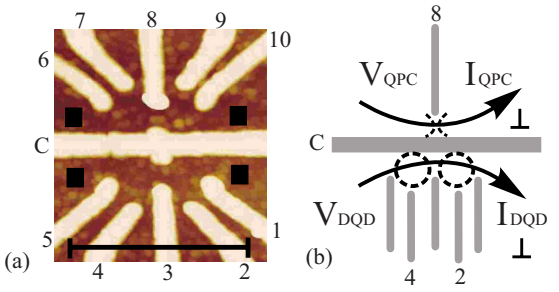

FIG. 35. (Color online) Double-dot quantum ratchet. (a) AFM micrograph of a double-quantum-dot device. Metal surface gates have a light color, black squares mark source and drain regions. The black scale bar marks the length of 1 μm. (b) Schematic diagram: A biased quantum point contact (QPC) provides the nonequilibrium fluctuation source for driving a tunneling current I_{DQD} in the asymmetric double quantum dot (DQD) (two dashed circles) (Khrapai *et al.*, 2006). The asymmetry is induced via gate voltages at the plunger gates 2 and 4. Figure provided by Vadim S. Khrapai.

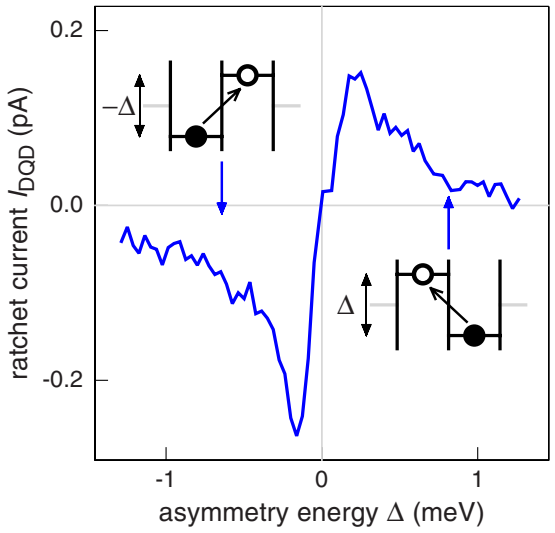

FIG. 36. (Color online) Experimental quantum ratchet current I_{DQD} measured through the double quantum dot as a function of its asymmetry energy Δ. The energy source is a nearby quantum point contact biased with $V_{QPC}=-1.55$ mV; see Fig. 35. An elastic contribution to I_{DQD} is subtracted (Khrapai *et al.*, 2006). The two insets sketch the corresponding inelastic tunneling processes which drive the ratchet current. Notably, this quantum ratchet current vanishes when $\Delta=0$ (i.e., no asymmetry). Figure provided by Stefan Ludwig.

and other asymmetric quantum-dot arrays, when subjected to unbiased ac drives, exhibit incoherent quantum ratchet currents. Such experimental realizations using 2D electron systems with broken spatial inversion symmetry have been reported by Lorke *et al.* (1998), Vidan *et al.* (2004), and Sassine *et al.* (2008). An even richer behavior of the quantum current, including, for example, multiple current reversals, emerges when this class of devices is operated in the *nonadiabatic* ac regime, as revealed by recent theoretical studies (Goychuk and Hanggi, 1998, 2005; Goychuck *et al.*, 1998a, 1998b; Grifoni *et al.*, 2002; Kohler *et al.*, 2005).

As a second example of an artificial quantum dot Brownian motor, we consider an experimental double-quantum-dot device where the two dots are independently coupled to a nonequilibrium energy source which is given by a biased quantum point contact. Moreover, the two quantum dots are embedded in independent electric circuits via a common central gate, marked by a C in Fig. 35. When its internal symmetry is broken by tuning the dot gate voltages, this double quantum dot acts as a quantum ratchet device (Khrapai *et al.*, 2006). For weak interdot tunneling, detuning of the quantum dot energy levels results in the localization of an electron in one dot, so that elastic electron transfer to the other dot is energetically forbidden. To operate as a quantum ratchet, the device still requires a nonequilibrium energy source. For this purpose, a strong tunable bias on the quantum point contact induces nonequilibrium energy fluctuations across the dividing central gate, thus promoting inelastic interdot tunneling inside the Coulomb-blockaded double quantum dot. This in turn leads to a net quantum ratchet current flow, as plotted in Fig. 36. In the insets of the same figure, the interdot tunneling process is sketched for the right-to-left transition $[m,n+1]\rightarrow[m+1,n]$, with asymmetry energy $\Delta \equiv E_{m+1,n}-E_{m,n+1}$, and for the opposite left-to-right transition with energy $-\Delta$. Notably, a finite ratchet current is observed only if the electron energy states in the dots are detuned asymmetrically, i.e., when $\Delta\neq 0$. In contrast, a likely inelastic ionization of one dot toward its adjacent lead, followed by recharging from the same lead, does not result in a net current. The nonequilibrium energy fluctuations, carried by the quantum point contact electrons and absorbed by the electrons in the double quantum dot, could consist of acoustic phonons, long-wavelength photons, or plasmons (Khrapai *et al.*, 2006).

The technology available to generate 2D electron gases can be generalized to ratchet not only charge but also spin carriers. The interplay of spatially periodic potentials, lateral confinement, spin-orbit or Zeeman-type interactions, and ac driving then gives rise to directed *spin ratchet* currents, as theoretically proposed in recent studies (Scheid, Bercioux, *et al.*, 2007; Scheid, Pfund, *et al.*, 2007). Of particular experimental relevance is the theoretically predicted phenomenon of a spin current which emerges via an unbiased ac charge current driving a dc spin current in a nonmagnetic, dissipative spin quantum ratchet which is composed of an asymmetric periodic structure with Rashba spin-orbit interactions (Flatte, 2008; Smirnov *et al.*, 2008). Remarkably, this spin current occurs although no magnetic fields are present.

Likewise, substantial rectification of a spin current can also be achieved by coupling impurities to spatially asymmetric Luttinger liquids under ac voltage rocking (Braunecker *et al.*, 2007). The transport mechanism in those schemes is governed by coherent tunneling processes, which will be addressed in the following section.

D. Coherent quantum ratchets

The study of quantum Brownian motors is far from being complete. In fact, there is an urgent need for fur-

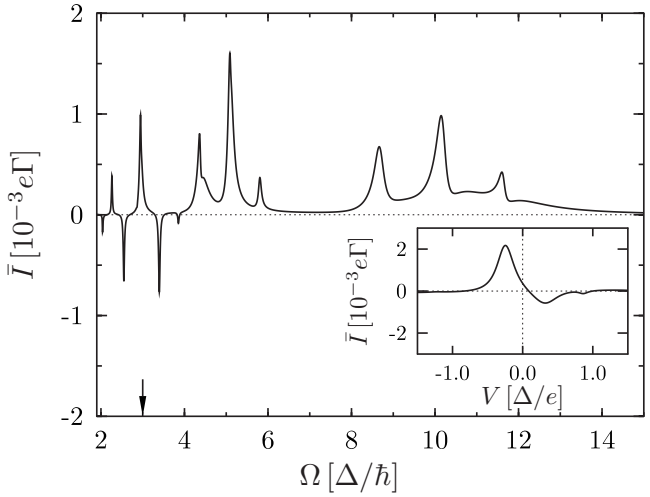

FIG. 37. Quantum Brownian motor from a molecular wire. Time-averaged current $\bar{I}$ (measured in units of the lead coupling strength $e\Gamma$) as a function of the infrared drive angular frequency Ω (measured in units of the tunneling matrix element $\Delta=0.1$ eV between sites for a laser amplitude $A=\Delta$; Lehmann *et al.*, 2002). The inset displays the dependence of $\bar{I}$ on the static voltage drop V applied along the molecule. Note that the current at zero voltage is finite, thereby indicating a ratchet effect. The driving frequency corresponds to the vertical arrow in the main panel.

ther development. In many cases the roles of incoherent tunneling and coherent transport channels cannot be clearly separated. For quantum devices built bottom up with engineered molecules or artificial molecules such as quantum dots, the role of coherent quantum transport typically plays a dominant role, as other interactions like electron-phonon processes turn out to be negligible. The key transport process for quantum ratcheting is then driven coherent quantum tunneling (Grifoni and Hänggi, 1998; Kohler *et al.*, 2005).

1. Quantum ratchets from molecular wires

This is the case of quantum Brownian motors consisting of nanowires formed by asymmetric molecular groups and subjected to infrared light sources (Lehmann *et al.*, 2002), or symmetric molecular wires with symmetry breaking now provided by irradiation of the wire with harmonic mixing signals (Lehmann *et al.*, 2003). The theoretically predicted quantum ratchet current through an asymmetric molecular wire irradiated by far-infrared light is displayed in Fig. 37.

In this class of quantum ratchets, transport proceeds coherently between two or more fermionic leads that ensure the dissipative mechanism for the transported electrons to relax toward equilibrium Fermi distributions. Such a ratchet current can also be used to sensitively probe the role of the electron correlations in the leads, as is the case with a ratchet device coupled to Luttinger liquids rather than to Fermi liquids (Komnik and Gogolin, 2003; Feldmann *et al.*, 2005).

2. Hamiltonian quantum ratchet for cold atoms

Surprisingly, systems governed by strictly Hamiltonian dynamics are able to yield directed transport as well. Directed transport may then take place even though no dissipation mechanisms are present. Trivial examples of this process are provided by integrable regular dynamics subjected to unbiased ac drives with fixed initial phase, i.e., not averaged over (Yevtushenko *et al.*, 2000; Goychuk and Hänggi, 2001). Much more intriguing are time-dependent driven Hamiltonian quantum Brownian motors exhibiting a nontrivial, mixed classical phase space structure (Flach *et al.*, 2000; Denisov and Flach, 2001; Schanz *et al.*, 2001, 2005). In these systems, the onset of a directed flow requires, apart from the necessity of breaking time-reversal symmetry, an additional dynamical symmetry breaking. As it turns out, in the semiclassical limit the corresponding directed flow then obeys a remarkable sum rule: Directed currents occurring in regular regimes of the underlying phase space dynamics are counterbalanced by directed flows occurring in chaotic regimes in phase space (Schanz *et al.*, 2001, 2005). As a result, if those individual directed currents are summed up over all disjoint regimes in (semi)classical mixed phase space, no net transport emerges.

The concept of Hamiltonian quantum Brownian motors extends as well to fully quantum systems governed by a unitary time evolution (Goychuk and Hänggi, 2000, 2001; Schanz *et al.*, 2001, 2005; Denisov *et al.*, 2006, 2007; Gong *et al.*, 2007). In fact, the issue of pure quantum coherence in the directed transport of chaotic Hamiltonian systems is presently a topic of active research. This in particular holds true for cold atoms loaded in optical lattices: If properly detuned, the intrinsic quantum dynamics is then practically dissipation-free, thus providing a paradigm for Hamiltonian quantum ratchet transport. Various experimental cold atom ratchets have been realized (Sec. IV). Relevant to the current topic is also the demonstration of sawtoothlike, asymmetric cold atom potentials by Salger *et al.* (2007). All these systems are currently employed to effectively steer cold matter on a quantum scale.

In the context of quantum ratchets for cold atoms, one must distinguish the common case of "rectification of velocity," implying that the mean position of particles is growing linearly in time, from the case with "rectification of force," i.e., with mean momentum growing linearly in time. The latter class is better referred to as "quantum ratchet accelerators" (Gong and Brumer, 2004, 2006). In the context of cold atom ratchets the first situation is obtained by rocking a cold atom gas with temporally asymmetric driving forces or temporally asymmetrically flashing, in combination with spatially asymmetric potential kicks (Denisov *et al.*, 2007). The accelerator case originates from the physics of quantum δ-kicked cold atoms displaying quantum chaos features such as the quantum suppression of classical chaotic diffusion (dynamical localization) and the diametrically opposite phenomenon of *quantum resonance* (occurring when the kicking period is commensurate with the in-

verse recoil frequency). Under the quantum resonance condition a linear (quadratic) increase of momentum (kinetic energy) takes place. These ratchet acceleration features, theoretically predicted in suitably modified kicked rotor models (Lundh and Wallin, 2005; Poletti, Carlo, *et al.*, 2007; Kenfack *et al.*, 2008), require tuning to exact resonance. In contrast, the accelerator models obtained from a generalization of either a quantum kicked rotor or a kicked Harper model (Gong and Brumer, 2004, 2006; Wang and Gong, 2008) are generic rectifiers of force in the sense that here no tuning to exact resonance is necessary. Interestingly, these fully quantum ratchet accelerators display unbounded linear growth of mean momentum, while the underlying classical dynamics is fully chaotic, a situation where classical quantum Brownian motor transport necessarily vanishes according to the above-mentioned classical sum rule (Schanz *et al.*, 2001, 2005). Thus, within this full quantum regime, which carries no clear relationship with the dynamics in the semiclassical regime, the quantum accelerator work by Gong and Brumer (2006) [see also Wang and Gong (2008)] presents a generic quantum mechanical exception to the classical sum rule.

Early quantum resonance experiments in quantum ratchets have already been successfully carried out. For a δ-kicked rotor model with time symmetry broken by a two-period kicking cycle (asymmetric temporal drive), directed growth of momentum has been detected by Jones *et al.* (2007). For a phase-dependent initial preparation of a Bose-Einstein condensate kicked at resonance, a momentum acceleration has been observed by Sadgrove *et al.* (2007) at zero quasimomentum, while for an arbitrary quasimomentum directed quantum Brownian transport has been realized by Dana *et al.* (2008). The last experiment also showed that the intrinsic experimentally nonavoidable finite width in quasimomentum causes a suppression of the acceleration, eventually leading to a saturation effect after short times.

This field of Hamiltonian quantum ratchets is presently undergoing rapid development. For example, it is possible to apply control schemes to the relative phases for the resulting single-particle quantum Brownian motor currents by harvesting Landau-Zener transitions (Morales-Molina *et al.*, 2008). Of particular theoretical and experimental interest is the study of the role of nonlinearity on the size of directed quantum currents in interacting cold gases, as described within mean-field theory by a nonlinear quantum ratchet evolution of the Gross-Pitaevskii type. There the interplay of time-dependent driving and nonlinear Floquet states yields new features, such as lifting of accidental symmetries (Poletti, Benenti, *et al.*, 2007) and a resonant enhancement of the directed ratchet currents (Morales-Molina and Flach, 2008).

IX. SUNDRY TOPICS

In the following we discuss some classes of nanosystems and devices which feature directed transport in the spirit of Brownian motors. In these systems, however, rectification of Brownian motion does not constitute the main element for directed transport. We recall that an artificial Brownian motor is mainly noise controlled, meaning that such a motor operates in an unpredictable manner. In contrast, we discuss next systems that exhibit directed transport predominantly as the result of strong-coupling schemes. Typical examples are adiabatic pump scenarios of the peristaltic type, or nanosystems which are driven by unbiased but asymmetric mechanical or chemical causes that are tightly coupled to the resulting motion.

A. Pumping of charge, spin, and heat

A first class of physical systems that comes to mind in relation to the working principles of artificial Brownian motors is nanoscale pump devices. Pumping is characterized by the occurrence of a net flux of particles, charges, spins, and soon, in response to time-dependent external manipulations of an otherwise unbiased system. This mechanism is well studied, and peristaltic pumps are widely exploited in technological applications. These systems do not require a periodic arrangement of components, nor is thermal Brownian motion an issue for their operation. In particular, adiabatic turnstiles and pumps for charge and other degrees of freedom have attracted considerable interest both experimentally (Kouwenhoven *et al.*, 1991; Pothier *et al.*, 1992; Switkes *et al.*, 1999; Hohberger *et al.*, 2001) and theoretically (Thouless, 1983; Spivak *et al.*, 1995; Brouwer, 1998; Zhou *et al.*, 1999; Shutenko *et al.*, 2000; Vavilov *et al.*, 2001; Brandes and Vorrath, 2002; Aono, 2003; Moskalets and Büttiker, 2004; Sinitsyn and Nemenman, 2007).

Realizations of artificial pumps on the nanoscale often involve coupled quantum dots or superlattices. Most notably, in such peristaltic devices the number of transferred charges, or, more generally, the number of transporting units per cycle, is directly linked to the cycle period. As a result, the output current becomes proportional to the driving frequency. This observation leads to the conclusion that high-frequency nonadiabatic pumping might become more effective. Indeed, nonadiabatic pumping of charge, spin (Scheid, Bercioux, *et al.*, 2007; Flatte, 2008; Smirnov *et al.*, 2008), or heat (Li *et al.*, 2008; Van den Broek and Van den Broeck, 2008) does exhibit a rich phenomenology, including resonances (Stafford and Wingreen, 1996; Moskalets and Büttiker, 2002; Platero and Aguado, 2004; Cota *et al.*, 2005; Kohler *et al.*, 2005; Arrachea *et al.*, 2007; Rey *et al.*, 2007) and other potentially useful noise-induced features (Strass *et al.*, 2005; Sanchez *et al.*, 2008), hence yielding a close interrelation between *nonadiabatic* pumping in the presence of noise and the physics of Brownian motors.

B. Synthetic molecular motors and machines

As emphasized in the Introduction, the field of Brownian motors has its roots in the study and applications of intracelluar transport in terms of molecular motors (Jülicher *et al.*, 1997; Astumian and Hänggi, 2002;

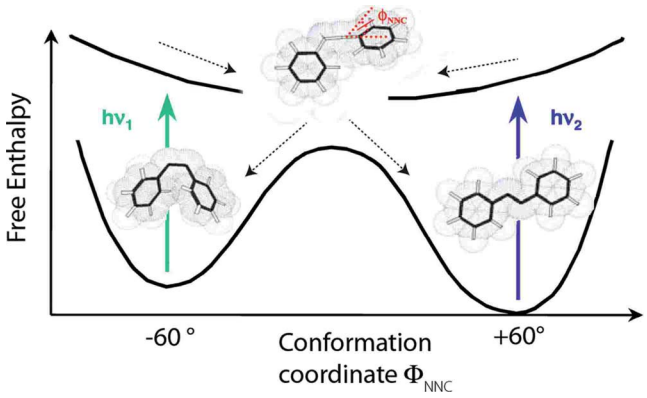

FIG. 38. (Color online) Free energy landscape of a single azobenzene molecule along the reaction coordinate of the conformation coordinate given by the bond angle Φ_{NNC}, which varies from about $-60°$ to $\sim+60°$. Transitions can be induced optically [$\lambda_1 \sim 420$ nm for the short *cis* form (0.6 nm) and $\lambda_2 \sim 365$ nm for the extended *trans* form (0.9 nm), respectively] from the singlet ground state S_0 into the excited singlet state S_1, from which the molecule subsequently relaxes fluctuation driven into either the *cis* or *trans* form. Notably, the *trans* form is thermally favored. The insets depict the corresponding conformations with the transition state located near $\Phi_{NNC} \sim 0°$. Figure provided by Thorsten Hugel.

Reimann, 2002; Reimann and Hänggi, 2002; Wang and Oster, 2002; Lipowsky and Klumpp, 2005). These molecular motors function in terms of structure and motility by use of specialized proteins in living systems. Such biological devices are fueled by ATP hydrolysis and are able to efficiently perform mechanical work on the nanoscale inside the cell structures (Howard, 2001; Schliwa, 2002).

Closely related to the topic of synthetic motors is the possibility of devising DNA-fueled artificial motors: several settings render it possible to biologically engineer nanomachines which move along tracks designed *a priori* (Yorke *et al.*, 2000; Turberfield *et al.*, 2003; Yin *et al.*, 2004).

An offspring of this topic is the engineering of nanomachines based on interlocked molecular species. This has spurred a flurry of new investigations within the physical biology and organic and physical chemistry communities, aimed at building bottom-up synthetic molecular systems which carry out such diverse functions as molecular switches, molecular rotors, and any other kind of molecular gear.

An example of this class of molecular motor is the light-powered molecular machine developed by Hugel *et al.* (2002). Bistable photosensitive azobenzene molecules can be synthesized into long chains, each containing molecules in either their *trans* or *cis* form. The free energy landscape corresponding to different molecular conformational states is sketched in Fig. 38 versus the reaction coordinate. Polymeric chains have the advantage of scaling up the length changes corresponding to the two different conformations of the constituents. The length changes of an azobenzene polymeric chain can then be transformed into mechanical energy by means of the lever arm of an atomic force microscope (AFM), which, in combination with the light sources, forms the core of the light-driven molecular motor of Fig. 39.

Such a molecular motor can be operated according to an idealized thermodynamic cycle of the Stirling type: Individual azobenzene polymers are made to stretch and contract by inducing optical *trans-cis* transitions of their constituents. This machine demonstrates optomechanical energy conversion in a single-molecule motor device. The analogy with a thermodynamic cycle, though, should not be taken too seriously. A thermal Stirling engine operates between baths of differing temperatures; here the "expansion" and "compression" of the

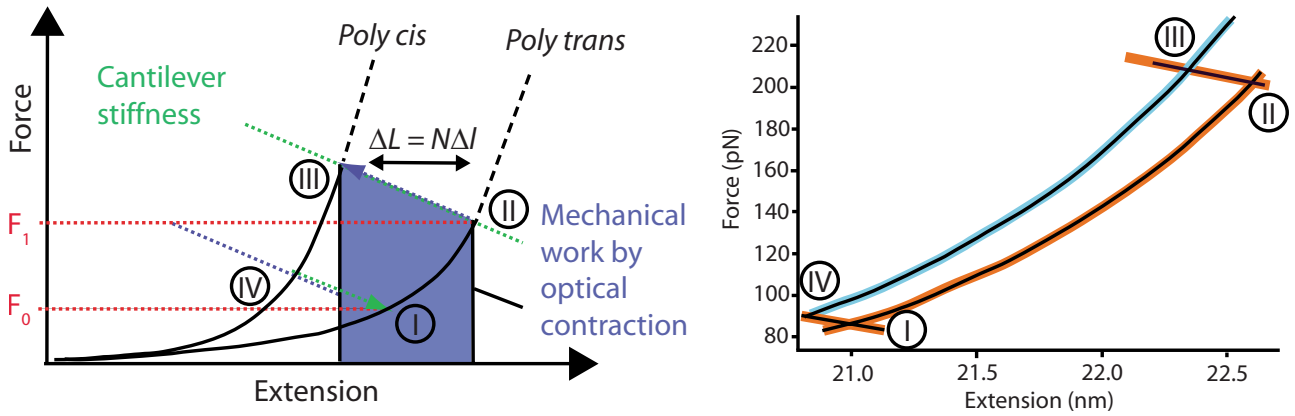

FIG. 39. (Color online) Operation of a light-powered molecular motor. (a) The schematic force extension cycle for the optomechanical energy conversion cycle of a single poly-azobenzene. In analogy to a thermodynamic Stirling cycle, the polymer is first stretched by the AFM tip acting as the piston (I→II). Then, the application of the first optical excitation with $\lambda_2 \simeq 365$ nm shortens the polymer by inducing a (poly)*trans*–(poly) *cis* transition. This yields the first part of the work in bending the AFM cantilever, which is clearly not as stiff as a piston in a common Stirling motor. In analogy to the Stirling cycle, another amount of work is done during the relaxation of the polymer (III→IV). Finally, a second optical excitation with $\lambda_1 \simeq 420$ nm is needed to reset the molecule into its starting (poly)*trans* state (IV→I). The total work output of the system is the mechanical energy corresponding to the contraction ($\Delta L = N\Delta l$) of the entire polymer chain of N azobenzenes against the external load. The experimental realization of a full single-molecule operating cycle (Hugel *et al.*, 2002) is depicted in (b). Figure provided by Thorsten Hugel.

molecular motor are performed at a fixed temperature and, most notably, by means of nonequilibrium light sources. This laser-operated molecular motor can also be used as a building block to devise a bioinspired molecular locomotive which can be guided back and forth on a preassigned track via a laser-assisted protocol (Wang, 2004).

In the operation of these synthetic nanoscale devices, especially when powered by light or chemical reactive additives, thermal noise does not necessarily play a major role, i.e., the function of these synthetic molecular motors is ruled predominantly by deterministic forces, forces that depend on the mechanical and chemical properties of the molecules (Neuert *et al.*, 2006). Yet this area of research is fascinating and we therefore refer the interested reader to recent items and tutorials (Porto *et al.*, 2000; Balzani *et al.*, 2006; Browne and Ferina, 2006; Astumian, 2007) and to consult the reviews by Kottas *et al.* (2005) and Kay *et al.* (2007) for more details.

X. CONCLUDING REMARKS

With this review we have taken a tour through the many intriguing and multifacetted applications that Brownian motion can offer in the most diverse areas of nanotechnology, when combined with spatiotemporal symmetry breaking, nonlinearity, and, possibly, collective interaction effects. The physics of classical and quantum Brownian motion is by now well established, by virtue of the breadth of the theoretical modeling and experimental realizations produced over the last century. Many research activities are still developing in interdisciplinary fields encompassing chemistry, biological research, information sciences, and even extending into social sciences and economics. The main lesson to be learned from Robert Brown's and Albert Einstein's work is therefore as follows: Rather than fighting thermal motion, we should put it to work to our advantage. Brownian motors use these ceaseless noise source to efficiently direct, separate, pump, and steer degrees of freedom of differing nature reliably and effectively.

In writing this overview we spared no efforts in covering a wide range of interesting developments and potential achievements. In doing so we nevertheless had to make some selective choices of topics and applications, which to some extent reflect our preferences and prejudices. Closely related topics of ongoing research were not reviewed due to space limits. For example, in Sec. IX.B we did not cover in sufficient detail the topic of ATP-driven molecular motors and DNA-fueled motors, for which we refer the reder to earlier reviews and books, such as Jülicher *et al.* (1997), Howard (2001), Schliwa (2002), and Lipowsky and Klumpp (2005). This is surely the case of the bottom-up design and operation of synthetic Brownian molecular devices, extensively covered by Kay *et al.* (2007). Another such topic is the question of so-called absolute negative mobility, which occurs via quantum tunneling events in quantum systems (Keay *et al.*, 1995; Aguado and Platero, 1997; Grifoni and Hänggi, 1998; Platero and Aguado, 2004) and through nonequilibrium-driven diffusive dynamics in classical systems (Eichhorn *et al.*, 2002a, 2002b; Ros *et al.*, 2005; Machura, Kostur, *et al.*, 2007; Kostur *et al.*, 2008).

Our main focus was on noise-assisted directional transport, shuttling, and pumping of individual or collective particle, charge, or matter degrees of freedom. The concept, however, extends as well to the transport of other degrees of freedom such as energy (heat) and spin modes (see also Sec. IX.A). Both topics are experiencing a surge of interest with new exciting achievements currently reported. The concept carries potential for yet other applications. Examples include the noise-assisted directional transport and transfer of informational degrees of freedom such as probability or entropy and, within a quantum context, the shuttling of entanglement information. These issues immediately relate to the energetics of artificial Brownian motors reviewed in Sec. II.E, including measures of open- and closed-loop control scenarios and other optimization schemes.

We have attempted to indicate the potential of Brownian motors in present nanotechnology by showing how they can be put to work; we discussed how such motors can be constructed and characterized, and how directional, Brownian-motion-driven transport can be controlled, measured, and optimized. Moreover, we are confident that the interdisciplinary style will encourage readers to develop new approaches and motivations in this challenging and fast-growing research area.

ACKNOWLEDGMENTS

This review would not have emerged without continuous support from and insightful discussions with our close collaborators and colleagues. We first express our gratitude to all members of our work groups among which special credit should be given to M. Borromeo, J. Dunkel, I. Goychuk, G.L. Ingold, S. Kohler, G. Schmid, P. Talkner, and U. Thiele for their scientific contributions and personal encouragement. A special thanks goes to our many colleagues and friends who are also engaged in the field of Brownian motors and, in particular, to R. D. Astumian, M. Bier, J. Casado, W. Ebeling, J. A. Freund, L. Gammaitoni, H. E. Gaub, E. Goldobin, M. Grifoni, D. Hennig, P. Jung, J. Kärger, I. Kosinska, M. Kostur, J. P. Kotthaus, B.-W. Li, H. Linke, J. Luczka, S. Ludwig, L. Machura, V. R. Misko, M. Morillo, F. Nori, J. Prost, P. Reimann, F. Renzoni, K. Richter, M. Rubí, S. Savel'ev, L. Schimansky-Geier, Z. Siwy, B. Spagnolo, C. Van den Broeck, and A. Vulpiani. In addition, we are indebted to M. Borromeo, M. Grifoni, T. Hugel, V. S. Khrapai, H. Linke, S. Ludwig, F. Müller, S. Savelev, U. Thiele, and C. Van den Broeck for providing us with original figures and unpublished material. F.M. wishes to thank Professor Hunggyu Park for his kind hospitality at the Korea Institute for Advanced Study and, likewise, the Physics Department of the National University of Singapore for kind hospitality: At these two institutions we were both given the opportunity to efficiently continue working on a preliminary version of this review.

P.H. acknowledges financial support by the Deutsche Forschungsgemeinschaft via the Collaborative Research Centre SFB-486, Project No. A10, B 13 and by the German Excellence Cluster "Nanosystems Initiative Munich" (NIM). Both authors thank the Alexander von Humboldt Stiftung, who made this joint project possible by granting to one of us (F.M.) a Humboldt Research Award to visit the Universität Augsburg, where most of the work was done.

REFERENCES

Abrikosov, A. A., 1957, "On the magnetic properties of superconductors of the second group," Sov. Phys. JETP **5**, 1174–1183.

Aghababaie, Y., G. I. Menon, and M. Plischke, 1999, "Universal properties of interacting Brownian motors," Phys. Rev. E **59**, 2578–2586.

Aguado, R., and G. Platero, 1997, "Dynamical localization and absolute negative conductance in an ac-driven double quantum well," Phys. Rev. B **55**, 12860–12863.

Ai, B.-Q., and L.-G. Liu, 2006, "Current in a three-dimensional periodic tube with unbiased forces," Phys. Rev. E **74**, 051114.

Ajdari, A., and J. Prost, 1992, "Drift induced by a spatially periodic potential of low symmetry -Pulsated dielctrophoresis," C. R. Acad. Sci., Ser. II: Mec., Phys., Chim., Sci. Terre Univers **315**, 1635–1639.

Aksimentiev, A., J. B. Heng, G. Timp, and K. Schulten, 2004, "Microscopic kinetics of DNA translocation through synthetic nanopores," Biophys. J. **87**, 2086–2097.

Altshuler, E., and T. H. Johansen, 2004, "*Colloquium*: Experiments in vortex avalanches," Rev. Mod. Phys. **76**, 471–487.

Ankerhold, J., P. Pechukas, and H. Grabert, 2001, "Strong friction limit in quantum mechanics: The quantum Smoluchowski equation," Phys. Rev. Lett. **87**, 086802; **101**, 119903(E) (2008).

Aono, T., 2003, "Adiabatic spin pumping through a quantum dot with a single orbital level," Phys. Rev. B **67**, 155303.

Arrachea, L., M. Moskalets, and L. Martin-Moreno, 2007, "Heat production and energy balance in nanoscale engines driven by time-dependent fields," Phys. Rev. B **75**, 245420.

Arvanitidou, E., and D. Hoagland, 1991, "Chain-length dependence of the electrophoretic mobility in random gels," Phys. Rev. Lett. **67**, 1464–1466.

Ashkenasy, N., J. Sánchez-Quesada, H. Bayley, and M. R. Ghadiri, 2005, "Recognizing a single base in an individual DNA strand: A step toward DNA sequencing in nanopores," Angew. Chem., Int. Ed. **44**, 1401–1404.

Astumian, R. D., 1997, "Thermodynamics and kinetics of a Brownian motor," Science **276**, 917–922.

Astumian, R. D., 2007, "Design principles for Brownian molecular machines: how to swim in molasses and walk in a hurricane," Phys. Chem. Chem. Phys. **9**, 5067–5083.

Astumian, R. D., and M. Bier, 1994, "Fluctuation driven ratchets: Molecular motors," Phys. Rev. Lett. **72**, 1766–1769.

Astumian, R. D., and I. Derényi, 1998, "Fluctuation driven transport and models of molecular motors and pumps," Eur. Polym. J. **27**, 474–489.

Astumian, R. D., and P. Hänggi, 2002, "Brownian motors," Phys. Today **55** (11), 33–39.

Babic, D., and C. Bechinger, 2005, "Noise-enhanced performance of ratchet cellular automata," Phys. Rev. Lett. **94**, 148303.

Babic, D., C. Schmitt, and C. Bechinger, 2005, "Colloids as model systems for problems in statistical physics," Chaos **15**, 026114.

Bader, J. S., R. W. Hammond, S. A. Henck, M. W. Deem, G. A. McDermott, J. M. Bustillo, J. W. Simpson, G. T. Mulhern, and J. M. Rothberg, 1999, "DNA transport by a micromachined Brownian ratchet device," Proc. Natl. Acad. Sci. U.S.A. **96**, 13165–13169.

Baker, G. L., and J. P. Gollub, 1990, *Chaotic Dynamics* (Cambridge University Press, Cambridge, England).

Baltanás, J. P., L. López, I. I. Blechman, P. S. Landa, A. Zaikin, J. Kurths, and M. A. F. Sanjuán, 2003, "Experimental evidence, numerics, and theory of vibrational resonance in bistable systems," Phys. Rev. E **67**, 066119.

Balzani, V., A. Credi, S. Silvi, and M. Venturi, 2006, "Artificial nanomachines based on interlocked molecular species: Recent advances," Chem. Soc. Rev. **35**, 1135–1149.

Bao, J. D., 1999, "Directed current of Brownian ratchet randomly circulating between two thermal sources," Physica A **273**, 286–293.

Barone, A., and G. Paternò, 1982, *Physics and Applications of the Josephson Effect* (Wiley, New York).

Bartussek, R., and P. Hänggi, 1995, "Brownsche Motoren: Wie aus Brownscher Bewegung makroskopischer Transport wird," Phys. Bl. **51** (6), 506–507.

Bartussek, R., P. Hänggi, and J. G. Kissner, 1994, "Periodically rocked thermal ratchets," Europhys. Lett. **28**, 459–464.

Bartussek, R., P. Reimann, and P. Hänggi, 1996, "Precise numerics versus theory for correlation ratchets," Phys. Rev. Lett. **76**, 1166–1169.

Baumgärtner, A., and J. Skolnick, 1995, "Spontaneous translocation of a polymer across a curved membrane," Phys. Rev. Lett. **74**, 2142–2145.

Beck, M., E. Goldobin, M. Neuhaus, M. Siegel, R. Kleiner, and D. Koelle, 2005, "High-efficiency deterministic Josephson vortex ratchet," Phys. Rev. Lett. **95**, 090603.

Berezhkovskii, A. M., M. Pustovoit, and S. M. Bezrukov, 2003, "Channel-facilitated membrane transport: Average lifetimes in the channel," J. Chem. Phys. **119**, 3943–3951.

Berger, J., 2004, "Noise rectification by a superconducting loop with two weak links," Phys. Rev. B **70**, 024524.

Bier, M., M. Kostur, I. Derényi, and R. D. Astumian, 2000, "Nonlinearly coupled flows," Phys. Rev. E **61**, 7184–7187.

Blatter, G., M. V. Feigel'man, V. B. Geshkenbein, A. I. Larkin, and V. M. Vinokur, 1994, "Vortices in high-temperature superconductors," Rev. Mod. Phys. **66**, 1125–1388.

Bleckman, I. I., 2000, *Vibrational Mechanics* (World Scientific, Singapore).

Bleil, S., P. Reimann, and C. Bechinger, 2007, "Directing Brownian motion by oscillating barriers," Phys. Rev. E **75**, 031117.

Borromeo, M., G. Costantini, and F. Marchesoni, 1999, "Critical hysteresis in a tilted washboard potential," Phys. Rev. Lett. **82**, 2820–2823.

Borromeo, M., G. Costantini, and F. Marchesoni, 2002, "Deterministic ratchets: Route to diffusive transport," Phys. Rev. E **65**, 041110.

Borromeo, M., S. Giusepponi, and F. Marchesoni, 2006, "Recycled noise rectification: An automated Maxwell's daemon," Phys. Rev. E **74**, 031121.

Borromeo, M., and F. Marchesoni, 1998, "Brownian surfers,"

Phys. Lett. A **249**, 199–203.
Borromeo, M., and F. Marchesoni, 2000, "Backward-to-forward jump rates on a tilted periodic substrate," Phys. Rev. Lett. **84**, 203–207.
Borromeo, M., and F. Marchesoni, 2004, "Asymmetric confinement in a noisy bistable device," Europhys. Lett. **68**, 783–789.
Borromeo, M., and F. Marchesoni, 2005a, "Mobility oscillations in high-frequency modulated devices," Europhys. Lett. **72**, 362–368.
Borromeo, M., and F. Marchesoni, 2005b, "Noise-assisted transport on symmetric periodic substrates," Chaos **15**, 026110.
Borromeo, M., and F. Marchesoni, 2006, "Vibrational ratchets," Phys. Rev. E **73**, 016142.
Borromeo, M., and F. Marchesoni, 2007a, "Artificial sieves for quasimassless particles," Phys. Rev. Lett. **99**, 150605.
Borromeo, M., and F. Marchesoni, 2007b, "Stochastic synchronization via noise recycling," Phys. Rev. E **75**, 041106.
Brandes, T., and T. Vorrath, 2002, "Adiabatic transfer of electrons in coupled quantum dots," Phys. Rev. B **66**, 075341.
Braunecker, B., D. E. Feldman, and F. Li, 2007, "Spin current and rectification in one-dimensional electronic systems," Phys. Rev. B **76**, 085119.
Brey, J., F. Moreno, R. García-Rojo, and M. J. Ruiz-Montero, 2001, "Hydrodynamic Maxwell demon in granular systems," Phys. Rev. E **65**, 011305.
Brouwer, P. W., 1998, "Scattering approach to parametric pumping," Phys. Rev. B **58**, R10135–R10138.
Browne, W. R., and B. L. Feringa, 2006, "Making molecular machines work," Nat. Nanotechnol. **1**, 25–35.
Bug, A. L. R., and B. J. Berne, 1987, "Shaking-induced transition to a nonequilibrium state," Phys. Rev. Lett. **59**, 948–948.
Buguin, A., L. Talini, and P. Silberzan, 2002, "Ratchet-like topological structures for the control of microdrops," Appl. Phys. A: Mater. Sci. Process. **75**, 207–212.
Burada, P. S., P. Hänggi, G. Schmid, and P. Talkner, 2009, "Diffusion in confined geometries," ChemPhysChem **10**, 45–54.
Bustamante, C., J. Liphardt, and F. Ritort, 2005, "The nonequilibrium thermodynamics of small systems," Phys. Today **58** (7), 43–48.
Caldeira, A. O., and A. J. Leggett, 1983, "Quantum tunneling in a dissipative system," Ann. Phys. (N.Y.) **149**, 374–456.
Caldeira, A. O., and A. J. Leggett, 1984, "Correction," Ann. Phys. (N.Y.) **153**, 445–445.
Carapella, G., and G. Costabile, 2001, "Ratchet effect: Demonstration of a relativistic fluxon diode," Phys. Rev. Lett. **87**, 077002.
Carlo, G. G., G. Benenti, G. Casati, and D. L. Shepelyansky, 2005, "Quantum ratchets in dissipative chaotic systems," Phys. Rev. Lett. **94**, 164101.
Chang, C. W., D. Okawa, A. Majumdar, and A. Zettl, 2006, "Solid-state thermal rectifier," Science **314**, 1121–1124.
Chauwin, J. F., A. Ajdari, and J. Prost, 1994, "Force-free motion in asymmetric structures—a mechanism without diffusive steps," Europhys. Lett. **27**, 421–426.
Chen, Y.-d., 1997, "Asymmetric cycling and biased movement of Brownian particles in fluctuating symmetric potentials," Phys. Rev. Lett. **79**, 3117–3120.
Chepelianskii, A. D., and D. L. Shepelyansky, 2005, "Directing transport by polarized radiation in the presence of chaos and dissipation," Phys. Rev. B **71**, 052508.
Chialvo, D., M. Dykman, and M. Millonas, 1997, "Fluctuation-induced transport in a periodic potential: Noise versus chaos," Phys. Rev. Lett. **78**, 1605.
Chou, C. F., O. Bakajin, S. W. P. Turner, T. A. J. Duke, S. S. Chan, E. C. Cox, H. G. Craighead, and R. Austin, 1999, "Sorting by diffusion: An asymmetric obstacle course for continuous molecular separation," Proc. Natl. Acad. Sci. U.S.A. **96**, 13762–13765.
Chow, W. W., J. Gea-Banacloche, L. M. Pedrotti, V. E. Sanders, W. Schleich, and M. O. Scully, 1985, "The ring laser gyro," Rev. Mod. Phys. **57**, 61–104.
Cleuren, B., and C. Van den Broeck, 2007, "Granular Brownian motor," EPL **77**, 50003.
Cole, D., S. Bending, S. Savel'ev, A. Grigorenko, T. Tamegai, and F. Nori, 2006, "Ratchet without spatial asymmetry for controlling the motion of magnetic flux quanta using time-asymmetric drives," Nature Mater. **5**, 305–311.
Collins, P. G., and P. Avouris, 2000, "Nanotubes for electronics," Sci. Am. (Int. Ed.) **283**, 62–69.
Constantin, D., and Z. S. Siwy, 2007, "Poisson-Nernst-Planck model of ion current rectification through a nanofluidic diode," Phys. Rev. E **76**, 041202.
Costantini, G., and F. Marchesoni, 1999, "Threshold diffusion in a tilted washboard potential," Europhys. Lett. **48**, 491–497.
Costantini, G., F. Marchesoni, and M. Borromeo, 2002, "String ratchets: ac driven asymmetric kinks," Phys. Rev. E **65**, 051103.
Costantini, G., U. M. B. Marconi, and A. Puglisi, 2007, "Granular Brownian ratchet model," Phys. Rev. E **75**, 061124.
Costantini, G., U. M. B. Marconi, and A. Puglisi, 2008, "Noise rectification and fluctuations of an asymmetric inelastic piston," EPL **82**, 50008.
Cota, E., R. Aguado, and G. Platero, 2005, "ac-driven double quantum dots as spin pumps and spin filters," Phys. Rev. Lett. **94**, 107202.
Craig, E. M., N. J. Kuwada, B. J. Lopez, and H. Linke, 2008, "Feedback control in flashing ratchets," Ann. Phys. **17**, 115–129.
Craig, E. M., B. R. Long, J. M. R. Parrondo, and H. Linke, 2008, "Effect of time delay on feedback control of a flashing ratchet," Europhys. Lett. **81**, 10002.
Crisan, A., A. Pross, D. Cole, S. J. Bending, R. Wördenweber, P. Lahl, and E. H. Brandt, 2005, "Anisotropic vortex channeling in $YBa_2Cu_3O_{7-\delta}$ thin films with ordered antidot arrays," Phys. Rev. B **71**, 144504.
Crooks, G. E., 1999, "Entropy production fluctuation theorem and the nonequilibrium work relation for free energy differences," Phys. Rev. E **60**, 2721–2726.
Curzon, F. L., and B. Ahlborn, 1975, "Efficiency of a Carnot engine at maximum power output," Am. J. Phys. **43**, 22–24.
Daiguji, H., Y. Oka, and K. Shirono, 2005, "Nanofluidic diode and bipolar transistor," Nano Lett. **5**, 2274–2280.
Dana, I., V. Ramareddy, I. Talukdar, and G. S. Summy, 2008, "Experimental realization of quantum-resonance ratchets at arbitrary quasimomenta," Phys. Rev. Lett. **100**, 024103.
Daniel, S., S. Sircar, J. Gliem, and M. K. Chaudhury, 2004, "Ratcheting motion of liquid drops on gradient surfaces," Langmuir **20**, 4085–4092.
Dekker, C., 1999, "Carbon nanotubes as molecular quantum wires," Phys. Today **52** (5), 22–28.
Dekker, C., 2007, "Solid-state nanopores," Nat. Nanotechnol. **2**, 209–215.
Denisov, S., and S. Flach, 2001, "Dynamical mechanisms of dc current generation in driven Hamiltonian systems," Phys. Rev. E **64**, 056236.

Denisov, S., S. Flach, and P. Hänggi, 2006, "Stationary Hamiltonian transport with dc bias," Europhys. Lett. **74**, 588–594.
Denisov, S., S. Kohler, and P. Hänggi, 2009, "Underdamped quantum ratchets," EPL **85**, 40003.
Denisov, S., L. Morales-Molina, S. Flach, and P. Hänggi, 2007, "Periodically driven quantum ratchets: Symmetries and resonances," Phys. Rev. A **75**, 063424.
Derényi, I., and A. Ajdari, 1996, "Collective transport of particles in a "flashing" periodic potential," Phys. Rev. E **54**, R5–R8.
Derényi, I., and T. Vicsek, 1995, "Cooperative transport of Brownian particles," Phys. Rev. Lett. **75**, 374–377.
Derouane, E. G., and Z. Gabelica, 1980, "A novel effect of shape selectivity—Molecular traffic control in zeolite ZSM-5," J. Catal. **65**, 486–489.
de Vondel, J. V., C. C. de Souza Silva, and V. V. Moshchalkov, 2007, "Diode effects in the surface superconductivity regime," Europhys. Lett. **80**, 17006.
de Vondel, J. V., C. C. de Souza Silva, B. Y. Zhu, M. Morelle, and V. V. Moshchalkov, 2005, "Vortex-rectification effects in films with periodic asymmetric pinning," Phys. Rev. Lett. **94**, 057003.
Dholakia, K., M. P. MacDonald, P. Zemanek, and T. Cizmar, 2007, "Cellular and colloidal separation using optical forces," Methods Cell Biol. **82**, 467–495.
Doering, C. R., W. Horsthemke, and J. Riordan, 1994, "Nonequilibrium fluctuation-induced transport," Phys. Rev. Lett. **72**, 2984–2987.
Dresselhaus, M. S., G. Dresselhaus, and P. C. Eklund, 1996, *The Science of Fullerenes and Carbon Nanotubes* (Academic, New York).
Drexler, K. E., 1992, *Nanosystems: Molecular Machinery, Manufacturing and Computation* (Wiley, New York).
Duke, T. A. J., and R. H. Austin, 1998, "Microfabricated sieve for the continuous sorting of macromolecules," Phys. Rev. Lett. **80**, 1552–1555.
Eggers, J., 1999, "Sand as Maxwell's demon," Phys. Rev. Lett. **83**, 5322–5325.
Eichhorn, R., P. Reimann, and P. Hänggi, 2002a, "Brownian motion exhibiting absolute negative mobility," Phys. Rev. Lett. **88**, 190601.
Eichhorn, R., P. Reimann, and P. Hänggi, 2002b, "Paradoxical motion of a single Brownian particle: Absolute negative mobility," Phys. Rev. E **66**, 066132.
Ellmann, H., J. Jersblad, and A. Kastberg, 2003, "Experiments with a 3D double optical lattice," Phys. Rev. Lett. **90**, 053001.
Engel, A., and P. Reimann, 2004, "Thermal ratchet effects in ferrofluids," Phys. Rev. E **70**, 051107.
Ertas, D., 1998, "Lateral separation of macromolecules and polyelectrolytes in microlithographic arrays," Phys. Rev. Lett. **80**, 1548–1551.
Falo, F., P. J. Martinez, J. J. Mazo, T. P. Orlando, K. Segall, and E. Trias, 2002, "Fluxon ratchet potentials in superconducting circuits," Appl. Phys. A: Mater. Sci. Process. **75**, 263–269.
Farkas, Z., F. Szalai, D. E. Wolf, and T. Vicsek, 2002, "Segregation of granular binary mixtures by a ratchet mechanism," Phys. Rev. E **65**, 022301.
Faucheux, L. P., L. S. Bourdieu, P. D. Kaplan, and A. J. Libchaber, 1995, "Optical thermal ratchet," Phys. Rev. Lett. **74**, 1504–1507.
Faucheux, L. P., and A. Libchaber, 1995, "Selection of Brownian particles," J. Chem. Soc., Faraday Trans. **91**, 3163–3166.
Feito, M., and F. J. Cao, 2007, "Information and maximum power in a feedback controlled Brownian ratchet," Eur. Phys. J. B **59**, 63–68.
Feito, M., and F. J. Cao, 2008, "Transport reversal in a delayed feedback ratchet," Physica A **387**, 4553–4559.
Feldman, D. E., S. Scheidl, and V. M. Vinokur, 2005, "Rectification in Luttinger liquids," Phys. Rev. Lett. **94**, 186809.
Fenzke, D., and J. Kärger, 1993, "On the correlation between the step rates and the diffusivities of guest molecules in microporous crystal," Z. Phys. D: At., Mol. Clusters **25**, 345–350.
Ferrando, R., R. Spadacini, and G. E. Tommei, 1995, "Retrapping and velocity inversion in jump diffusion," Phys. Rev. E **51**, 126–130.
Festa, R., and E. G. d'Agliano, 1978, "Diffusion coefficient for a Brownian particle in a periodic field of force: I. Large friction limit," Physica A **90**, 229–244.
Feynman, R. P., 1960, *There's Plenty of Room at the Bottom* (Caltech's Engineering & Science Magazine, Pasadena).
Feynman, R. P., R. B. Leighton, and M. Sands, 1963, *The Feynman Lectures on Physics* (Addison-Wesley, Reading, MA), Vol. I.
Flach, S., O. Yevtushenko, and Y. Zolotaryuk, 2000, "Directed current due to broken time-space symmetry," Phys. Rev. Lett. **84**, 2358–2361.
Flatte, M. E., 2008, "Spin ratchets: A one-way street for spin current," Nat. Phys. **4**, 587–588.
Fleischer, R. L., P. B. Price, and R. M. Walker, 1975, *Nuclear Tracks in Solids. Principles and Applications* (University of California Press, Berkeley).
Freund, J. A., and L. Schimansky-Geier, 1999, "Diffusion in discrete ratchets," Phys. Rev. E **60**, 1304–1309.
Gallavotti, G., and E. G. D. Cohen, 1995, "Dynamical ensembles in nonequilibrium statistical mechanics," Phys. Rev. Lett. **74**, 2694–2697.
Gammaitoni, L., P. Hänggi, P. Jung, and F. Marchesoni, 1998, "Stochastic resonance," Rev. Mod. Phys. **70**, 223–287.
Gao, Y. H., and Y. Bando, 2002, "Carbon nanothermometer containing gallium—Gallium's macroscopic properties are retained on a miniature scale in this nanodevice," Nature (London) **415**, 599–599.
Geisel, T., and J. Nierwetberg, 1982, "Onset of diffusion and universal scaling in chaotic systems," Phys. Rev. Lett. **48**, 7–10.
Gerland, U., R. Bundschuh, and T. Hwa, 2004, "Translocation of structured polynucleotides through nanopores," Phys. Biol. **1**, 19–26.
Gillijns, W., A. V. Silhanek, V. V. Moshchalkov, C. J. O. Reichhardt, and C. Reichhardt, 2007, "Origin of reversed vortex ratchet motion," Phys. Rev. Lett. **99**, 247002.
Gommers, R., S. Bergamini, and F. Renzoni, 2005, "Dissipation-induced symmetry breaking in a driven optical lattice," Phys. Rev. Lett. **95**, 073003.
Gommers, R., M. Brown, and F. Renzoni, 2007, "Symmetry and transport in a cold atom ratchet with multifrequency driving," Phys. Rev. A **75**, 053406.
Gommers, R., S. Denisov, and F. Renzoni, 2006, "Quasiperiodically driven ratchets for cold atoms," Phys. Rev. Lett. **96**, 240604.
Gommers, R., V. Lebedev, M. Brown, and F. Renzoni, 2008, "Gating ratchet for cold atoms," Phys. Rev. Lett. **100**, 040603.
Gong, J., and P. Brumer, 2004, "Directed anomalous diffusion without a biased field: A ratchet accelerator," Phys. Rev. E **70**, 016202.

Gong, J., and P. Brumer, 2006, "Generic quantum ratchet accelerator with full classical chaos," Phys. Rev. Lett. **97**, 240602.
Gong, J., D. Poletti, and P. Hänggi, 2007, "Dissipationless directed transport in rocked single-band quantum dynamics," Phys. Rev. A **75**, 033602.
Gonzalez, M., N. O. Nunez, J. V. Anguita, and J. L. Vicent, 2007, "Transverse rectification in superconducting thin films with arrays of asymmetric defects," Appl. Phys. Lett. **91**, 062505.
Gorman, M., M. el Hamdi, B. Pearson, and K. A. Robbins, 1996, "Ratcheting motion of concentric rings in cellular flames," Phys. Rev. Lett. **76**, 228–231.
Gorre, L., E. Ioannidis, and P. Silberzan, 1996, "Rectified motion of a mercury drop in an asymmetric structure," Europhys. Lett. **33**, 267–272.
Goychuk, I., 2006, "Chemically driven electron tunneling pumps," Mol. Simul. **32**, 717–725.
Goychuk, I., M. Grifoni, and P. Hänggi, 1998a, "Nonadiabatic quantum Brownian rectifiers," Phys. Rev. Lett. **81**, 649–652.
Goychuk, I., M. Grifoni, and P. Hänggi, 1998b, "Addendum," Phys. Rev. Lett. **81**, 2837–2837.
Goychuk, I., and P. Hänggi, 1998, "Quantum rectifiers from harmonic mixing," Europhys. Lett. **43**, 503–509.
Goychuk, I., and P. Hänggi, 2000, "Directed current without dissipation: Reincarnation of a Maxwell-Loschmidt-demon," Lect. Notes Phys. **557**, 7–20.
Goychuk, I., and P. Hänggi, 2001, "Minimal quantum Brownian rectifiers," J. Phys. Chem. B **105**, 6642–6647.
Goychuk, I., and P. Hänggi, 2005, "Quantum dynamics in strong fluctuating fields," Adv. Phys. **54**, 525–584.
Grier, D. G., 2003, "A revolution in optical manipulation," Nature (London) **424**, 810–816.
Grifoni, M., M. S. Ferreira, J. Peguiron, and J. B. Majer, 2002, "Quantum ratchets with few bands below the barrier," Phys. Rev. Lett. **89**, 146801.
Grifoni, M., and P. Hänggi, 1998, "Driven quantum tunneling," Phys. Rep. **304**, 229–354.
Grigorenko, A., S. Bending, T. Tamegai, S. Ooi, and M. Henini, 2001, "A one-dimensional chain state of vortex matter," Nature (London) **414**, 728–731.
Gross, M., 1999, *Travels to the Nanoworld* (Perseus, New York).
Grossmann, S., and H. Fujisaka, 1982, "Diffusion in discrete nonlinear dynamical systems," Phys. Rev. A **26**, 1779–1782.
Grynberg, G., and C. Robilliard, 2001, "Cold atoms in dissipative optical lattices," Phys. Rep. **355**, 335–451.
Han, J., and H. G. Craighead, 2000, "Separation of long DNA molecules in a microfabricated entropic trap array," Science **288**, 1026–1029.
Han, J., S. W. Turner, and H. G. Craighead, 1999, "Entropic trapping and escape of long DNA molecules at submicron size constriction," Phys. Rev. Lett. **83**, 1688–1691.
Hänggi, P., and R. Bartussek, 1996, "Browninan rectifiers: How to convert Brownian motion into directed transport," Lect. Notes Phys. **476**, 294–308.
Hänggi, P., R. Bartussek, P. Talkner, and J. Luczka, 1996, "Noise-induced transport in symmetric periodic potentials: White shot noise versus deterministic noise," Europhys. Lett. **35**, 315–317.
Hänggi, P., and G.-L. Ingold, 2005, "Fundamental aspects of quantum Brownian motion," Chaos **15**, 026105.
Hänggi, P., P. Jung, and F. Marchesoni, 1989, "Escape driven by strongly colored noise," J. Stat. Phys. **54**, 1367–1380.
Hänggi, P., F. Marchesoni, and F. Nori, 2005, "Brownian motors," Ann. Phys. **14**, 51–70.
Hänggi, P., M. Ratner, and S. Yaliraki, 2002, "Transport in molecular wires, Preface," Chem. Phys. **281**, 111–111.
Hänggi, P., P. Talkner, and M. Borkovec, 1990, "Reaction-rate theory: Fifty years after Kramers," Rev. Mod. Phys. **62**, 251–341.
Hänggi, P., and H. Thomas, 1982, "Stochastic processes: Time-evolution, symmetries and linear response," Phys. Rep. **88**, 207–319.
Harada, K., O. Kamimura, H. Kasai, T. Matsuda, A. Tonomura, and V. V. Moshchalkov, 1996, "Direct observation of vortex dynamics in superconducting films with regular arrays of defects," Science **274**, 1167–1170.
Harms, T., and R. Lipowsky, 1997, "Driven ratchets with disordered tracks," Phys. Rev. Lett. **79**, 2895–2898.
Harris, T. E., 1974, "Contact interactions on a lattice," Ann. Probab. **2**, 969–988.
Hartl, F. U., 1996, "Molecular chaperones in cellular protein folding," Nature (London) **304**, 571–580.
Haw, M., 2007, *Middle World: The Restless Heart of Matter and Life* (Macmillan, New York).
Healy, K., 2007, "Nanopore-based single-molecule DNA analysis," Nanomedicine **2**, 459–481.
Healy, K., B. Schiedt, and A. P. Morrison, 2007, "Solid-state nanopore technologies for nanopore-based DNA analysis," Nanomedicine **2**, 875–897.
Hechtfischer, G., R. Kleiner, A. V. Ustinov, and P. Müller, 1997, "Non-Josephson emission from intrinsic junctions in $Bi_2Sr_2CaCu_2O_{8+y}$: Cherenkov radiation by Josephson vortices," Phys. Rev. Lett. **79**, 1365–1368.
Heinsalu, E., M. Patriarca, and F. Marchesoni, 2008, "Dimer diffusion in a washboard potential," Phys. Rev. E **77**, 021129.
Heller, M., and H. Bruus, 2008, "A theoretical analysis of the resolution due to diffusion and size dispersion of particles in deterministic lateral displacement devices," J. Micromech. Microeng. **18**, 075030.
Hohberger, E. M., A. Lorke, W. Wegscheider, and M. Bichler, 2001, "Adiabatic pumping of two-dimensional electrons in a ratchet-type lateral superlattice," Appl. Phys. Lett. **78**, 2905–2907.
Holt, J. K., H. G. Park, Y. M. Wang, M. Stadermann, A. B. Artyukhin, C. P. Grigoropoulos, A. Noy, and O. Bakajin, 2006, "Fast mass transport through sub-2-nanometer carbon nanotubes," Science **312**, 1034–1037.
Howard, J., 2001, *Mechanics of Motor Proteins and the Cytoskeleton* (Sinauer Press, Sunderland MA).
Huang, L. R., E. C. Cox, R. H. Austin, and J. C. Sturm, 2004, "Continuous particle separation through deterministic lateral displacement," Science **304**, 987–990.
Huberman, B. A., J. P. Crutchfield, and N. H. Packard, 1980, "Noise phenomena in Josephson junctions," Appl. Phys. Lett. **37**, 750–752.
Hugel, T., N. B. Holland, A. Cattani, L. Moroder, M. Seitz, and H. E. Gaub, 2002, "Single-molecule optomechanical cycle," Science **296**, 1103–1106.
Im, W., and B. Roux, 2002, "Ion permeation and selectivity of OmpF porin: A theoretical study based on molecular dynamics, Brownian dynamics, and continuum electrodiffusion theory," J. Mol. Biol. **322**, 851–869.
Jaeger, H. M., S. R. Nagel, and R. P. Behringer, 1996, "Granular solids, liquids, and gases," Rev. Mod. Phys. **68**, 1259–1273.

Jarzynski, C., 1997, "Nonequilibrium equality for free energy differences," Phys. Rev. Lett. **78**, 2690–2693.
Jarzynski, C., 2007, "Comparison of far-from-equilibrium work relations," C. R. Phys. **8**, 495–506.
Jepsen, D. W., 1965, "Dynamics of a simple many-body system of hard rods," J. Math. Phys. **6**, 405–413.
Jessen, P. S., and I. H. Deutsch, 1996, "Optical lattices," Adv. At., Mol., Opt. Phys. **37**, 95–138.
John, K., P. Hänggi, and U. Thiele, 2008, "Ratched-driven fluid transport in bounded two-layer films of immiscible liquids," Soft Matter **4**, 1183–1195.
John, K., and U. Thiele, 2007, "Liquid transport generated by a flashing field-induced wettability ratchet," Appl. Phys. Lett. **90**, 264102.
Jones, P. H., M. Goonasekera, D. R. Meacher, T. Jonckheere, and T. S. Monteiro, 2007, "Directed motion for delta-kicked atoms with broken symmetries: Comparison between theory and experiment," Phys. Rev. Lett. **98**, 073002.
Jülicher, F., A. Ajdari, and J. Prost, 1997, "Modeling molecular motors," Rev. Mod. Phys. **69**, 1269–1281.
Jung, P., and P. Hänggi, 1991, "Amplification of small signals via stochastic resonance," Phys. Rev. A **44**, 8032–8041.
Jung, P., J. G. Kissner, and P. Hänggi, 1996, "Regular and chaotic transport in asymmetric periodic potentials: Inertia ratchets," Phys. Rev. Lett. **76**, 3436–3439.
Kafri, Y., and D. Nelson, 2005, "Sequence heterogeneity and the dynamics of molecular motors," J. Phys.: Condens. Matter **17**, S3871–S3886.
Kalman, E., K. Healy, and Z. S. Siwy, 2007, "Tuning ion current rectification in asymmetric nanopores by signal mixing," EPL **78**, 28002.
Kärger, J., 2008a, "Diffusion measurements by NMR techniques," Mol. Sieves **7**, 85–133.
Kärger, J., 2008b, "Single-file diffusion in zeolites," Mol. Sieves **7**, 329–366.
Kärger, J., and D. M. Ruthven, 1992, *Diffusion in Zeolites and Other Microporous Solids* (Wiley, New York).
Kärger, J., R. Valiullin, and S. Vasenkov, 2005, "Molecular dynamics under confinement to one dimension: Options of measurement and accessible information," New J. Phys. **7**, 15.
Karnik, R., C. Duan, K. Castelino, H. Daiguji, and A. Majumdar, 2007, "Rectification of ionic current in a nanofluidic diode," Nano Lett. **7**, 547–551.
Kasianowicz, J. J., E. Brandin, D. Branton, and D. W. Deamer, 1996, "Characterization of individual polynucleotide molecules using a membrane channel," Proc. Natl. Acad. Sci. U.S.A. **93**, 13770–13773.
Kay, E. R., D. A. Leigh, and F. Zerbetto, 2007, "Synthetic molecular motors and mechanical machines," Angew. Chem., Int. Ed. **46**, 72–191.
Keay, B., S. Zeuner, S. Allen, K. Maranowski, A. Gossard, U. Bhattacharya, and M. Rodell, 1995, "Dynamic localization, absolute negative conductance, and stimulated, multiphoton emission in sequential resonant-tunneling semiconductor superlattices," Phys. Rev. Lett. **75**, 4102–4105.
Kenfack, A., J. Gong, and A. K. Pattanayak, 2008, "Controlling the ratchet effect for cold atoms," Phys. Rev. Lett. **100**, 044104.
Kettner, C., P. Reimann, P. Hänggi, and F. Müller, 2000, "Drift ratchet," Phys. Rev. E **61**, 312–323.
Khrapai, V. S., S. Ludwig, J. P. Kotthaus, H. P. Tranitz, and W. Wegscheider, 2006, "Double-dot quantum ratchet driven by an independently biased quantum point contact," Phys. Rev. Lett. **97**, 176803.
Kohler, S., J. Lehmann, and P. Hänggi, 2005, "Driven quantum transport on the nanoscale," Phys. Rep. **406**, 379–443.
Kolomeisky, A. B., 2007, "Channel-facilitated molecular transport across membranes: Attraction, repulsion, and asymmetry," Phys. Rev. Lett. **98**, 048105.
Komnik, A., and A. O. Gogolin, 2003, "Transport, optical properties, and quantum ratchet effects for quantum dots and molecules coupled to Luttinger liquids," Phys. Rev. B **68**, 235323.
Koshelev, A. E., 1999, "Crossing lattices, vortex chains, and angular dependence of melting line in layered superconductors," Phys. Rev. Lett. **83**, 187.
Kosinska, I. D., I. Goychuk, M. Kostur, G. Schmid, and P. Hänggi, 2008, "Rectification in synthetic conical nanopores: A one-dimensional Poisson-Nernst-Planck model," Phys. Rev. E **77**, 031131.
Koss, B. A., and D. G. Grier, 2003, "Optical peristalsis," Appl. Phys. Lett. **82**, 3985–3987.
Kostur, M., L. Machura, P. Talkner, P. Hänggi, and J. Luczka, 2008, "Anomalous transport in biased ac-driven Josephson junctions: Negative conductances," Phys. Rev. B **77**, 104509.
Kostur, M., M. Schindler, P. Talkner, and P. Hänggi, 2006, "Chiral separation in microflows," Phys. Rev. Lett. **96**, 014502.
Kosztin, I., and K. Schulten, 2004, "Fluctuation-driven molecular transport through an asymmetric membrane channel," Phys. Rev. Lett. **93**, 238102.
Kottas, G. S., L. I. Clarke, D. Horinek, and J. Michl, 2005, "Artificial molecular motors," Chem. Rev. (Washington, D.C.) **105**, 1281–1376.
Kouwenhoven, L. P., A. T. Johnson, N. C. van der Vaart, C. J. P. M. Harmans, and C. T. Foxon, 1991, "Quantized current in a quantum-dot turnstile using oscillating tunnel barriers," Phys. Rev. Lett. **67**, 1626–1629.
Kwok, W. K., R. J. Olsson, G. Karapetrov, U. Welp, V. Vlasko-Vlasov, K. Kadowaki, and G. W. Crabtree, 2002, "Modification of vortex behavior through heavy ion lithography," Physica C **382**, 137–141.
Landa, P. S., and P. V. E. McClintock, 2000, "Vibrational resonance," J. Phys. A **33**, L433–L438.
Läuger, P., 1991, *Electrogenic Ion Pumps Cytoskeleton* (Sinauer Associates, Sunderland, MA).
Lebowitz, J. L., and J. K. Percus, 1967, "Kinetic equations and density expansions: Exactly solvable one-dimensional system," Phys. Rev. **155**, 122–138.
Lee, C.-S., B. Jankó, I. Derényi, and A.-L. Barabási, 1999, "Reducing vortex density in superconductors using the "ratchet effect," " Nature (London) **400**, 337–340.
Lee, K. H., 2003, "Ratchet effect in an ac-current driven Josephson junction array," Appl. Phys. Lett. **83**, 117–119.
Lee, S.-H., K. Ladavac, M. Polin, and D. G. Grier, 2005, "Observation of flux reversal in a symmetric optical thermal ratchet," Phys. Rev. Lett. **94**, 110601.
Leff, H. S., and A. F. Rex, 2003, Eds., *Maxwell's Daemon 2: Entropy, Classical and Quantum Information, Computing*, 2nd ed. (IOP, London).
Lehmann, J., S. Kohler, P. Hänggi, and A. Nitzan, 2002, "Molecular wires acting as coherent quantum ratchets," Phys. Rev. Lett. **88**, 228305.
Lehmann, J., S. Kohler, P. Hänggi, and A. Nitzan, 2003, "Rectification of laser-induced electronic transport through molecules," J. Chem. Phys. **118**, 3283–3293.

Levitt, D. G., 1973, "Dynamics of a single-file pore: Non-Fickian behavior," Phys. Rev. A **8**, 3050–3054.
Li, J., D. Stein, C. McMullan, D. Branton, M. J. Aziz, and J. A. Golovchenko, 2001, "Ion-beam sculpting at nanometre length scales," Nature (London) **412**, 166–169.
Li, N., P. Hänggi, and B. W. Li, 2008, "Ratcheting heat flux against a thermal bias," EPL **84**, 40009.
Lindner, B., L. Schimansky-Geier, P. Reimann, P. Hänggi, and M. Nagaoka, 1999, "Inertia ratchets: A numerical study versus theory," Phys. Rev. E **59**, 1417–1424.
Linke, H., 2002, "Ratchets and Brownian motors: Basics, experiments and applications," Appl. Phys. A: Mater. Sci. Process. **75**, 167.
Linke, H., B. J. Alemán, L. D. Melling, M. J. Taormina, M. J. Francis, C. C. Dow-Hygelund, V. Narayanan, R. P. Taylor, and A. Stout, 2006, "Self-propelled Leidenfrost droplets," Phys. Rev. Lett. **96**, 154502.
Linke, H., T. E. Humphrey, P. E. Lindelof, A. Lofgren, R. Newbury, P. Omling, A. O. Sushkov, R. P. Taylor, and H. Xu, 2002, "Quantum ratchets and quantum heat pumps," Appl. Phys. A: Mater. Sci. Process. **75**, 237–246.
Linke, H., T. E. Humphrey, A. Lofgren, A. O. Sushkov, R. Newbury, R. P. Taylor, and P. Omling, 1999, "Experimental tunneling ratchets," Science **286**, 2314–2317.
Linke, H., W. Sheng, A. Löfgren, H. Xu, P. Omling, and P. E. Lindelof, 1998, "A quantum dot ratchet: Experiment and theory," Europhys. Lett. **44**, 341–347.
Lipowsky, R., and S. Klumpp, 2005, "Life is motion: Multiscale motility of molecular motors," Physica A **352**, 53–112.
Lopez, B. J., N. J. Kuwada, E. M. Craig, B. R. Long, and H. Linke, 2008, "Realization of a feedback controlled flashing ratchet," Phys. Rev. Lett. **101**, 220601.
Lorke, A., S. Wimmer, B. Jager, J. P. Kotthaus, W. Wegscheider, and M. Bichler, 1998, "Far-infrared and transport properties of antidot arrays with broken symmetry," Physica B **249-251**, 312–316.
Luchsinger, R. H., 2000, "Transport in nonequilibrium systems with position-dependent mobility," Phys. Rev. E **62**, 272–275.
Luczka, J., R. Bartussek, and P. Hänggi, 1995, "White-noise-induced transport in periodic structures," Europhys. Lett. **31**, 431–436.
Lundh, E., and M. Wallin, 2005, "Ratchet effect for cold atoms in an optical lattice," Phys. Rev. Lett. **94**, 110603.
Machura, L., M. Kostur, P. Hänggi, P. Talkner, and J. Łuczka, 2004, "Consistent description of quantum Brownian motors operating at strong friction," Phys. Rev. E **70**, 031107.
Machura, L., M. Kostur, P. Talkner, J. Łuczka, and P. Hänggi, 2007, "Absolute negative mobility induced by thermal equilibrium fluctuations," Phys. Rev. Lett. **98**, 040601.
Machura, L., M. Kostur, P. Talkner, J. Łuczka, F. Marchesoni, and P. Hänggi, 2004, "Brownian motors: Current fluctuations and rectification efficiency," Phys. Rev. E **70**, 061105.
Machura, L., J. Luczka, P. Talkner, and P. Hänggi, 2007, "Transport of forced quantum motors in the strong friction limit," Acta Phys. Pol. B **38**, 1855–1863.
Magnasco, M. O., 1993, "Forced thermal ratchets," Phys. Rev. Lett. **71**, 1477–1481.
Majer, J. B., J. Peguiron, M. Grifoni, M. Tusveld, and J. E. Mooij, 2003, "Quantum ratchet effect for vortices," Phys. Rev. Lett. **90**, 056802.
Marchesoni, F., 1986, "Harmonic mixing signal: Doubly dithered ring laser gyroscope," Phys. Lett. A **119**, 221–224.
Marchesoni, F., 1996, "Thermal ratchets in 1+1 dimensions," Phys. Rev. Lett. **77**, 2364–2367.
Marchesoni, F., 1997, "Transport properties in disordered ratchet potentials," Phys. Rev. E **56**, 2492–2495.
Marchesoni, F., 1998, "Conceptual design of a molecular shuttle," Phys. Lett. A **237**, 126–130.
Marchesoni, F., S. Savel'ev, and F. Nori, 2006a, "Achieving optimal rectification using underdamped rocked ratchets," Phys. Rev. E **73**, 021102.
Marchesoni, F., S. Savel'ev, and F. Nori, 2006b, "Driven binary mixtures: Clustering and giant diffusion," Europhys. Lett. **73**, 513–519.
Marchesoni, F., P. Sodano, and M. Zanetti, 1988, "Supersymmetry and bistable soft potentials," Phys. Rev. Lett. **61**, 1143–1146.
Marchesoni, F., and A. Taloni, 2006, "Subdiffusion and long-time anticorrelations in a stochastic single file," Phys. Rev. Lett. **97**, 106101.
Marquet, C., A. Buguin, L. Talini, and P. Silberzan, 2002, "Rectified motion of colloids in asymmetrically structured channels," Phys. Rev. Lett. **88**, 168301.
Martinez, P. J., and R. Chacon, 2008, "Disorder induced control of discrete soliton ratchets," Phys. Rev. Lett. **100**, 144101.
Maruyama, K., F. Nori, and V. Vedral, 2008, "The physics of Maxwell's demon and information," Rev. Mod. Phys. **81**, 1–23.
Mateos, J. L., 2000, "Chaotic transport and current reversal in deterministic ratchets," Phys. Rev. Lett. **84**, 258–261.
Mateos, J. L., 2003, "Current reversals in chaotic ratchets: The battle of the attractors," Physica A **325**, 92–100.
Matsuda, T., O. Kamimura, H. Kasai, K. Harada, T. Yoshida, T. Akashi, A. Tonomura, Y. Nakayama, J. Shimoyama, K. Kishio, T. Hanaguri, and K. Kitazawa, 2001, "Oscillating rows of vortices in superconductors," Science **294**, 2136–2138.
Matthias, S., and F. Müller, 2003, "Asymmetric pores in a silicon membrane acting as massively parallel Brownian ratchets," Nature (London) **424**, 53–57.
Mel'nikov, V. I., 1991, "The Kramers problem: Fifty years of development," Phys. Rep. **209**, 1–71.
Menghini, M., J. V. de Vondel, D. G. Gheorghe, R. J. Wijngaarden, and V. V. Moshchalkov, 2007, "Asymmetry reversal of thermomagnetic avalanches in Pb films with a ratchet pinning potential," Phys. Rev. B **76**, 184515.
Mennerat-Robilliard, C., D. Lucas, S. Guibal, J. Tabosa, C. Jurczak, J.-Y. Courtois, and G. Grynberg, 1999, "Ratchet for cold rubidium atoms: The asymmetric optical lattice," Phys. Rev. Lett. **82**, 851–854.
Millonas, M. M., and M. I. Dykman, 1994, "Transport and current reversal in stochastically driven ratchets," Phys. Lett. A **185**, 65–69.
Morales-Molina, L., and S. Flach, 2008, "Resonant ratcheting of a Bose-Einstein condensate," New J. Phys. **10**, 013008.
Morales-Molina, L., J. B. Gong, and S. Flach, 2008, "Quantum raatchet control—Harvesting on Landau-Zener transitions," Europhys. Lett. **83**, 40005.
Moskalets, M., and M. Büttiker, 2002, "Floquet scattering theory of quantum pumps," Phys. Rev. B **66**, 205320.
Moskalets, M., and M. Büttiker, 2004, "Floquet scattering theory for current and heat noise in large amplitude adiabatic pumps," Phys. Rev. B **70**, 245305.
Movileanu, L., 2008, "Squeezing a single polypeptide through a nanopore," Soft Matter **4**, 925–931.
Müller, F., A. Birner, J. Schilling, U. Gösele, C. Kettner, and P. Hänggi, 2000, "Membranes for micropumps from

macroporous silicon," Phys. Status Solidi A **182**, 585–590.
Nagel, J., D. Speer, A. Sterck, R. Eichhorn, P. Reimann, K. Illin, M. Siegel, D. Koelle, and R. Kleiner, 2008, "Observation of negative absolute resistance in a Josephson junction," Phys. Rev. Lett. **100**, 217001.
Neuert, G., T. Hugel, R. Netzt, and H. Gaub, 2006, "Elasticity of polyazobenzene-peptides," Macromolecules **39**, 789–797.
Neugebauer, N., P. Bräuer, and J. Kärger, 2000, "Reactivity enhancement by molecular traffic control," J. Catal. **194**, 1–3.
Nigg, E. A., 1997, "Nucleocytoplasmic transport: Signals, mechanisms and regulation," Nature (London) **386**, 779–787.
Nishiyama, M., H. Higuchi, and T. Yanagida, 2002, "Chemomechanical coupling of the ATPase cycle to the forward and backward movements of single kinesin molecules," Nat. Cell Biol. **4**, 790–797.
Nishiyama, M., E. Muto, Y. Inoue, T. Yanagida, and H. Higuchi, 2001, "Substeps within the 8-nm step of the ATPase cycle of single kinesin molecules," Nat. Cell Biol. **3**, 425–428.
Olson, C. J., C. Reichhardt, B. Jankó, and F. Nori, 2001, "Collective interaction-driven ratchet for transporting flux quanta," Phys. Rev. Lett. **87**, 177002.
Ooi, S., S. Savel'ev, M. B. Gaifullin, T. Mochiku, K. Hirata, and F. Nori, 2007, "Nonlinear nanodevices using magnetic flux quanta," Phys. Rev. Lett. **99**, 207003.
Ooi, S., T. Shibauchi, N. Okuda, and T. Tamegai, 1999, "Novel angular scaling of vortex phase transitions in $Bi_2Sr_2CaCu_2O_{8+y}$," Phys. Rev. Lett. **82**, 4308–4311.
Park, P. J., and W. Sung, 1999, "Dynamics of a polymer surmounting a potential barrier: The Kramers problem for polymers," J. Chem. Phys. **111**, 5259–5266.
Parrondo, J., and B. de Cisneros, 2002, "Energetics of Brownian motors: A review," Appl. Phys. A: Mater. Sci. Process. **75**, 179–191.
Parrondo, J. M. R., and P. Español, 1996, "Criticism of Feynman's analysis of the ratchet as an engine," Am. J. Phys. **64**, 1125–1130.
Platero, G., and R. Aguado, 2004, "Photon-assisted transport in semiconductor nanostructures," Phys. Rep. **395**, 1–157.
Plourde, B. L. T., D. J. Van Harlingen, R. Besseling, M. B. S. Hesselberth, and P. H. Kes, 2000, "Vortex dynamics in thin superconducting strips observed by scanning SQUID microscopy," Physica C **341-348**, 1023–1026.
Poletti, D., G. Benenti, G. Casati, and B. Li, 2007, "Interaction-induced quantum ratchet in a Bose-Einstein condensate," Phys. Rev. A **76**, 023421.
Poletti, D., G. G. Carlo, and B. Li, 2007, "Current behavior of a quantum Hamiltonian ratchet in resonance," Phys. Rev. E **75**, 011102.
Pollak, E., J. Bader, B. J. Berne, and P. Talkner, 1993, "Theory of correlated hops in surface diffusion," Phys. Rev. Lett. **70**, 3299–3302.
Popescu, M. N., C. M. Arizmendi, A. L. Salas-Brito, and F. Family, 2000, "Disorder induced diffusive transport in ratchets," Phys. Rev. Lett. **85**, 3321–3324.
Porto, M., M. Urbakh, and J. Klafter, 2000, "Atomic scale engines: Cars and wheels," Phys. Rev. Lett. **84**, 6058–6061.
Pothier, H., P. Lafarge, C. Urbina, D. Esteve, and M. H. Devoret, 1992, "Single-electron pump based on charging effects," Europhys. Lett. **17**, 249–254.
Prost, J., J. F. Chauwin, L. Peliti, and A. Ajdari, 1994, "Asymmetric pumping of ratchets," Phys. Rev. Lett. **72**, 2652–2655.
Purcell, E. M., 1977, "Life at low Reynolds number," Am. J. Phys. **45**, 3–11.
Quéré, D., and A. Ajdari, 2006, "Liquid drops: Surfing the hot spot," Nature Mater. **5**, 429–430.
Rapaport, D. C., 2002, "The wonderful world of granular ratchets," Comput. Phys. Commun. **147**, 141–144.
Regan, B. C., S. Aloni, R. O. Ritchie, U. Dahmen, and A. Zettl, 2004, "Carbon nanotubes as nanoscale mass conveyors," Nature (London) **428**, 924–927.
Reguera, D., G. Schmid, P. S. Burada, J. M. Rubí, P. Reimann, and P. Hänggi, 2006, "Entropic transport: Kinetics, scaling, and control mechanisms," Phys. Rev. Lett. **96**, 130603.
Reichhardt, C., C. J. Olson, and F. Nori, 1998, "Commensurate and incommensurate vortex states in superconductors with periodic pinning arrays," Phys. Rev. B **57**, 7937–7943.
Reichhardt, C. J. O., and C. Reichhardt, 2005, "Rectification and flux reversals for vortices interacting with triangular traps," Physica C **432**, 125–132.
Reimann, P., 2001, "Supersymmetric ratchets," Phys. Rev. Lett. **86**, 4992–4995.
Reimann, P., 2002, "Brownian motors: Noisy transport far from equilibrium," Phys. Rep. **361**, 57–265.
Reimann, P., R. Bartussek, R. Häussler, and P. Hänggi, 1996, "Brownian motors driven by temperature oscillations," Phys. Lett. A **215**, 26–31.
Reimann, P., M. Grifoni, and P. Hänggi, 1997, "Quantum ratchets," Phys. Rev. Lett. **79**, 10–13.
Reimann, P., and P. Hänggi, 1998, "Quantum features of Brownian motors and stochastic resonance," Chaos **8**, 629–642.
Reimann, P., and P. Hänggi, 2002, "Introduction to the physics of Brownian motors," Appl. Phys. A: Mater. Sci. Process. **75**, 169–178.
Reimann, P., R. Kawai, C. Van den Broeck, and P. Hänggi, 1999, "Coupled Brownian motors: Anomalous hysteresis and zero-bias negative conductance," Europhys. Lett. **45**, 545–551.
Reimann, P., C. Van den Broeck, H. Linke, P. Hänggi, J. M. Rubí, and A. Pérez-Madrid, 2001, "Giant acceleration of free diffusion by use of tilted periodic potentials," Phys. Rev. Lett. **87**, 010602.
Reimann, P., C. Van den Broeck, H. Linke, P. Hänggi, J. M. Rubi, and A. Perez-Madrid, 2002, "Diffusion in tilted periodic potentials: Enhancement, universality, and scaling," Phys. Rev. E **65**, 031104.
Rěmskar, M., 2004, "Inorganic nanotubes," Adv. Mater. (Weinheim, Ger.) **16**, 1497–1504.
Rey, M., M. Strass, S. Kohler, P. Hänggi, and F. Sols, 2007, "Nonadiabatic electron heat pump," Phys. Rev. B **76**, 085337.
Risken, H., 1984, *The Fokker-Planck Equation* (Springer, Berlin).
Ritt, G., C. Geckeler, T. Salger, G. Cennini, and M. Weitz, 2006, "Fourier synthesis of optical potentials for atomic quantum gases," Phys. Rev. A **74**, 063622.
Ros, A., R. Eichhorn, J. Regtmeier, T. Duong, P. Reimann, and D. Anselmetti, 2005, "Brownian motion—Absolute negative particle mobility," Nature (London) **436**, 928.
Rosato, A., K. J. Strandburg, F. Prinz, and R. H. Swendsen, 1987, "Why the Brazil nuts are on top: Size segregation of particulate matter by shaking," Phys. Rev. Lett. **58**, 1038–1040.
Rousselet, J., L. Salome, A. Ajdari, and J. Prost, 1994, "Directional motion of Brownian particles induced by a periodic asymmetric potential," Nature (London) **370**, 446–448.
Rozenbaum, V., D. Yang, S. Lin, and T. Tsong, 2004, "Catalytic

wheel as a Brownian motor," J. Phys. Chem. B **108**, 15880–15889.
Sadgrove, M., M. Horikoshi, T. Sekimura, and K. Nakagawa, 2007, "Rectified momentum transport for a kicked Bose-Einstein condensate," Phys. Rev. Lett. **99**, 043002.
Salger, T., C. Geckeler, S. Kling, and M. Weitz, 2007, "Atomic Landau-Zener tunneling in Fourier-synthesized optical lattices," Phys. Rev. Lett. **99**, 190405.
Sanchez, R., F. J. Kaiser, S. Kohler, P. Hänggi, and G. Platero, 2008, "Shot noise in spin pumps," Physica E (Amsterdam) **40**, 1276–1278.
Sassine, S., Y. Krupko, J. C. Portal, Z. D. Kvon, R. Murali, K. P. Martin, G. Hill, and A. D. Wieck, 2008, "Experimental investigation of the ratchet effect in a two-dimensional electron system with broken spatial inversion symmetry," Phys. Rev. B **78**, 045431.
Savel'ev, S., F. Marchesoni, P. Hänggi, and F. Nori, 2004a, "Transport via nonlinear signal mixing in ratchet devices," Phys. Rev. E **70**, 066109.
Savel'ev, S., F. Marchesoni, P. Hänggi, and F. Nori, 2004b, "Nonlinear signal mixing in a ratchet device," Europhys. Lett. **67**, 179–185.
Savel'ev, S., F. Marchesoni, and F. Nori, 2003, "Controlling transport in mixtures of interacting particles using Brownian motors," Phys. Rev. Lett. **91**, 010601.
Savel'ev, S., F. Marchesoni, and F. Nori, 2004a, "Manipulating small particles in mixtures far from equilibrium," Phys. Rev. Lett. **92**, 160602.
Savel'ev, S., F. Marchesoni, and F. Nori, 2004b, "Stochastic transport of interacting particles in periodically driven ratchets," Phys. Rev. E **70**, 061107.
Savel'ev, S., V. Misko, F. Marchesoni, and F. Nori, 2005, "Separating particles according to their physical properties: Transverse drift of underdamped and overdamped interacting particles diffusing through two-dimensional ratchets," Phys. Rev. B **71**, 214303.
Savel'ev, S., and F. Nori, 2002, "Experimentally realizable devices for controlling the motion of magnetic flux quanta in anisotropic superconductors," Nature Mater. **1**, 179–184.
Schanz, H., T. Dittrich, and R. Ketzmerick, 2005, "Directed chaotic transport in Hamiltonian ratchets," Phys. Rev. E **71**, 026228.
Schanz, H., M.-F. Otto, R. Ketzmerick, and T. Dittrich, 2001, "Classical and quantum Hamiltonian ratchets," Phys. Rev. Lett. **87**, 070601.
Scheid, M., D. Bercioux, and K. Richter, 2007, "Zeeman ratchets: Pure spin current generation in mesoscopic conductors with non-uniform magnetic fields," New J. Phys. **9**, 401.
Scheid, M., A. Pfund, D. Bercioux, and K. Richter, 2007, "Coherent spin ratchets: A spin-orbit based quantum ratchet mechanism for spin-polarized currents in ballistic conductors," Phys. Rev. B **76**, 195303.
Schemmert, U., J. Kärger, C. Krause, R. A. Rákoczy, and J. Weitkamp, 1999, "Monitoring the evolution of intracrystalline concentration," Europhys. Lett. **46**, 204–210.
Schiavoni, M., L. Sanchez-Palencia, F. Renzoni, and G. Grynberg, 2003, "Phase control of directed diffusion in a symmetric optical lattice," Phys. Rev. Lett. **90**, 094101.
Schliwa, M., 2002, *Molecular Motors* (Wiley-VCH, Weinheim).
Schneider, W., and K. Seeger, 1966, "Harmonic mixing of microwaves by warm electrons in germanium," Appl. Phys. Lett. **8**, 133–135.
Sekimoto, K., 1998, "Langevin equation and thermodynamics," Prog. Theor. Phys. Suppl. **130**, 17–27.
Shalóm, D. E., and H. Pastoriza, 2005, "Vortex motion rectification in Josephson junction arrays with a ratchet potential," Phys. Rev. Lett. **94**, 177001.
Shushin, A. I., 2002, "Specific features of threshold diffusion in a tilted periodic potential. Simple model and analytical results in the underdamped regime," Europhys. Lett. **60**, 525–531.
Shutenko, T. A., I. L. Aleiner, and B. L. Altshuler, 2000, "Mesoscopic fluctuations of adiabatic charge pumping in quantum dots," Phys. Rev. B **61**, 10366–10375.
Silva, C. C. D., J. V. de Vondel, M. Morelle, and V. V. Moshchalkov, 2006, "Controlled multiple reversals of a ratchet effect," Nature (London) **440**, 651–654.
Silva, C. C. D., A. V. Silhanek, J. Van de Vondel, W. Gillijns, V. Metlushko, B. Ilic, and V. V. Moshchalkov, 2007, "Dipole-induced vortex ratchets in superconducting films with arrays of micromagnets," Phys. Rev. Lett. **98**, 117005.
Simon, S. M., C. S. Peskin, and G. F. Oster, 1992, "What drives the translocation of proteins," Proc. Natl. Acad. Sci. U.S.A. **89**, 3770–3774.
Sinitsyn, N. A., and I. Nemenman, 2007, "Universal geometric theory of mesoscopic stochastic pumps and reversible ratchets," Phys. Rev. Lett. **99**, 220408.
Siwy, Z., and A. Fuliński, 2002, "Fabrication of a synthetic nanopore ion pump," Phys. Rev. Lett. **89**, 198103.
Siwy, Z., and A. Fuliński, 2004, "A nanodevice for rectification and pumping ions," Am. J. Phys. **72**, 567–574.
Siwy, Z., I. D. Kosińska, A. Fuliński, and C. R. Martin, 2005, "Asymmetric diffusion through synthetic nanopores," Phys. Rev. Lett. **94**, 048102.
Sjölund, P., S. J. H. Petra, C. M. Dion, S. Jonsell, M. Nylén, L. Sanchez-Palencia, and A. Kastberg, 2006, "Demonstration of a controllable three-dimensional Brownian motor in symmetric potentials," Phys. Rev. Lett. **96**, 190602.
Slater, G. W., H. L. Guo, and G. I. Nixon, 1997, "Bidirectional transport of polyelectrolytes using self-modulating entropic ratchets," Phys. Rev. Lett. **78**, 1170–1173.
Smirnov, S., D. Bercioux, M. Grifoni, and K. Richter, 2008, "Quantum dissipative Rashba spin ratchets," Phys. Rev. Lett. **100**, 230601.
Smoluchowski, M., 1912, "Experimentell nachweisbare, der üblichen Thermodynamik widersprechende Molekularphänomene," Phys. Z. **13**, 1069–1080.
Son, W. S., J. W. Ryu, D. U. Hwang, S. Y. Lee, Y. J. Park, and C. M. Kim, 2008, "Transport control in a deterministic ratchet system," Phys. Rev. E **77**, 066213.
Speer, D., R. Eichhorn, and P. Reimann, 2007, "Transient chaos induces anomalous transport properties of an underdamped Brownian particle," Phys. Rev. E **76**, 051110.
Spivak, B., F. Zhou, and M. T. Beal Monod, 1995, "Mesoscopic mechanisms of the photovoltaic effect and microwave absorption in granular metals," Phys. Rev. B **51**, 13226–13230.
Squires, T. M., and S. R. Quake, 2005, "Microfluidics: Fluid physics at the nanoliter scale," Rev. Mod. Phys. **77**, 977–1026.
Stafford, C. A., and N. S. Wingreen, 1996, "Resonant photon-assisted tunneling through a double quantum dot: An electron pump from spatial Rabi oscillations," Phys. Rev. Lett. **76**, 1916–1919.
Stein, D., M. Kruithof, and C. Dekker, 2004, "Surface-charge-governed ion transport in nanofluidic channels," Phys. Rev. Lett. **93**, 035901.
Sterck, A., R. Kleiner, and D. Koelle, 2005, "Three-junction

SQUID rocking ratchet," Phys. Rev. Lett. **95**, 177006.
Sterck, A., S. Weiss, and D. Koelle, 2002, "SQUID ratchets: Basics and experiments," Appl. Phys. A: Mater. Sci. Process. **75**, 253–262.
Storm, A. J., J. H. Chen, X. S. Ling, H. W. Zandbergen, and C. Dekker, 2003, "Fabrication of solid-state nanopores with single-nanometre precision," Nature Mater. **2**, 537–540.
Strass, M., P. Hänggi, and S. Kohler, 2005, "Nonadiabatic electron pumping: Maximal current with minimal noise," Phys. Rev. Lett. **95**, 130601.
Stroock, A. D., R. F. Ismagilov, H. A. Stone, and G. M. Whitesides, 2003, "Fluidic ratchet based on Marangoni-Benard convection," Langmuir **19**, 4358–4362.
Suzuki, D., and T. Munakata, 2003, "Rectification efficiency of a Brownian motor," Phys. Rev. E **68**, 021906.
Switkes, M., C. M. Marcus, K. Campman, and A. C. Gossard, 1999, "An adiabatic quantum electron pump," Science **283**, 1905–1908.
Talkner, P., P. Hänggi, and M. Morillo, 2008, "Microcanonical quantum fluctuation theorems," Phys. Rev. E **77**, 051131.
Talkner, P., E. Lutz, and P. Hänggi, 2007, "Fluctuation theorems: Work is not an observable," Phys. Rev. E **75**, 050102.
Taloni, A., and F. Marchesoni, 2006, "Single-file diffusion on a periodic substrate," Phys. Rev. Lett. **96**, 020601.
Tessier, F., and G. W. Slater, 2002, "Strategies for the separation of polyelectrolytes based on non-linear dynamics and entropic ratchets in a simple microfluidic device," Appl. Phys. A: Mater. Sci. Process. **75**, 285–291.
Thouless, D. J., 1983, "Quantization of particle transport," Phys. Rev. B **27**, 6083–6087.
Togawa, Y., K. Harada, T. Akashi, H. Kasai, T. Matsuda, F. Nori, A. Maeda, and A. Tonomura, 2005, "Direct observation of rectified motion of vortices in a niobium superconductor," Phys. Rev. Lett. **95**, 087002.
Tsong, T. Y., 2002, "Na,K-ATPase as a Brownian motor: Electric field-induced conformational fluctuation leads to uphill pumping of cation in the absence of ATP," J. Biol. Phys. **28**, 309–325.
Tu, Z. C., 2008, "Efficiency at maximum power of Feynman's ratchet as a heat engine," J. Phys. A **41**, 312003.
Turberfield, A. J., J. C. Mitchell, B. Yurke, A. P. Mills, M. I. Blakey, and F. C. Simmel, 2003, "DNA fuel for free-running nanomachines," Phys. Rev. Lett. **90**, 118102.
Ustinov, A. V., C. Coqui, A. Kemp, Y. Zolotaryuk, and M. Salerno, 2004, "Ratchetlike dynamics of fluxons in annular Josephson junctions driven by biharmonic microwave fields," Phys. Rev. Lett. **93**, 087001.
Van den Broeck, C., 2005, "Thermodynamic efficiency at maximum power," Phys. Rev. Lett. **95**, 190602.
Van den Broeck, C., 2007, "Carnot efficiency revisited," Adv. Chem. Phys. **135**, 189–201.
Van den Broeck, C., and R. Kawai, 2006, "Brownian refrigerator," Phys. Rev. Lett. **96**, 210601.
Van den Broeck, C., R. Kawai, and P. Meurs, 2004, "Microscopic analysis of a thermal Brownian motor," Phys. Rev. Lett. **93**, 090601.
Van den Broeck, C., P. Meurs, and R. Kawai, 2005, "From Maxwell demon to Brownian motor," New J. Phys. **7**, 10.
Van den Broek, M., and C. Van den Broeck, 2008, "Chiral Brownian heat pump," Phys. Rev. Lett. **100**, 130601.
van der Heyden, F. H. J., D. Stein, K. Besteman, S. G. Lemay, and C. Dekker, 2006, "Charge inversion at high ionic strength studied by streaming currents," Phys. Rev. Lett. **96**, 224502.
van der Meer, D., P. Reimann, K. van der Weele, and D. Lohse, 2004, "Spontaneous ratchet effect in a granular gas," Phys. Rev. Lett. **92**, 184301.
van der Meer, D., K. van der Weele, P. Reimann, and D. Lohse, 2007, "Compartmentalized granular gases: Flux model results," J. Stat. Mech.: Theory Exp. **2007**, P07021.
Van Look, L., B. Y. Zhu, R. Jonckheere, B. R. Zhao, Z. X. Zhao, and V. V. Moshchalkov, 2002, "Anisotropic vortex pinning in superconductors with a square array of rectangular submicron holes," Phys. Rev. B **66**, 214511.
van Oudenaarden, A., and S. G. Boxer, 1999, "Brownian ratchets: Molecular separations in lipid bilayers supported on patterned arrays," Science **285**, 1046–1048.
Vavilov, M. G., V. Ambegaokar, and I. L. Aleiner, 2001, "Charge pumping and photovoltaic effect in open quantum dots," Phys. Rev. B **63**, 195313.
Vercoutere, W. A., S. Winters-Hilt, V. S. DeGuzman, D. Deamer, S. E. Ridinoa, J. T. Rodgers, H. E. Olsen, A. Marziali, and M. Akeson, 2003, "Discrimination among individual Watson-Crick base pairs at the termini of single DNA hairpin molecules," Nucleic Acids Res. **31**, 1311–1318.
Vidan, A., R. M. Westervelt, M. Stopa, M. Hanson, and A. C. Gossard, 2004, "Triple quantum dot charging rectifier," Appl. Phys. Lett. **85**, 3602–3604.
Villegas, J. E., S. Savel'ev, F. Nori, E. M. Gonzalez, J. V. Anguita, R. Garcia, and J. L. Vicent, 2003, "A superconducting reversible rectifier that controls the motion of magnetic flux quanta," Science **302**, 1188–1191.
Vlassiouk, I., and Z. S. Siwy, 2007, "Nanofluidic diode," Nano Lett. **7**, 552–556.
Wambaugh, J. F., C. Reichhardt, C. J. Olson, F. Marchesoni, and F. Nori, 1999, "Superconducting fluxon pumps and lenses," Phys. Rev. Lett. **83**, 5106–5109.
Wang, H., and G. Oster, 2002, "Ratchets, power strokes, and molecular motors," Appl. Phys. A: Mater. Sci. Process. **75**, 315–323.
Wang, J., and J. Gong, 2008, "Quantum ratchet accelerator without a bichromatic lattice potential," Phys. Rev. E **78**, 036219.
Wang, Z. S., 2004, "Bioinspired laser-operated molecular locomotive," Phys. Rev. E **70**, 031903.
Weiss, S., D. Koelle, J. Müller, R. Gross, and K. Barthel, 2000, "Ratchet effect in dc SQUIDs," Europhys. Lett. **51**, 499–505.
Wonneberger, W., and H. J. Breymayer, 1981, "Asymptotics of harmonic microwave mixing in a sinusoidal potential," Z. Phys. B: Condens. Matter **43**, 329–334.
Wördenweber, R., P. Dymashevski, and V. R. Misko, 2004, "Guidance of vortices and the vortex ratchet effect in high-T_c superconducting thin films obtained by arrangement of antidots," Phys. Rev. B **69**, 184504.
Xie, T. D., P. Marszalek, Y. D. Chen, and T. Y. Tsong, 1994, "Recognition and processing of randomly fluctuating electric signals by Na, K-ATPase," Biophys. J. **67**, 1247–1251.
Xu, C., W. Rice, W. He, and D. Stokes, 2002, "A structural model for the catalytic cycle of Ca^{2+}-ATPase," J. Mol. Biol. **316**, 201–211.
Yevtushenko, O., S. Flach, and K. Richter, 2000, "ac-driven phase-dependent directed diffusion," Phys. Rev. E **61**, 7215–7218.
Yevtushenko, O., S. Flach, Y. Zolotaryuk, and A. A. Ovchinikov, 2001, "Rectification of current in ac-driven nonlinear systems and symmetry properties of the Boltzmann equation," Europhys. Lett. **54**, 141–147.

Yin, P., H. Yan, X. G. Daniell, A. J. Turberfield, and J. H. Reif, 2004, "A unidirectional DNA walker that moves autonomously along a track," Angew. Chem., Int. Ed. **43**, 4906–4911.

Yorke, B., A. J. Turberfield, A. P. Mills, F. C. Simmel, and J. L. Neumann, 2000, "A DNA-fuelled molecular machine made of DNA," Nature (London) **406**, 605–608.

You, J. Q., and F. Nori, 2005, "Superconducting circuits and quantum information," Phys. Today **58** (11), 42–47.

Yu, K., T. W. Heitmann, C. Song, M. P. DeFeo, B. L. T. Plourde, M. B. S. Hesselberth, and P. H. Kes, 2007, "Asymmetric weak-pinning superconducting channels: Vortex ratchets," Phys. Rev. B **76**, 220507.

Zapata, I., R. Bartussek, F. Sols, and P. Hänggi, 1996, "Voltage rectification by a SQUID ratchet," Phys. Rev. Lett. **77**, 2292–2295.

Zapata, I., J. Łuczka, F. Sols, and P. Hänggi, 1998, "Tunneling center as a source of voltage rectification in Josephson junctions," Phys. Rev. Lett. **80**, 829–832.

Zhou, F., B. Spivak, and B. Altshuler, 1999, "Mesoscopic mechanism of adiabatic charge transport," Phys. Rev. Lett. **82**, 608–611.

Zhu, B. Y., L. V. Look, V. V. Moshchalkov, B. R. Zhao, and Z. X. Zhao, 2001, "Vortex dynamics in regular arrays of asymmetric pinning centers," Phys. Rev. B **64**, 012504.

Zhu, B. Y., F. Marchesoni, V. V. Moshchalkov, and F. Nori, 2003, "Controllable step motors and rectifiers of magnetic flux quanta using periodic arrays of asymmetric pinning defects," Phys. Rev. B **68**, 014514.

Zhu, B. Y., F. Marchesoni, and F. Nori, 2003, "Biologically inspired devices for easily controlling the motion of magnetic flux quanta," Physica E (Amsterdam) **18**, 318–319.

Zhu, B. Y., F. Marchesoni, and F. Nori, 2004, "Controlling the motion of magnetic flux quanta," Phys. Rev. Lett. **92**, 180602.

Zitzmann, J., A. V. Ustinov, M. Levitchev, and S. Sakai, 2002, "Super-relativistic fluxon in a Josephson multilayer: Experiment and simulation," Phys. Rev. B **66**, 064527.

Zueco, D., and J. L. Garcia-Palacios, 2005, "Quantum ratchets at high temperatures," Physica E (Amsterdam) **29**, 435–441.

Zwolak, M., and M. Di Ventra, 2008, "Physical approaches to DNA sequencing and detection," Rev. Mod. Phys. **80**, 141–165.